AD-781 995

THE EFFECT OF EUTECTIC MICROSTRUC-
TURES ON THE MECHANICAL PROPERTIES
OF CERAMIC OXIDES

Charles O. Hulse, et al

United Aircraft Research Laboratories

Prepared for:

Office of Naval Research

May 1974

REPORT DOCUMENTATION PAGE		READ INSTRUCTIONS BEFORE COMPLETING FORM
1. REPORT NUMBER N910803-10	2. GOVT ACCESSION NO.	3. RECIPIENT'S CATALOG NUMBER AD-781995
4. TITLE (and Subtitle) THE EFFECT OF EUTECTIC MICROSTRUCTURE ON THE MECHANICAL PROPERTIES OF CERAMIC OXIDES		5. TYPE OF REPORT & PERIOD COVERED Final Report 1 Feb 1969 – 31 Dec 1973
		6. PERFORMING ORG. REPORT NUMBER
7. AUTHOR(s) Charles O. Hulse and John A. Batt		8. CONTRACT OR GRANT NUMBER(s) N00014-69-C-0073
9. PERFORMING ORGANIZATION NAME AND ADDRESS United Aircraft Corporation Research Laboratories East Hartford, Connecticut 06108		10. PROGRAM ELEMENT, PROJECT, TASK AREA & WORK UNIT NUMBERS
11. CONTROLLING OFFICE NAME AND ADDRESS Department of the Navy Office of Naval Research Arlington, Virginia 22217		12. REPORT DATE May 1974
		13. NUMBER OF PAGES 137
14. MONITORING AGENCY NAME & ADDRESS(if different from Controlling Office)		15. SECURITY CLASS. (of this report) Unclassified
		15a. DECLASSIFICATION/DOWNGRADING SCHEDULE

16. DISTRIBUTION STATEMENT (of this Report)

Reproduction in whole or in part is permitted for any purpose of
The United States Government.

17. DISTRIBUTION STATEMENT (of the abstract entered in Block 20, if different from Report)

19. KEY WORDS (Continue on reverse side if necessary and identify by block number)

Eutectics	Mechanical Properties	Crystal Growth
Directional Solidification	Microstructure	Floating Molten Zone
Oxides	High Temperature	Work-to-Fracture

20. ABSTRACT (Continue on reverse side if necessary and identify by block number)

Various experimental techniques for the production of unidirectionally
solidified oxide eutectics were examined. These included a modified Bridgman-
Starkbarger technique and bottom cooling of melts held in platinum crucibles.
It was concluded that the best approach, at least for experimental purposes,
was the floating molten zone technique and the successful use of a number of
variations of this technique was demonstrated. Scale-up of this basic

20.

technique to produce plates and cylindrical ingots up to 1 3/8 in. in diameter was demonstrated. Many different eutectic systems were directionally solidified and the mechanical properties of the $Al_2O_3-ZrO_2$ (Y_2O_3), $Y_2O_3-ZrO_2$, $CaZrO_3-ZrO_2$ and MgO-CaO systems are described in considerable detail. The strength results indicate that oxide materials prepared in this manner can exhibit exceptional strengths and significant increases in toughness at elevated temperatures. The various reasons and requirements for obtaining exceptional mechanical properties in this class of materials are considered. Continued research should result in new materials with further mechanical property improvements for use in demanding high temperature technological applications.

United Aircraft Research Laboratories

UA

UNITED AIRCRAFT CORPORATION

EAST HARTFORD, CONNECTICUT

Report N910803-10

The Effect of Eutectic Microstructures on the
Mechanical Properties of Ceramic Oxides

FINAL REPORT

Contract N00014-69-C-0073

REPORTED BY _C. O. Hulse_

C. C. Hulse

J. A. Batt

J. A. Batt

APPROVED BY _E. R. Thompson_

E. R. Thompson, Chief
Advanced Metallurgy

DATE _May 1974_

NO. OF PAGES ___140___   COPY NO. _____

ABSTRACT

Various experimental techniques for the production of unidirectionally solidified oxide eutectics were examined. These included a modified Bridgman-Starkbarger technique and bottom cooling of melts held in platinum crucibles. It was concluded that the best approach, at least for experimental purposes, was the floating molten zone technique and the successful use of a number of variations of this technique was demonstrated. Scale-up of this basic technique to produce plates and cylindrical ingots up to 1 3/8 in. in diameter was demonstrated. Many different eutectic systems were directionally solidified and the mechanical properties of the Al_2O_3-ZrO_2 (Y_2O_3), Y_2O_3-ZrO_2, $CaZrO_3$-ZrO_2 and MgO-CaO systems are described in considerable detail. The strength results indicate that oxide materials prepared in this manner can exhibit exceptional strengths and significant increases in toughness at elevated temperatures. The various reasons and requirements for obtaining exceptional mechanical properties in this class of materials are considered. Continued research should result in new materials with further mechanical property improvements for use in demanding high temperature technological applications.

The Effect of Eutectic Microstructures on the
Mechanical Properties of Ceramic Oxides

TABLE OF CONTENTS

INTRODUCTION

This final summary report reviews four years of a research investigation directed toward an examination of the properties of oxide-oxide eutectics unidirectionally solidified to form composite microstructures. The results of earlier portions of this investigation have been described in previous reports and publications (Refs. 1-6). This report describes the results obtained using a variety of different preparation techniques and the mechanical properties of a number of unidirectionally solidified, high melting point eutectic systems.

Pure oxide ceramics have a number of properties which make them of interest as potential engineering materials: high melting points, good resistance to corrosion by liquids and gases, and high potential strength to weight ratios. Because of these properties, there has always been an interest in employing ceramics to solve the materials problem in the highest temperature sections of gas turbine engines. Demands for operation at higher gas turbine temperatures continue because such increases lead directly to increased efficiency and decreased pollution.

Recognition of the needs for higher temperature materials and the known properties of ceramic materials led to the initiation of a multimillion dollar effort sponsored by ARPA to construct gas turbine engines containing ceramic components. These gas turbines are to be used in automotive heavy equipment and for base load electric power generation and will be made using presently available ceramic materials. The engineering design difficulties associated with the development of gas turbine engines containing brittle components for these types of applications are clearly much less difficult than they would be for engines to be used in aircraft power plants. This ARPA-sponsored effort has prompted an increased interest in the development of ceramics with superior mechanical properties for use not only i these engine applications, but for use in ships and eventually in aircraft. The use of ceramic materials in these applications will depend not only on superior engineering design but more importantly on the availability of ceramics with a significant advantage in high temperature strength over presently available nickel and cobalt base superalloys.

One of the earliest approaches for increasing the mechanical strength of ceramic materials was by firing at a high temperature so that some of the components melted or by adding an extra amount of glassy phase to promote densification and a reduction in porosity at a lower temperature. It was later realized that these lower melting (glassy) phases were beneficial only

with regard to the low temperature strength, and were in fact very detrimental
to the mechanical properties at high temperatures. The problem of obtaining
high strength at high temperatures became one of creating high density in a
pure single phase. The two principal approaches to achieve this have been the
incorporation of small amounts of very specialized additives before firing to
assist sintering and single-phase consolidation by hot pressing. In both
cases optimum densification is accomplished by beginning with extremely fine
powders.

A large portion of the recent efforts in ceramic research have dealt with
understanding how to create high strength ceramics by hot pressing. This work
has resulted in the fabrication of many different single-phase materials with
excellent mechanical strengths and even good optical transparency. It has
been clearly demonstrated in a number of these systems that, in addition to
near theoretical density and extreme purity, the presence of a very fine micro-
structure is necessary in order to obtain the highest strength.

Unfortunately, some important problems are associated with the fabrication
of ceramics for high temperature strength applications using the hot-pressing
approach. Extremely fine, reactive charge powders must be employed in order
to hot press at low enough temperatures to achieve both theoretical density and
a fine grain size. These fine, reactive powders tend to pick up gases which
cannot generally be removed without destroying the reactivity so essential to
successful hot pressing. When many transparent hot-pressed ceramic materials
are subsequently heated to high temperatures, the gases contained within the
piece tend to form voids and pieces may actually explode (Ref. 7).

Another difficulty with hot-pressed materials, perhaps more serious, is
that fine grain size material necessarily contains many grain boundaries. These
boundaries are not thermodynamically stable and at high temperatures grain
boundary area tends to be reduced by grain growth. Thus, the advantage of the
original fine grain size (microstructure) is significantly reduced. Even if
grain growth were avoided, the presence of grain boundaries is detrimental to
strength at high temperatures. The major mechanisms of creep and fracture at
high temperatures are associated with enhanced diffusion along grain boundaries
and grain boundary sliding and separation (Refs. 8,9). Grain boundaries are
perhaps a more serious defect in ionic structures than metals because of their
greater complexity in crystal structure brought about by valence balance
requirements.

Another possible approach to the creation of ceramics with superior high
temperature strength is to use the material in single crystal form. Although
crystals can be made in this form with very high purity and with zero porosity,
they do not usually contain a fine scale microstructure. In general, ceramic

2

single crystals are observed to fracture by cleavage at low temperature and to be relatively ductile at very high temperatures because there are no micro-structural features present to impede the motion of cracks or dislocations.

The metal superalloys which are presently used in the highest temperature sections of gas turbines are normally made by casting from the liquid state. More recently, improved metal superalloys have been made by directional solidification (Ref. 10) so that vanes and blades are either single crystals (containing dendrites and precipitates) or a collection of large, columnar grains. The crystal boundaries are parallel to the direction of solidification and are oriented in the airfoil parallel to the direction of maximum stress. Even stronger and equally stable metal superalloys have been made by the uni-directional solidification of eutectic compositions. This produces a composite material containing a uniform dispersion of fine oriented whiskers or lamellae which effectively reinforce a more ductile matrix phase (Refs. 11,12). It has been shown that whiskers removed from these composites have strengths of the order of 10^6 psi (Ref. 13).

This report describes efforts to examine the effects of a unidirectionally solidified eutectic microstructure on the mechanical properties of refractory oxides. In view of the advantages and importance of casting from the melt in the metallurgical industry, an examination of the properties of ceramics with microstructures which can be obtained only by melt solidification appears appropriate. Several investigators (Refs. 14-16) have recently demonstrated with completely different systems that the mechanical properties of ceramics can be improved by the incorporation of a hard, second phase using hot-pressing techniques. The growth of a eutectic structure from the melt would theoretically be a much more satisfactory way to obtain the finest, most stable and most uni-form composite microstructure.

Obvious reasons why so little research has been directed to this area are the difficulties associated with containment and the control of a molten ceramic. Because of the difficulties involved in obtaining precise control over the solidification process and because of the need to demonstrate as soon as possible that ingots of potentially useful size could be produced, a major portion of this research effort was concerned with the development of the best solidification technique. Although much was accomplished, there is a great need for continued effort in this direction.

There are a number of circumstances which could produce improvements in the mechanical properties of ceramic materials with a directional eutectic microstructure over that available from hot-pressed ceramics. An immediate possibility is that at high temperatures the minor phase will have the high

strength characteristic of a material in whisker form and that this phase will
directionally reinforce the somewhat ductile matrix in a typical composite
manner. The reality of this possibility has been demonstrated in numerous
metallic eutectic systems. Figure 1 shows that over a wide range of tempera-
tures, similar Petch type equations relate strength to the spacing between
phases in a relatively brittle intermetallic eutectic (Ref. 17) just as they
relate the strength to grain size in hot-pressed ceramics.

An important advantage of unidirectionally solidified eutectics for high
temperature strength applications is that their microstructure is extremely
stable, practically to the melting point (Ref. 18). This stability results
from the fact that their microstructures are produced directly from the molten
state under conditions of thermodynamic equilibrium. If grain boundaries are
present in these microstructures they are relatively few in number and generally
parallel to the axis of primary reinforcement.

The strength of a eutectic composite at lower temperatures, where both
phases are brittle, may be enhanced by a suitable selection of phases so that
the matrix phase is placed in compression upon cooling due to differences in
thermal expansion between the phases. A tensile stress applied to the bulk
composite then will not result in a tensile stress in the continuous matrix
phase until the compressive prestress is overcome. Tension is the primary
failure mode of ceramic materials. The effectiveness of prestressing in
increasing the strength of a ceramic matrix composite has been demonstrated
(Ref. 16) and surface type prestressing is of considerable commercial impor-
tance in the glass industry. If, in addition to the prestress contribution,
the matrix has a lower elastic modulus than the reinforcing phase, the amount
of stress seen by the matrix phase during tensile loading of the composite
will be even further reduced. A proportionately larger fraction of the applied
stress is carried by the minor phase as the ratio of the modulus of rein-
forcing to matrix phase is increased.

The fracture of brittle materials is usually believed to involve the
sudden growth of very fine flaws, called "Griffith Microcracks", which are
always present in these materials. The importance of a flaw depends upon its
size. Fracture normally involves the growth of the "critical" flaw which is
the largest microcrack with the appropriate orientation to the applied load.
Because the distribution of these flaws is random, the actual strengths of
ceramics show a statistical distribution which is also a function of volume
stressed. Some encouraging efforts have been made to limit the size of micro-
cracks by the presence of a fine dispersion of second phase particles. If
ceramic eutectics with a very fine, uniform microstructure can be produced,
improved mechanical properties may be observed because the size of these
microcracks are significantly limited.

The impact strengths of ceramics are generally so low that they are not usable in many important applications for which they might otherwise be well suited. The main mechanism by which energy is absorbed during fracture of brittle materials is through the production of new surfaces. The presence of a finely dispersed, high modulus fibrous or lamellar phase may function to deviate cracks and thus increase the amount of fracture surface produced during failure. These energies can be increased significantly if cracks are deflected so as to follow the dispersed phase-matrix interface. The Ni_3Al-Ni_3Cb intermetallic eutectic is an example where cracks are blunted and deflected along these interfaces rather than propagating in the usual brittle manner. Figure 2 shows some examples of this process occurring in a fatigue specimen. Although this eutectic material shows practically no tensile ductility at room temperatures, it has a room temperature Charpy impact strength of about 1.75 ft-lbs for half-sized, notched samples.

LITERATURE SURVEY

The first published research on directionally solidified oxide eutectics of which we are aware was by Galasso, et al at the United Aircraft Research Laboratories (Ref. 19) in 1968. In the following year, Harrison (Ref. 20) described the directional solidification of an oxide-oxide eutectic system in which one of the phases solidified as a glass. In the next year, Rowcliffe, et al (Ref. 21) reported on two directionally solidified eutectics in the alumina-titania system. They used a special electron beam heating technique with a traveling molten zone. Although cracking was observed in many of their samples, they noted that fine primary dendrites appeared to impede the movement of cracks. A series of papers by Viechnicki and Schmid (Refs. 22-26) followed in which directional solidification was obtained primarily by the bottom cooling of crucibles containing the molten oxides. Although they reported the first real strength data, their materials were not exceptionally strong. At present the only other place besides UARL where oxide-oxide eutectic systems are being studied is at Pennsylvania State University (Refs. 27-30).

Presently, there are active research programs both in the United States and in Europe concerned with the preparation and properties of metal oxide-metal eutectic systems (Refs. 31-38). Studies have also been made of salt eutectics (Refs. 39-41), an oxide-nonmetallic system (Ref. 42) and a devitrified glass system (Ref. 43).

TECHNIQUES USED FOR DIRECTIONAL SOLIDIFICATION

Certain requirements must be met in order to develop optimum eutectic microstructures. One important requirement is that the components must be of high purity. It is believed (Ref. 44) that the presence of impurities is the primary reason for localized constitutional supercooling and the formation of a cellular interface at the boundary between the liquid and solid during solidification. The details of the resultant colony microstructure in the final ingot have been described elsewhere (Ref. 45). These microstructures are characterized by parallel elongated volumes of relatively perfect eutectic structure with the axis of the colony oriented parallel to the direction of solidification. The material between the colonies contains a higher concentration of impurities than the eutectic material within the colonies and thus it solidifies at a lower temperature. Because of the differences in melting point, the material between the colonies solidifies after the eutectic within the colonies and the liquid-solid interface contains cusps or depressions around the colonies which would resemble cells if the liquid-solid interface could be viewed directly through the liquid. The mechanical properties of metallic eutectics with colony microstructures are almost always inferior to those obtained where a planar liquid-solid interface has been maintained.

In addition to the more obvious requirements for extremely uniform movement of the liquid-solid interface during solidification and precise control of temperature, an important requirement is that the thermal gradient across the liquid-solid interface be as high as possible. The general formulation of this requirement which has been verified for a number of metallic eutectic systems is (Ref. 46):

$$G/R \leq \frac{M_T C_O}{D} \quad \frac{1 - K_{\alpha\beta}^C}{K_{\alpha\beta}^C} \qquad (2)$$

where G = temperature gradient in the liquid at the interface
  R = rate of solidification
  M_T = slope of liquidus trough
  C_O = third element concentration
  D = diffusion coefficient of third element in the liquid
  $K_{\alpha\beta}^C$ = weighted average of the distribution coefficient of c for the α and β phases.

The magnitude of the gradient (G) limits directly the maximum rate at which solidification can occur without the undesirable breakdown of the planar liquid-solid interface and the formation of a colony microstructure. In addition to the economic advantages of increased production and/or some relaxation of the

requirements for high purity when a high liquid-solid thermal gradient is present, higher speed solidification results in a finer microstructure and generally more desirable properties. Figure 1 shows how strength at all temperatures increases with a finer microstructure in directionally solidified Ni_3Al-Ni_3Cb eutectic. If the thermal gradient can be made sufficiently high, it has been shown that with certain metallic systems, composite growth can also be established over a wide range of off-eutectic compositions.

Container-Held Melts

At the time this work was initiated, very little was known about directionally solidified oxide-oxide eutectic systems. Only three papers had been published and in one of these the matrix was a glass. Hunt and Jackson (Ref. 47) have suggested that phases which have high entropies of fusion will grow in a faceted manner and if one or both phases in a eutectic grow in this manner, coupled, composite growth would not be predicted. Because ceramic materials often solidify in a faceted manner, the initial objectives of this program were to develop inexpensive and convenient techniques to fabricate many ingots of low temperature model ceramic systems. The decision was made to work with refractory ceramic oxide crucibles and eutectics which solidify below 1000°C. It was hoped that in this way reactions with the containers could be minimized and that the expense of using platinum to contain the melts could be avoided. Refractory metal containers had the limitations of cost and the fact that many low temperature ceramic melts are not sufficiently stable in the absence of oxygen.

Initial solidification experiments were conducted using equipment previously developed to produce unidirectionally solidified metal eutectics. This consisted of slowly lowering a 5/8 in. I.D. alumina crucible from a furnace, resistively heated by a carbon helix resistor in an argon atmosphere. For solidification of ceramics, a longer crucible than normal was used so that the upper end might be exposed to air. These experiments showed that poor directionality occurred after the first few inches of growth, apparently because of poor heat flow through the already solidified section of the ceramic ingot.

A modified Bridgman-Starktarger solidification furnace, shown diagrammatically in Fig. 3, was then built specifically for this program and used for most of the unidirectional solidification experiments during the first year. Its main features are its use of refractory oxide tubes as containers and its ability to maintain a high liquid-solid temperature gradient independent of ingot length. A liquid-solid temperature gradient of 143°C/cm was measured using an alumina shielded thermocouple in an ingot of V_2O_5 (m.p. 685°C).

8

In this device, water is continually sprayed on the outside of the refractory oxide tube containing the melt as it is slowly lowered from a Pt-Rd wire wound furnace. The water is present almost up to the center of the furnace as is shown in Fig. 3. The water is prevented from leaking further up into the hot zone by a copper washer which fits loosely around the ceramic tube. Just above this spray arrangement, a porous oxide (firebrick) ring provides a baffle zone to limit radial heat flow from the melt. A flat liquid-solid interface can then be attained by adjusting the furnace temperature so that the liquid-solid interface is in the baffle zone. If the furnace is too hot so that the ingot is melted below the baffle, the solid at the interface will be concave; if the furnace temperature is too low so that the liquid-solid interface is above the baffle, the solid at the interface will be convex. No problems were encountered with the oxide containment tube cracking because of the presence of a high thermal gradient.

A serious problem that developed during the use of this apparatus was the development of porosity after about the first 3/4 in. of solidification. These pores were usually elongated and parallel to the growth direction. This effect was apparently due to gases dissolved in the melt whose concentration increased at the interface as additional material solidified. The process is analogous to that which creates the so-called "ice worms" in common ice cubes. This problem could be overcome either by creating a vacuum over the melt and then back-filling with oxygen prior to solidification or by insertion of a vibrator into the melt during solidification. Figure 4 shows a typical containment tube with seals for creation of a vacuum and also the vibrator assembly which was used. Figure 5 shows longitudinally sectioned ingots with and without the porosity problem.

Although many solidification experiments on a number of systems were carried out, cellular eutectic microstructures were developed in all cases. This was believed to be due to a small degree of contamination by the oxide container. Table I gives the chemical analysis of some low temperature eutectics after solidification in this apparatus. Because of the contamination problem, it was concluded that in further experiments the expense of working with platinum crucibles was justified.

A second unidirectional solidification arrangement for making short lengths of large diameter ingots is shown in Fig. 6. This device depended upon cooling only from the bottom by means of a water-cooled post and it also involved the use of refractory oxide crucibles to hold the melt. Solidification occurred as the cold post was slowly traversed up to the bottom of the crucible. Very few experiments were made after this equipment was assembled because it was decided that the emphasis should be shifted to work with precious metal crucibles and to the construction of the higher temperature equipment described below.

Table I

Chemical Analysis of Some Low Temperature Eutectics
Melted in Oxide Containers in Air

Eutectic	Container	Furnace Temp °C	Time or Solidification Rate	Analysis W/O		
				Al	Si	Mg
$5PbO \cdot 3GeO - 3PbO \cdot GeO$	Al_2O_3	1000	2 cm/hr	.60	.03	.005
$PbO - 2PbO \cdot Fe_2O_3$	Al_2O_3	1180	2 cm/hr	.33	.06	.006
$PbO - 3PbO \cdot Nb_2O_5$	Al_2O_3	1165	2 cm/hr	1.02	.12	.12
$Bi_2O_3 \cdot Fe_2O_3 - 20Bi_2O_3 \cdot Fe_2O_3$	$Al_2O_3 \cdot MgO$	985	16 hr	.27	--	.07
$Bi_2O_3 \cdot Fe_2O_3 - 20Bi_2O_3 \cdot Fe_2O_3$	Al_2O_3	985	16 hr	.47	--	.007

Two additional pieces of equipment for unidirectional solidification were constructed near the end of the first contract year. They were similar in concept and differed primarily in that one was heated by Globars in air and was therefore capable of reaching about $1525^{\circ}C$, while the second was heated by a SiC tube heater in an argon atmosphere and could reach temperatures of $1700^{\circ}C$. Both could operate with the melt in an air, vacuum or oxygen environment. A diagram of the lower temperature unit is shown in Fig. 7.

The temperature gradient in these furnaces was adjustable depending upon the distance between the water-cooled probe and the bottom of the crucible. In the typical procedure, the contents of the crucible were completely melted and then the probe was raised until it contacted the bottom of the crucible. Once the probe was positioned, unidirectional solidification occurred by slowly lowering the furnace temperature through a controlled cooling cycle. The sample was never physically moved and it was felt that this would be helpful in eliminating banding which can be a severe problem in techniques when the sample must be moved. It was hoped that at higher temperatures, where heat transfer by radiation is appreciable, bottom cooling alone might be sufficient to grow ingots of appreciable length. Viechnicki and Schmid had successfully used bottom cooling at somewhat higher temperatures to produce directionally solidified ingots of the $Al_2O_3-Y_2Al_5O_{12}$ eutectic (m.p. $1800^{\circ}C$).

Two techniques were developed to remove samples from their precious metal containers without causing damage to the crucibles. The first approach consisted of diamond core drilling almost to the bottom of the crucible and then tapping the crucible bottom until the undamaged core fell out. In the second approach, the sides of the crucibles were plasma sprayed with a coating of mullite. During the cooling of an ingot held in this crucible, the low thermal expansion of the mullite pulled the platinum away from the melt and the whole ingot could be removed intact. Figure 8 shows a mullite-platinum composite crucible with some sample melts in which this removal process was used successfully.

Poor microstructures were generally obtained from our melts which were slowly solidified upward from the bottom of platinum or iridium crucibles. Examination of flats polished on the sides of samples revealed directional but poorly oriented microstructures. Extensive nucleation of new grains occurred near the bottom of the crucibles but these grains were only approximately oriented. At least one-half inch of solidification was required before the better oriented grains began to predominate, but soon after the grain orientation became random. Figure 9 presents thermocouple data on thermal gradients present in a $BaWO_4-WO_3$ eutectic after different amounts of solidification. The liquid-solid thermal gradients are generally low and decrease as the amount of solidification increases. This steady decrease in liquid-solid thermal gradient

resulted from the increasingly effective thermal insulation presented by the solidified eutectic as it grew in length. On the basis of these results it was concluded that a different type of technique should be developed which would yield a higher liquid-solid thermal gradient which would be independent of the length of ingot solidified.

Floating Molten Zone Experiments

It was decided that better eutectic microstructures would be obtained if ingots were prepared by the floating molten zone technique. In this approach, a molten zone, held in place by surface tension, is slowly traversed up a pre-fired charge rod. Since no containers are required, gases dissolved in the melt have relatively short paths for escape via free liquid surfaces, and high liquid-solid thermal gradients can be obtained independent of the length of solidified ingot. In contrast to the earlier approach, the poor thermal conductivity of ceramics acts to promote a high liquid-solid thermal gradient.

In initial experiments, two mil thick platinum resistance strip heaters were placed around premelted and cast eutectic rods and used to obtain narrow molten zones. These molten zones, held in place by surface tension forces, were slowly moved up the rods by moving the heater. Figure 10 shows a temperature profile measured during directional solidification of the $PbO-3PbO \cdot Nb_2O_5$ eutectic. The slope of the line at the melting point yields a liquid-solid thermal gradient of $576^\circ C/cm$. These values represent a significant improvement over the gradients obtainable using the previous techniques. For this measurement a eutectic charge rod containing a thermocouple buried along its axis was made by repeated dipping of a sheathed chromel-alumel thermocouple into a melt of the eutectic held in a platinum crucible.

In general, the heat transfer between the strip heaters and the melts was so poor that the heaters had to be ~500°C above the temperature of the melt. This limited the work to eutectics with melting points below ~1200°C. Much higher temperatures could be reached if the melts actually wetted the strip heaters as shown in Fig. 11. This greatly improved the heat transfer and the temperature of the melt and heater were measured by an optical pyrometer to be essentially the same. Thus, a melt temperature of ~1700°C in air could be conveniently reached using an iridium heater and ~1600°C using a platinum heater without radiation shields. The melts usually wetted the outside as well as the insides of the strip heaters and this suggested that internal heating by complete immersion might be beneficial. Figure 12 shows a further modification in which this was purposely accomplished by using several concentric loops of resistively heated wires embedded within the melt. This resulted in a very narrow and stable molten zone. It was also found that

these hot wires could be moved transversely out of the rod after a molten zone pass and then reinserted (melted in) near the initial starting point and the whole process repeated again and again. The possibilities of zone refining to high purities and of eliminating all grain boundaries by this approach presented very interesting possibilities for further work.

Despite these encouraging results, further work with these systems was delayed after a discussion with Dr. Diness of ONR in favor of investigations of higher temperature systems with more potential for useful mechanical properties. Because the useful limit of even the iridium heaters in contact with the melt appeared to be ~1700°C, various tungsten and molybdenum strip and wire configurations were examined. Melts of the Al_2O_3-ZrO_2 eutectic (m.p. 1890°C) and pure alumina (m.p. 2050°C) in contact with these heaters were made with results which were initially encouraging. However, with further work and closer examination, extremely small visual specks of apparent metal pickup were observed which could not be avoided.

Rather than continue with this approach, radiation heaters using tungsten and/or tungsten-rhenium wires were developed to overcome this contamination. These wires were wound vertically on short, slotted thoria tubes as shown in Fig. 13. A typical heater consisted of about 19 in. of 20 mil diameter wire and required ~31 amps at 26 volts (800 watts) to melt a column of the Al_2O_3-ZrO_2 eutectic ~1/2 in. long. A liquid-solid thermal gradient of at least 1000°C/cm was estimated in the Al_2O_3-ZrO_2 eutectic (m.p. 1890°C) using an optical pyrometer.

The main difficulty encountered with heaters of this type was associated with making a good electrical contact between the heater and the power supply. If care was not taken, the thermal expansion of the wire upon heating caused stresses in the wire and heater failure. This difficulty was overcome by avoiding a rigid physical connection between the wires and the water-cooled copper electrodes. The heating wires were held in position by the slotted thoria tube which rested on heat shields as shown in Fig. 13. Support of the heat shields was provided by alumina plates which rested on the electrodes. The ends of the heating wires were braided and extended down from the furnace into vertical wells in the electrodes which were filled with the Ga-In-Sn eutectic which is liquid at room temperature. The liquid metal made a good electrical connection and did not physically restrain the tungsten wires from moving as they were heated.

Also shown in Fig. 13 is a wire basket which supported the melt and fixed its position in the center of the heater. Although the melt could freely pass through the basket, surface tension forces kept the melt largely inside the basket and this helped to establish a long liquid column which eliminated porosity in the ingots. The baskets were made from about four turns of 20 mil diameter tungsten or molybdenum wire spot-welded to three or more support wires.

Although the facility shown in Fig. 13 was used quite successfully to prepare unidirectionally solidified ingots of the Al_2O_3-ZrO_2 (Y_2O_3) eutectic, it was experimentally difficult to ensure that the solid eutectic never came in contact with and damaged the wire basket. Also, we realized that there were only a limited number of systems which would not react or become contaminated with the tungsten or molybdenum wire. In order to avoid these problems, equipment and procedures were developed for melting using R.F. power. A Model J Westinghouse zone refiner, designed for use with metal systems was made available for our work. This unit includes a large chamber for work in inert gas or vacuum atmospheres and various traverse controls. A 50 kw Lepel power generator operating at ~500 K.C. supplies R.F. power to the work coil through Lepel L.C.T.-4 step down transformer. Figure 14 is a diagrammatic view of the heater arrangement. Because ceramics are poor electrical conductors, the actual heating is accomplished by radiation from small carbon ring susceptors about 1/8 in. thick.

As will be discussed later, one of the problems which developed in the initial heater arrangement was that the thermal gradients were so high that cracks occurred in ingots prepared at high solidification speeds. The effect of this problem was reduced by the use of an after-heater (additional susceptor) or more insulation just below the heater to cut down on the rate of cooling in the solidified ingot. Because this tended to decrease the liquid-solid thermal gradient, which we wanted to be as high as possible, and because we wanted to keep the macroscopic liquid-solid interface as flat as possible, these additions were not made immediately adjacent to the heater assembly. In the final arrangement, used to obtain the data presented later, there was a gap of about 3/16 in. between the heater and the thermal insulation. This gap allowed the ingot to lose heat by radiation and made it easier to observe the melt.

Near the end of the program, some attention was given to possible modifications of the floating molten zone technique which would permit the preparation of ingots of larger sizes and/or shapes. The first modification is shown diagrammatically in Fig. 15. A molybdenum crucible was used to hold the melt and the melt was fed by a charge rod which slowly entered the crucible from above. The crucible was surrounded and heated by a carbon susceptor and the appropriate R.F. coils in an argon atmosphere. Four small holes in the bottom of the crucible allowed the melt to pass through the crucible and to solidify on the ingot being pulled slowly away from the bottom of the crucible. This process is similar to the Tyco process (Ref. 48) except that gravity instead of capillary forces are used to feed the melt, the charge feed is continuous and the final ingot is pulled downward instead of upward. The molybdenum crucible used in a subsequent version of this concept is shown in Fig. 16. Except for support hangers, the sides of the crucible were removed in an attempt to facilitate the removal of gases from the melt.

Using the above technique we were able to prepare an ingot of the Al_2O_3-ZrO_2 (Y_2O_3) eutectic 1 in. in diameter. Although only a few experiments were tried, the tendency for gases to collect on the bottom surface of the crucible was identified as an important problem. The problem could not be avoided by using as a charge rod material which had previously been zone melted several times.

Although the crucible technique just described would create high liquid-solid thermal gradients independent of ingot length and would also lend itself to the preparation of shapes, it has the serious limitation that it requires the liquid to be in direct contact with a container. Because of the severe requirements for high purity in order to grow the most perfect eutectic micro-structures, it would be better if this contact could be completely avoided. There are many ceramic systems which could never use this process because no suitable container material exists.

Figure 17 shows diagrammatically a modification to the floating molten zone technique which can be used to prepare larger size ingots without the presence of any additional container phase. In this approach, the insulation beneath part of the ring susceptor (shown previously in Fig. 14) has been removed so that heat is directed downward as well as towards the center of the ring susceptor. The upper traverse is now moved downward faster than the solidified ingot so that the resultant piece can be much larger in diameter than the charge rod. The final arrangement is similar in some respects to the Verneuil process. With this arrangement, the problems of supporting a column of liquid against the force of gravity is avoided because, except just at the liquid-solid interface, the liquid column is always much smaller in diameter than the solidified ingot which supports it. Another feature of this process is that gases dissolved in the melt have easy access to large areas of free surface from which to escape.

Figure 18 shows an ingot of the Al_2O_3-ZrO_2 (Y_2O_3) eutectic whose diameter has been increased to 1 3/8 in. by gradually increasing the rate of charge rod feed while the ingot lowering speed remained fixed with the heater modified as shown in Fig. 17. The experiment was terminated at this diameter because the charge rod had been expended. The authors feel that ingots with considerably larger diameters can be directionally solidified using this technique.

Because all the heat is introduced from the sides in our usual float zone procedure, the liquid-solid interface tends to be convex with respect to the solid. This is undesirable - the liquid-solid interface for optimum micro-structures should be perfectly flat. In the solidification approach just described (Fig. 17) the final heating is from above and the interface should be flattened. By appropriate control of the radial heat loss (insulation, cooling, etc.), it should be possible to make the solid at the liquid-solid interface concave, flat or convex.

One final variation of the floating molten zone technique which permitted the preparation of directionally solidified plates was briefly examined. Again, this variation did not require the presence of any additional inert container material which could result in contamination. A diagram of the final arrangement is shown in Fig. 19. The initial charge material is in the form of a plate and two susceptors are used, one on each side of the plate. The power is increased until a zone of molten material passing completely through the plate is produced and then the plate is traversed down through the zone heating furnace. The lateral width of the plate is larger than the lateral dimension of the carbon susceptor so that the liquid zone does not extend completely to either edge of the plate. Surface tension forces and the wetting of the unmelted edges of the plate by the liquid keeps the melt from contracting and forming a cylindrical ingot. Figure 20 shows a successful example experiment using the $Al_2O_3-ZrO_2$ (Y_2O_3) eutectic system. In this picture the edges of the plate which were not melted are still attached. The run was abruptly terminated when the power drifted too high and the liquid zone extended all the way to the right-hand edge of the plate.

CHARGE MATERIAL PREPARATION

Because it was known that the presence of impurities usually results in poor microstructure, attempts were made to work primarily with high purity materials after preliminary experiments with lower purity, less expensive materials. Table II lists the sources and purities of the powders used in this program.

For experiments in which eutectics were held in containers, the melts were always prehomogenized by complete melting of the batch in platinum crucibles. A convenient technique was found for the preparation of rods for use in the modified Bridgman-Starkbarger solidification facility (Fig. 3) and for use in floating molten zone experiments with relatively low melting eutectic systems (Figs. 10 and 11). The eutectic composition was first melted in a platinum crucible and then the contents poured into a clean quartz tube standing on a copper heat sink as shown in Fig. 21. The first melt to be poured solidified immediately at the bottom, thereby sealing the tube, and the remainder of the liquid solidified as a rod. In some instances, it was necessary to pour slowly to avoid the formation of shrinkage voids and excessive cracking. In all cases, the rods shrank away from the quartz upon cooling without reaction and were easily removed.

Charge rods for high melting point systems for floating molten zone processing were made by isostatic pressing at 10,000 psi followed by firing for approximately one hour in air at $1500^{\circ}C$. After firing the rods were usually still soft enough to be hand sanded, if necessary, into perfectly straight, round rods. The ends of the rods were sanded into points which were inserted into the ends of refractory oxide support tubes rigidly held by the traverse mechanisms. Commercial tubes of Al_2O_3, ZrO_2 and MgO have been used for supports depending upon the system. The two ends of the charge rod, first the bottom and then the top, were next fused to their oxide support tubes using the R.F. heater assembly. Zone melting was usually initiated in the rod just above the lower attachment point and the rod was then slowly traversed downward. At least two, and often three or more, melt traverses were usually made in an attempt to develop the optimum microstructure.

Table II

Raw Materials

Oxide	Source	Approximate Price	Approximate Purity, %
PbO	Fisher Cert.	$ 1.95/lb	99.5
Fe_2O_3	Fisher Cert.	1.95/lb	99.5
Fe_2O_3	Hall Labs		99.999
Nb_2O_5	Alfa Inorganics	9.40/100gm	99.5
V_2O_5	Alfa Inorganics	16.00/250gm	99.5
GeO_2	Alfa Inorganics	35.00/100gm	99.999
BaO	Alfa Inorganics	7.80/kg	97.0
WO_3	Alfa Inorganics	11.70/250gm	99.5
Bi_2O_3	Fisher Cert.	14.25/lb	99.7
Bi_2O_3	Poly Research		99.999
ZnO	Alfa Inorganics	9.30/kg	99.9
Cr_2O_3	Alfa Inorganics	6.20/lb	99.0
Li_2WO_4	Alfa Inorganics	11.80/100gm	99.0
$MnCO_3$	Fisher Cert.	3.90/lb	99.8
NiO	Fisher Cert.	9.50/lb	99.5
CaO	Fisher Cert.	6.60/lb	99.9
CoO	Fisher Cert.	1.70/lb	99.0
Mn_2O_3	Poly Research		99.9
TiO_2	Fisher Cert.	2.55/lb	99.9
$SrCO_3$	Allied Chem.		99.0
$MgCO_3$	Fisher Cert.	7.20/lb	99.4

Table II (Cont'd)

Oxide	Source	Approximate Price	Approximate Purity, %
La_2O_3	A. D. MacKay		99.99
Y_2O_3	Moly Corp.	$ 32/lb	99.99
Gd_2O_3	A. D. MacKay		99.9
Gd_2O_3	Res. Chem. Inc.		99.9
SiO_2	Penn. Pulverizing Co.		99.91
Na_2CO_3	Fisher Cert.	1.35/lb	99.5
H_3BO_3	Fisher Cert.	1.95/lb	99.8
$MgCO_3$	United Mineral & Chem.		99.999
Al_2O_3	Materials Res. Corp.	144/lb	99.999
ZrO_2	Wah Chang	90/100 gm	99.99+
$CaCO_3$	United Mineral & Chem.		99.99
ZrO_2	Materials Res. Corp.	60/lb	99.97
Fe_2O_3	Materials Res. Corp.	200/lb	99.995

EVALUATION PROCEDURES

The polished microstructures of all the samples prepared were carefully examined with an optical microscope up to 1000X. Some etched microstructures were also examined using the scanning electron microscope. The SEM was the primary tool used to reveal the details on fracture surfaces. Some eutectic structures were also examined using an AMR/3 electron microprobe manufactured by Philips Electronic Instruments.

The crystallographic orientation of some eutectics relative to the solidification direction was determined using X-ray techniques. The typical procedure was to mount a transverse slice of the eutectic on a standard Norelco Pole Figure device and then make a spiral scan (vary α and ϕ together) for a fixed value of 2θ corresponding to a major crystal plane.

Three-point bend strengths parallel to the direction of solidification were determined using a 60,000 lb capacity Tinius Olsen Universal Testing machine. The 15, 30, and 120 lbs full scale readout ranges were used in this program. For high temperature bend testing, 2 in. diameter solid alumina loading rams are used. These rams are rigidly attached to the crossheads and extend into a split furnace using SiC heater elements. Figure 22 shows the testing machine with the high temperature rams in place. For testing above 1525°C, an extra small booster furnace inside the usual furnace is employed. The booster furnace consists of Pt-40% Rh heater wire wound and cemented onto a thin walled alumina tube. This furnace fits closely around the hot ends of the loading rams and the sample testing fixture. This furnace has been used for testing in air up to 1670°C. The booster furnace can be seen setting separately at the front on the lower testing crosshead in the left side of Fig. 22. The white alumina rams can be seen behind this surrounded by the partially opened clam-shell furnace.

Typical flexural strength samples were 0.156 x 0.066 x 0.875 in. with a 0.75 in. test span. Tensile sample edges were beveled and all surfaces were polished down to 6µ diamond. All fixture parts were polycrystalline alumina with single crystal sapphire loading pins 3/16 in. in diameter.

All work-of-fracture testing was done using the same testing machine with the solid alumina rams. Samples were nominally 1/4 x 1/4 x 2 in. with a central notch made using .011 in. thick diamond blade. The notch was cut so that only 1/4 of the cross-sectional area remained as suggested by Simpson and others (Refs. 49,50). The crosshead loading rate for all testing was .0025 in. per minute. Fracture energy values are quoted per area of crack so that the surface energies would be one-half of the values given.

Because of the large dimensions of the alumina loading rams, it was usually possible to make only one high temperature test per day without risk of cracking the rams due to thermal shock. A second testing machine was constructed at UARL during this program in response to our mechanical testing needs. This machine employs a furnace with Super Kanthal heaters and zircar insulation and is capable of 1700°C. Although tests can be made in air using the same alumina rams mentioned above, the test results reported here for the bend strengths of the CaO-MgO eutectic system were made in an argon atmosphere using carbon (Pocco Graphite) rams. The fixtures were also made of the same material except for the loading pins which were 3/16 in. diameter tungsten rods.

RESULTS AND DISCUSSION BY SYSTEM

Various Lower Melting Temperature Eutectics

Initial experiments in this program were concerned with the selection of model ceramic systems whose behavior during and after unidirectional solidification would subsequently be studied in detail. A summary of all the preliminary casting experiments is given in Table III. Most of these melts were made in alumina crucibles which gave the same results as some comparison melts in platinum crucibles. The fact that a number of these melts showed dendritic-like structures may be more a measure of errors in composition during batch preparation or errors in phase diagram values than an indication that the eutectic cannot be controlled. Figure 23 shows the $SrO \cdot WO_3-WO_3$ eutectic microstructure which is an example of faceted growth in the minor phase. This system and many of the systems in Table III appeared to be suitable candidates for unidirectional solidification.

A general summary of all the unidirectionally solidified experiments with low melting point eutectics is given in Table IV. Figures 24-29 show the microstructures of some of these systems. Although selected areas showed good microstructures, the general control and uniformity of these ingots have not been of sufficient quality to justify any property examination other than metallographic. Figure 24 shows a multigrain lamellar structure in the $PbO-3PbO \cdot Nb_2O_3$ eutectic. Figure 25 shows a typical colony structure in the $PbO-2PbO \cdot Fe_2O_3$ lamellar eutectic. The matrix in this eutectic undergoes a solid state decomposition reaction so there are three phases present in this figure.

Figure 26 shows a typical rod-like structure in a selected area of the $Bi_2O_3-Bi_2O_3 \cdot Fe_2O_3$ eutectic. This eutectic tended to form colony structures as shown in the upper photograph of Fig. 27. These were notable because each colony appeared to contain whiskers of three slightly different orientations. Each colony had three walls of clear matrix which met near the center of the colony and divided the colony into three volumes as shown in the lower photograph of Fig. 27. The whiskers in each volume appeared to grow at a slight angle to each other. The upper photograph in Fig. 27 shows the intersection of the three different zones. A similar growth was observed in earlier work with the $MgO-MgO \cdot Al_2O_3$ eutectic. In that system each colony consisted of four volumes. These observations are not understood but may indicate that the matrix grows in a faceted manner or that the whiskers prefer to grow in the matrix at some other angle than perpendicular to the liquid-solid interface. Another possibility is that the melt has an excess of the matrix phase which grows dendritically ahead of each colony.

Table III

Summary of Oxide Eutectic Castings

Sample No.	System	Composition	Eutectic Temp. °C	Microstructure	Potential for Controllability	Crucible	Comment
	$PbO-Fe_2O_3$	12.8 w/o Fe_2O_3	730	broken lamellar*	good	Al_2O_3, Pt	solid state tranf. at 650- 2-phase matrix
2	$PbO-Nb_2O_5$	6.85 w/o Nb_2O_5	835	rough lamellar*	good	Al_2O_3, Pt	
3A	$PbO-V_2O_5$	5.7 w/o V_2O_5	760	very rough lamellar	fair	Pt	controllability uncertain
3B	$PbO-V_2O_5$	46.1 w/o V_2O_5	490	dendritic		Pt	glassy (?)
4	$PbO-GeO_2$	15 w/o GeO_2	707	rod-like	poor	Al_2O_3, Pt	glassy (?)
5	$BaO-WO_3$	18.5 w/o BaO	935			Al_2O_3	soluble in water, mechanically weak
6	V_2O_5-BaO	32.2 w/o BaO	550			Al_2O_3	glassy
7	$Bi_2O_3-GeO_2$	10.3 w/o GeO_2	880	directional dendritic	fair	Al_2O_3	
8	V_2O_5-ZnO	14.2 w/o ZnO	640	directional dendritic	poor	Al_2O_3	
9	$PbO-WO_3$	17.6 w/o WO_3	725		very poor	Pt	mica-like appearance, very weak mechanically, many fragments
10	Bi_2O_3-ZnO	1.24 w/o ZnO	750	rod-like*	good	Al_2O_3, Pt	nonuniform rod spacing

23

Table III (Cont'd)

Sample No.	System	Composition	Eutectic Temp. °C	Microstructure	Potential for Controllability	Crucible	Comment
11	Bi_2O_3-Fe_2O_3	1.14 w/o Fe_2O_3	790	rod-like*	good	Al_2O_3	Whiskers axes at small angle to ingot axis
12	V_2O_5-Cr_2O_3	19.0 w/o Al_2O_3	640	dendritic, large grains	very poor	Al_2O_3	somewhat porous
14	V_2O_5-Cr_2O_3	18.6 w/o Cr_2O_3	665	randomly shaped grains	very poor	Al_2O_3	
15	Li_2WO_4-WO_3	18.1 w/o WO_3	695	porous			very soluble in water
16	V_2O_5-MnO	9.13 w/o $MnCO_3$	660	directional dendritic	poor	Al_2O_3	porous
17	V_2O_5-NiO	9.2 w/o NiO	650	dendritic	very poor	Al_2O_3	very porous
18	V_2O_5-CuO	12.72 w/o CuO	620	dendritic	very poor	Al_2O_3	porous
19	Bi_2O_3-Al_2O_3	0.67 w/o Al_2O_3	810	dendritic	poor	Pt	
20	V_2O_5-CaO	2.74 w/o CaO	618	dendritic	very poor	Al_2O_3	
21	Bi_2O_3-Mn_2O_3	13.2 w/o Mn_2O_3	790	lamellar (?)	fair	Al_2O_3	
22	Bi_2O_3-TiO_2	.535 w/o TiO_2	835	rough, broken lamellar	fair	Al_2O_3	
23	CaO-WO_3	7.46 w/o CaO	1135	broken lamellar	good	Al_2O_3	color - green
24	SrO-WO_3	17.il w/o $SrCO_3$	1073	triangular rods*	good	Pt	

24

Table III (Cont'd)

Sample No.	System	Composition	Eutectic Temp. °C	Microstructure	Potential for Controllability	Crucible	Comment
25	$MgO-WO_3$	12.65 w/o $MgCO_3$	1120	not well defined irregular cross-section rods	good	Pt	
26	$Fe_2O_3-La_2O_3$	28.5 w/o La_2O_3	1490	rod-like*	very good	Pt	rods transparent in thin section cleaves perpendicular to whisker axes
27	$Fe_2O_3-Y_2O_3$	15.9 w/o Y_2O_3	1455	rod-like	good	Pt	
28	$Fe_2O_3-Gd_2O_3$	15.0 w/o Gd_2O_3	1500	rod-like			
29	$Nb_2O_5-Bi_2O_3$	49.2 w/o Bi_2O_3	1180	rod-like	poor	Al_2O_3	

*Microstructure shown in figures

25

Table IV

Summary of Unidirectionally Solidified Oxide Eutectic Experiments

Sample No.	System	Wt %	Phases	Eutectic Temp. (°C)	Furnace Temp. (°C)	Crucible	Rate of Solid.	Microstructure—Comment
A69-051-1	PbO-Fe$_2$O$_3$	12.8 w/o Fe$_2$O$_3$	PbO-2PbO.Fe$_2$O$_3$	730	1080	Al$_2$O$_3$	2 cm/hr	broken lamellar, 2-phase matrix, cellular structure, bubbles observed
A69-051-2	PbO-Fe$_2$O$_3$	--	--	---	1050	Al$_2$O$_3$	2 cm/hr	vacuum*, crucible cracked, cellular structure
A69-051-3	PbO-Fe$_2$O$_3$	--	--	---	1050	Al$_2$O$_3$	.5 cm/hr	vacuum*, cellular structure
A69-051-4	PbO-Fe$_2$O$_3$	--	--	---	1050	Al$_2$O$_3$	.5 cm/hr	vacuum*, cracked crucible, cellular structure
A69-051-5	PbO-Fe$_2$O$_3$	--	--	---	1050	Al$_2$O$_3$	.5 cm/hr	vacuum*, cellular structure
A69-051-6	PbO-Fe$_2$O$_3$	--	--	---	1050	Al$_2$O$_3$	.5 cm/hr	vibrator** (5000 cps), cellular structure
A69-471-1	PbO-GeO$_2$	15% GeO$_2$	4PbO.GeO$_2$-3PbO.2GeO$_2$	707	1025	Al$_2$O$_3$	1.45cm/hr	bubble formation, did not control
A69-053-1	PbO-Nb$_2$O$_5$	6.85% Nb$_2$O$_5$	PbO-3PbO.Nb$_2$O$_5$	835	1165	Al$_2$O$_3$	2 cm/hr	melt leaked, traverse failure
A69-053-2	PbO-Nb$_2$O$_5$	--	--	---	1140	Al$_2$O$_3$	2 cm/hr	only a short area controlled, traverse failure, broken lamellar, cellular
A69-053-3	PbO-Nb$_2$O$_5$	--	--	---	1010	Al$_2$O$_3$	2 cm/hr	extensive bubble formation

Table IV (Cont'd)

Sample No.	System	Wt %	Phases	Eutectic Temp. (°C)	Furnace Temp. (°C)	Crucible	Rate of Solid.	Microstructure-Comment
A69-054-1	V_2O_5-MnO	9.13% $MnCO_3$	V_2O_5-Mn$(VO_3)_2$	660	930	Al_2O_3	2 cm/hr	dendritic long grains
A69-212-1	SiO_2-Na_2O-BaO glass + Fe_2O_3	40 w/o Fe_2O_3, 10 w/o SiO_2, 50 w/o $Na_2O.SiO_2$	--	---	1360	Al_2O_3	2 cm/hr	glass, no precipitate
A69-055-1	Bi_2O_3-Fe_2O_3	4.6% Fe_2O_3	γBi_2O_3-$BiFeO_3$	790	1050	Al_2O_3	2 cm/hr	rod-like colony structure, some bubble formation
A69-055-2	Bi_2O_3-Fe_2O_3	--	--	---	1050	Al_2O_3	.5 cm/hr	colony structure
A69-055-3	Bi_2O_3-Fe_2O_3	--	--	---	1000	Al_2O_3	.5 cm/hr	large amount of bubble formation
A69-055-4	Bi_2O_3-Fe_2O_3	--	--	---	990	SiO_2	.5 cm/hr	Pt sheet used, melt leaked
A69-055-5	Bi_2O_3-Fe_2O_3	--	--	---	1050	ZrO_2	.5 cm/hr	bubble formation
A69-055-6	Bi_2O_3-Fe_2O_3	--	--	---	1050	spinel	.5 cm/hr	vacuum* oxygen
A69-055-7	Bi_2O_3-Fe_2O_3	--	--	---	1050	Al_2O_3	.5 cm/hr	water in vacuum system
A69-055-8	Bi_2O_3-Fe_2O_3	--	--	---	1050	Al_2O_3	.5 cm/hr	vacuum*

27

Table IV (Cont'd)

Sample No.	System	Wt %	Phases	Eutectic Temp. (°C)	Furnace Temp. (°C)	Crucible	Rate of Solid.	Microstructure-Comment
A69-055-9	Bi_2O_3-Fe_2O_3	--	--	--	1050	SiO_2 lined with Pt foil	.5 cm/hr	colony structure, no porosity noted
A69-055-10	Bi_2O_3-Fe_2O_3	--	--	--	1050	Al_2O_3	.5 cm/hr	vacuum vibrator, no porosity
A69-055-11	Bi_2O_3-Fe_2O_3	--	--	--	1050	Al_2O_3	.5 cm/hr	vibratory, no porosity
A69-056-1	Bi_2O_3-Fe_2O_3	--	--	--	1050	Al_2O_3		furnace #2* solid. too rapid, no control
A69-056-2	Bi_2O_3-Fe_2O_3	--	--	--	1300	Pt lined mullite cruc.	2.5 cm/hr	furnace #3* no control, thermal grad. too low
A69-056-3	Bi_2O_3-Fe_2O_3	--	--	--	1300	Pt lined mullite cruc.	2.5 cm/hr	thermal grad. increased, control somewhat improved
A69-057-1	Bi_2O_3-ZnO	24% ZnO	--	750	1030	Al_2O_3	2 cm/hr	rod-like eutectic, bubble formation
A69-166	$BaO.TiO_2$-SiO_2	9.9 w/o SiO_2 90.06 w/o $BaTiO_2$	$BaO.TiO_2$-$BaO.TiO_2.SiO_2$	1260	1400	Al_2O_3	2 cm/hr	not completely oxidized, reaction with crucible, furnace #4*

Table IV (Cont'd)

Sample No.	System	Wt %	Phases	Eutectic Temp. (°C)	Furnace Temp. (°C)	Crucible	Rate of Solid.	Microstructure-Comment
A69-177	PbO-SiO₂-B₂O₃	50 w/o PbO, 20 w/o SiO₂, 30 w/o B₂O₃	2 immis-cible glasses	---	1150	Al₂O₃	5 cm/hr	glasses separated but not directionally, reaction with crucible, furnace #4
A69-	TiO₂-SiO₂-B₂O₃-Na₂O	25 w/o TiO₂, 49 w/o SiO₂, 11 w/o B₂O₃, 15	glass + TiO₂ whiskers	---	1200	Pt	1.5 cm/hr	poor directionality, insufficient mixing

*Applied vacuum over melt until gas evolution ended, back filled with oxygen

**Vibrating alumina probe held in melt about 1 cm above liquid-solid interface during solidification

All samples run in Bridgman-Starkbarger furnace (Fig. 1), except where otherwise indicated. Furnace #2 shown in Fig. 2, furnace #3 shown in Fig. 3, furnace #4 normally used for metal eutectics but modified for air exposure over melt.

Figure 28 shows rod-like growth in the $Bi_2O_3-15Bi_2O_3 \cdot 2ZnO$ eutectic. This system appeared unusual in that the rod spacing was not uniform and the rods appeared to occur in occasional rows.

Figure 29 is a view in transmitted light of the $Fe_2O_3-LaFe_{12}O_{19}$ eutectic. The piece shown was observed parallel to the axes of the whiskers and was about .001 in. thick. The whiskers, which are believed to be the $LaFe_{12}O_{19}$ phase, transmit light and are also magnetic. If polarized light is passed through the whiskers the rotation direction of the plane of polarization of the light depends upon the direction of magnetization of the whiskers. Thus, in the lower picture, viewed with partially crossed Nicols, some of the whiskers transmit light and some do not. If the direction of magnetization could be adjusted by heating individual whiskers or groups of whiskers with a laser beam in a weak magnetic field, a chip of this material might be used for high density information storage.

Figure 30 shows selected transverse and longitudinal micrographs of the $BaWO_4-WO_3$ eutectic made with the bottom cooling apparatus previously shown in Fig. 6. This system grew nonfaceted and it should be possible to grow it in a controlled manner. Figure 31 shows the relationship between the inter-lamellar spacing and solidification speed for the $PbO-3PbO \cdot Nb_2O_5$ eutectic made using the floating molten zone technique with strip heater not in contact with the melt. The spacing varied from 0.78μ at 34.0 cm/hr to 2.04μ at 2.1 cm/hr. Figure 32 shows an example of how cracks around a hardness indent in this eutectic can be deflected by the microstructure to travel preferentially along the lamellar interfaces. This crack-blunting type behavior might impart a quality of toughness to this material. Figure 33 shows the longitudinal microstructure of the $BaTiO_3-Ba_2TiO_4$ eutectic (m.p. 1565°C), which was solidified at 2.2 cm/hr using an iridium strip heater in direct contact with the melt.

$Al_2O_3-ZrO_2$ (Y_2O_3) System

This eutectic melts at about 1890°C and all the results reported here were obtained for material prepared using the floating molten zone technique with R.F. heating in an argon atmosphere. This system has recently become of considerable commercial importance because of the outstanding properties exhibited by grinding wheels made using grits obtained from quenched eutectic melts.

The microstructure of this eutectic consists of a matrix of Al_2O_3 containing a whisker-like reinforcement phase of ZrO_2. Approximately 15.0 w/o of the ZrO_2 phase was replaced by Y_2O_3 in order to stabilize the ZrO_2 in the cubic form. This avoids the weakening effects of the monoclinic/tetragonal crystal

inversion and also creates a desirable thermal expansion mismatch between the phases in which the matrix phase is placed in compression upon cooling. By comparison of the microstructure of various melts, a composition for the eutectic of 54.50 w/o Al_2O_3, 38.66 w/o ZrO_2 and 6.84 w/o Y_2O_3 was determined. Assuming that all the Y_2O_3 is in the cubic ZrO_2 and estimating the density of the ZrO_2 (Y_2O_3) from available data (Ref. 51), the volume fraction of the ZrO_2 reinforcement was calculated to be 26.0 v/o.

If the effects of Poissons ratio are neglected, the stresses in the two phases can be estimated from Eqs. (2) and (3) (Ref. 16).

$$\sigma_f = \frac{\Delta\alpha \; \Delta T \; E_f}{1 + \dfrac{V_f \; E_f}{V_m \; E_m}} \qquad (2)$$

$$\sigma_m = \frac{\Delta\alpha \; \Delta T \; E_m}{1 + \dfrac{V_m \; E_m}{V_f \; E_f}} \qquad (3)$$

where σ_f = stress in fiber
$\Delta\alpha$ = difference in coefficient of thermal expansion
ΔT = temperature drop
V_f = volume fraction of fiber
V_m = volume fraction of matrix
E_f = elastic modulus of fiber
E_m = elastic modulus of matrix

If it is assumed that both phases behave elastically below about 1600°C, thermal expansion data (Ref. 51) can be used to estimate that the total differential internal strain produced in this eutectic upon cooling to room temperature is approximately .004. Substitution into Eqs. (1) and (2) yields estimates of 116 ksi (tension) for the ZrO_2 phase and 42 ksi (compression) for the Al_2O_3 phase.

Schmid and Viechnicki (Ref. 23) have grown unidirectionally solidified ingots of the same eutectic containing unstabilized ZrO_2 in molybdenum crucibles. They observed microcracking and pullouts which they suggest was due to the ZrO_2 crystal inversion and the residual tensile stress in the Al_2O_3 matrix due to the difference in thermal expansion between the phases. In later work they unidirectionally solidified the same eutectic with the ZrO_2 stabilized with Y_2O_3. They reported more difficulty in controlling this system and that their ingots again contained cracks. Typical bend strengths were 40 ksi and 25 ksi

31

in the longitudinal and transverse directions, respectively. They suggested that most of their difficulties in obtaining good ingots reflected the effect of the relatively low liquid-solid thermal gradient associated with their technique.

Ingots of the Al_2O_3-ZrO_2 (Y_2O_3) eutectic produced in our R.F. heated apparatus, which does not contain any possible source of tungsten contamination, exhibited the same eutectic microstructure as that produced by our earlier tungsten wire heated facility. Figure 34 shows in the longitudinal section the microstructure produced with plane front growth conditions (noncellular microstructures) at a solidification speed of 0.8 cm/hr. The whiskers are relatively short and irregular.

At solidification speeds above 0.8 cm/hr, cellular microstructures are produced. Figure 35 shows a transverse section through several cells in an ingot solidified at 2.5 cm/hr. Typical ingots were 3/8 in. in diameter and showed no evidence of cracking except at solidification speeds of 10 cm/hr and above.

Figure 36 shows stress-strain curves in three point bending for the eutectic solidified at 2.5 and 5 cm/hr compared with commercial polycrystalline Al_2O_3 (Wesgo 995) at 1575°C. The superiority of the eutectic is obvious and the data supports the assumption that the fine microstructure produced by the unidirectional solidification of an oxide eutectic can be mechanically superior to that produced by a more conventional technique.

The effect of solidification rate on bend strength at 1575°C is shown in Fig. 37. The strength tends to increase with increasing speed (finer micro-structure) as expected up to 5 cm/hr. Above 5 cm/hr the strength decreased perhaps because of the thermal shock associated with the high thermal gradients produced by this solidification technique. We estimated these gradients to be of the order 1000°C/cm. Apparatus modifications were made as mentioned earlier, to provide some annealing of the as-produced material and this allowed uncracked ingots to be produced at speeds up to 20 cm/hr.

The effects of post annealing of ingots with an after-heater chamber and the strengths which can therefore be obtained at higher solidification speeds are shown in Fig. 38. Optimum data for hot-pressed Al_2O_3 are also shown in Fig. 38 for purpose of comparison (Ref. 51). Although room temperature strengths above 100 ksi have been obtained for very fine grain size material, the data presented here are probably realistic for the bend strengths of hot-pressed Al_2O_3 at high temperatures. Also shown in Fig. 38 are strength data for the best hot-pressed Si_3N_4 currently available (Ref. 52) and a cast nickel-base superalloy, B-1900, (Ref. 53). To our knowledge, the strength value of 76,000 psi at 1575°C is the highest ever reported for an oxide material.

The effects of post annealing and the relationships of various other parameters on strength have not yet been carefully examined. It is hoped that further strength improvements can be obtained by: (a) additional improvement in the ingot annealing procedure, (b) solidification at higher or perhaps lower speeds, (c) evaluation of the optimum amount of Y_2O_3 stabilizer, (d) determination of the optimum eutectic composition for solidification at the higher speeds and (e) purification and/or better removal of dissolved gases by making more preliminary molten zone passes at lower speeds.

Transverse views of the eutectic microstructures produced by solidification at 20 cm/hr are shown in Figs. 39 and 40. The cells produced at higher speeds are larger than those produced at slower solidification speeds, which is the reverse of expected behavior. Each cell contains a central 3-web spine of Al_2O_3 with an extremely fine eutectic structure between the webs. The axes of the zirconia whiskers between the webs lie at an angle of about 50° to the axis of the web and to the direction of solidification. Within a particular grain, each web is parallel to one web in another cell. The cell walls are preferentially attacked by the etch (dilute HF) which suggests that these interfaces are relatively weak and contain higher concentrations of impurities.

Some experimental energies required to propagate a crack through this eutectic structure transverse to the solidification direction as a function of temperature are presented in Fig. 41. Also shown are similarly determined energies for polycrystalline and single crystal alumina. The energies required to propagate a crack in the eutectic are significantly greater especially at the higher temperatures.

A typical feature observed on room temperature fracture surfaces is shown in Fig. 42. The figure shows that in passing through a colony, the crack is deflected to pass parallel to the axes of the ZrO_2 whiskers which results in a raised triangular pyramid on one face and a similar depression in the opposite face. During a grinding operation the continual splintering away of these whiskers could result in continual presentation of sharp cutting edges.

The fracture surfaces produced at elevated temperatures are much different. The surfaces are generally flatter and covered with small "dimples" or depressions. and spherical balls of zirconia. A general SEM view of a fracture surface produced at 1500°C is shown in Fig. 43 while a more magnified picture is presented in Fig. 44. A suggested fracture sequence which could explain these unusual observations is described by Fig. 45. At these temperatures, both phases can deform at the crack tip and as this deformation proceeds, the bonds between the two phases ruptures. Eventually the matrix phase fails and the whiskers are left connected between the two fracture faces. Eventually these break, usually at the "grip" or point of attachment with one of the fracture faces. The extended, deformed whisker is not stable without the matrix surrounding it and spheroidized by diffusion processes to form a faceted ball.

An X-ray examination of a unidirectionally solidified ingot revealed that the [110] of the ZrO_2 and the C-axis of the Al_2O_3 are parallel to the growth direction. From an examination of various ingots, it was concluded that the ZrO_2 phase will grow as long, straight-sided whiskers when it is allowed to grow at an angle of about 50° to the C-axis of the Al_2O_3 matrix. Experiments in which the eutectic was seeded using a single crystal of sapphire with the [02$\bar{2}$4] parallel to the solidification direction resulted in microstructures shown in Fig. 46. Because of the perfection of this structure it should have outstanding strength. It was difficult to avoid renucleation of the C-axis alumina and the study was not pursued long enough to obtain samples of sufficient size for mechanical measurement. It is possible that a small adjustment in composition to prevent the presence of excess alumina would have solved the problem.

Several preliminary attempts were made to locate and directionally solidify the Al_2O_3-ZrO_2 eutectic with the ZrO_2 phase stabilized in the cubic form by additions of CaO. Figure 47 shows a longitudinal view of directionally solidified composition.

The two phases seen at low magnification in this figure are each different two-phase eutectics. Figure 48 shows the microstructure in several grains of the continuous matrix eutectic at higher magnification. The microstructure of this eutectic looks identical to that of the Al_2O_3-ZrO_2 (Y_2O_3) eutectic in which the ZrO_2 is not forced to grow parallel to the C-axis of the alumina.

The composition of the continuous matrix eutectic using the electron probe was 53 m/o Al_2O_3, 21.2 m/o ZrO_2, and 25.8 m/o CaO. Directional solidification of this composition resulted in a double eutectic microstructure. These results may be caused by the presence of a peritectic reaction in the eutectic trough. Although we have no X-ray confirmation, one eutectic may be between Al_2O_3 and ZrO_2 (CaO) while the second may be between CaO·Al_2O_3 and ZrO_2 (CaO).

ZrO_2-Y_2O_3 System

The system ZrO_2-Y_2O_3 was selected for study primarily because of its high melting point (2260°C), the fact that it responded to directional solidification in a controlled manner, and because it is a lamellar eutectic. A noticeable degree of toughness might be observed in a brittle lamellar system in which cracks are deflected, perhaps because of weak bonding between the phases, to travel primarily parallel to the lamellae.

34

The generally accepted phase diagram for this system is shown in Fig. 49 (Ref. 54). Chemical analyses and electron probe investigations of our controlled ingots indicated that the eutectic occurs at 10.2 w/o ZrO_2 and that the matrix phase is Y_2O_3, in conflict with earlier suggestions (Refs. 54,55). By comparing the weights of sections of SEM photographs containing the two eutectic phases, the amount of the ZrO_2 phase in the eutectic was calculated to be 6.38 v/o. Although SEM and optical microscope examinations indicated that the lamellae grew relatively parallel to the growth axis, it was not possible from X-ray studies to make an exact crystallographic statement of either the preferred growth direction or the relationship between the two phases because the grains were too small and too randomly oriented.

Figures 50 and 51 show transverse and longitudinal structures in ingots solidified at 5.7 and 40 cm/hr. The transverse view shows that in some areas the eutectic may solidify in a rod-like morphology. Initial ingots were 5/16 in. diameter and these always contained cellular microstructures along their center lines when grown at 40 cm/hr. In this microstructure the center of the cells grew with the lamellar morphology with rod-like growth near the colony walls. The liquid-solid thermal gradient was not high enough to permit plane front growth near the center of the ingot at these high speeds. Subsequent ingots, which were used for all the other data presented here, were 3/16 in. in diameter and grew in a plane front manner throughout. Plane front growth could be obtained with the system at speeds up to 100 cm/hr near the outside of the ingot, where an extremely high thermal gradient always existed.

Examination of polished sections revealed that the liquid-solid interface was not completely flat but instead represented a small section from a hemisphere about 3/4 in. in radius. Perhaps because of the resultant poor lamellar alignment relative to the tensile axis, fracture usually initiated from the tensile edge of the sample bars. The lamellar spacing as a function of solidification speed was measured and the results, shown in Fig. 52, corresponded well to the following equation:

$$\lambda^2 R = 2.38 \times 10^{-6} \text{ cm}^3/\text{hr} \qquad (4)$$

where λ = distance between lamellae
        R = solidification rate.

The spacing measurements were made using scanning electron microscope photos of grains mounted and polished so that the lamellae could be examined at surfaces 90° to each other, in order to assure that the measurements were not affected by either the small curvature of the liquid-solid interface or the scatter in orientation of the grains about the solidification direction.

In this eutectic system, the ZrO_2 phase contains approximately 60 m/o Y_2O_3 which stabilizes it in the cubic form. At room temperature the total elastic strain present in this eutectic due to the differences in thermal expansion between the phases was estimated as approximately 1 percent. This estimate was made using available thermal expansion data for the eutectic phases which contained much less or none of the other phases dissolved in it with the assumption also that mismatch strains were not relieved by plastic flow below 2000°C. Neglecting Poisson's ratio effects, the stresses in the two phases were estimated from Eqs. (2) and (3), to be approximately 181 ksi (tension) for the ZrO_2 phase and 12 ksi (compression) for the Y_2O_3 phase. The fact that the matrix is prestressed in compression by the minor phase upon cooling could enhance the strength of this eutectic system.

The effects of heat treatment on room temperature bend strength are shown in Table V. All heat treatments were made in air with the samples resting on platinum sheet. The as-made eutectic was black but became clear and fairly transparent during the above heat treatments. There were no measurable changes in weight associated with this bleaching process. The results shown in Table V can be compared with strengths of 17 ksi reported by General Electric for the commercial transparent Y_2O_3 material "Yttralox". The strengths presented in Table V show the typical scatter associated with brittle materials and that the strength increases with the amount of annealing. These results suggest that the stresses produced during ingot fabrication and/or sample preparation resulted in mechanical damage which could, at least partially, be removed by annealing.

The bend strengths at room temperature of samples solidified at speeds from 1.5 to 40 cm/hr and then annealed for 2 hrs at 1400°C are shown in Fig. 53. The more slowly grown ingots were difficult to prepare without cracking and, in order to obtain crack-free test samples, it was necessary to hand polish away the larger dimension (breadth) until the samples were almost square in cross section. As can be seen in Fig. 53, after anneal, the strengths were essentially independent of solidification speed. One reason for this behavior may be that the strength is controlled by flaws created during fabrication and/or sample preparation independent of the microstructures.

The critical flaw size required to initiate fracture can be estimated from the modified Griffith equation (Refs. 56,57):

$$\sigma = 1/Y \, [E \, (2 \, \gamma_1)/C]^{1/2} \tag{5}$$

where σ = fracture strength

Y = size factor ($\sim$2)

E = elastic modulus

γ_1 = surface energy

C = critical flaw size.

Table V

Room Temperature Bend Strengths after Various Thermal
Treatments of ZrO_2-Y_2O_3 Eutectic Directionally
Solidified at 10 cm/hr

Sample	Treatment	Bend Strength (ksi)	Average Strength (ksi)
59-3	As Made	23.2	26.3
60-3	As Made	29.3	
60-2	2 hrs at 1400°C	46.8	
59-2	2 hrs at 1400°C	30.6	
78-1	2 hrs at 1400°C	30.3	34.8
78-2	2 hrs at 1400°C	46.1	
79-1	2 hrs at 1400°C	23.3	
79-2	2 hrs at 1400°C	31.8	
45	2 hrs at 1400°C + 3 hrs at 1545°C	53.0	
56	2 hrs at 1400°C + 3 hrs at 1545°C	21.8	38.0
59-1	2 hrs at 1400°C + 3 hrs at 1545°C	39.0	

If we substitute $E = 16.6 \times 10^6$ lbs/in^2 (Ref. 51) and assume that γ_1 is of the order of 1000 ergs/cm^2, the critical flaw which would initiate fracture is about 1μ. One explanation for the insensitivity of strength to changes in inter-lamellar spacings may be that the critical flaw size is small with respect to the spacings obtained with this system, even at a solidification speed of 40 cm/hr.

The effect of temperature on the bend strengths of samples solidified at 40 cm/hr and then annealed for 2 hrs at 1400°C is shown in Fig. 54. These results may reflect the stability of the eutectic structure and/or the fact that this eutectic has a very high melting point. There was no indication from the machine traces of the stress-strain curves of any plastic yielding in any of these samples.

Fracture surfaces were examined with the optical and the scanning electron microscope. Figure 55 shows a selected area in which the surface is completely covered with steps or perturbations where the crack front was deflected by the presence of the lamellae. From cracks seen on edge in polished metallographic samples, it is clear that cracks always run in the Y_2O_3 phase, equidistant between the lamellae. When cracks run perpendicular to the plane of the lamellae, there is little, if any, perturbation in the fracture surface. An example of this is seen in Fig. 56 where the fracture has run vertically and the lamellae lie perpendicular to the fracture direction.

At elevated temperatures, evidence that the eutectic substructure deflected cracks was less evident. Figure 57 shows an area of the sample broken at 1500°C which indicates some effect and also that, in this particular sample, the initial lamellae were tending toward the rod-like form.

CaO·ZrO$_2$-ZrO$_2$ System

The CaO·ZrO$_2$-ZrO$_2$ system was of particular interest because of its high melting point (2300°C) and the fact that it solidified with a lamellar structure which might lend itself to crack blunting by delamination processes. Also, it has been reported that the similar compound SrO·ZrO$_2$ and solid solutions of CaO·ZrO$_2$ in SrO·ZrO$_2$ can be plastically deformed at room temperatures by a twinning process (Refs. 58,59). Both phases are cubic and the thermal expansion coefficients of the two phases are identical (Ref. 51) so therefore possible effects due to this variable should not be observed.

This eutectic always solidified in the lamellar form with the spacing between the lamellae being approximately 3μ when solidified at 10 cm/hr. The volume fraction of ZrO$_2$ as determined from optical photographs was 32 v/o which may be compared with 41 v/o as calculated from the published equilibrium phase diagrams.

Near the surface of the ingots and inward typically for about 1/8 in., relatively perfect lamellar eutectic microstructures were always obtained. Figure 58 shows an example of this microstructure in longitudinal section wherein the lamellae are parallel to the direction of solidification. Extensive areas of apparent twins are observed in the $CaO \cdot ZrO_2$ matrix phase, apparently resulting from the stresses generated during mechanical polishing.

The effect of solidification speed on flexural strength is presented in Fig. 59. The strength levels are relatively high for a ceramic and show only a slight tendency to increase at the higher rates of solidification. The fact that a Petch type dependency was not observed suggests either that the controlling flaws are smaller than the spacing or, more probably, that the strengths are being controlled by microstructure defects caused by poor solidification or compositional control. The effect of temperature on flexural strength is presented in Fig. 60. The strength is relatively unaffected by temperatures up to 1500°C. The strength value of 85,000 psi at 1450°C is probably indicative of the true potential of this material with optimum structure.

Despite considerable effort, eutectic ingots sufficient for the preparation of 0.25 x 0.25 in. square work-to-fracture bars could not be prepared with uniform eutectic microstructures throughout. One reason for this was that there was always some loss of CaO during the zone melting which made it difficult to hold the ingots to exact composition. The batch composition finally selected consisted of 24 w/o CaO with the rest ZrO_2. Near the centers of the ingots, the liquid-solid thermal gradients were not sufficiently high to produce comparable microstructures. Figure 61 shows a transverse view of this microstructure which contains eutectic colonies and dendrites. At least half of the fracture process in work-to-fracture samples prepared from these ingots and reported here, was through imperfect microstructures similar to those shown in Fig. 61.

Stable crack growth could be obtained in work-to-fracture experiments at room temperatures but the details on the fracture face were difficult to interpret because of the irregular nature of the crack faces and the nonuniform microstructures. There was no evidence of delamination between the two phases.

The effect of the eutectic microstructure on fracture was orientation dependent. In case 1, in which the direction of fracture was perpendicular to the plane of the lamellae, there was no observable interaction. In case 2, however, in which the normal to the lamellae is rotated in the plane of the fracture surface, there was noticeable interaction between the fracture path and the microstructure. In case 3, in which the normal to the lamellae is rotated out of the plane of fracture there was also interaction as shown in Fig. 62.

The force deflection curves obtained for several work-to-fracture samples at different temperatures are shown in Fig. 63. As can be seen, at 1500°C the force to propagate the crack is higher than at room temperature and a considerable amount of plasticity is observed. Figure 64 shows additional data and the dramatic increase in toughness that occurs in this material upon heating to temperatures above 1000°C. The energy required to propagate a crack through this material at 1500°C is approximately 28 times greater than that required at room temperature. Also shown in Fig. 64 are data for polycrystalline Al_2O_3. At 1500°C this material comes apart at grain boundaries and is relatively weak.

The fracture surfaces and the work-to-fracture energy at 1000°C were similar to those obtained at room temperature. Figure 65 shows how the fracture path for case 2 can be affected by the eutectic microstructure at 1000°C.

Examination of the fracture surfaces obtained at 1500°C, as shown in Fig. 66, support the view that at these temperatures the eutectic behaves in a typical composite manner with the more ductile $CaO \cdot ZrO_2$ matrix being reinforced by the stronger ZrO_2 phase. Energy is absorbed in deforming the more ductile calcium zirconate phase and in the shear processes involved in pulling the ZrO_2 phase out of this matrix. Figure 67 shows the partially extracted ZrO_2 phase in more detail. The ZrO_2 phase when removed from the matrix has begun to spheroidize by surface diffusion processes. A similar even more extreme example of this process was observed in the Al_2O_3-ZrO_2 (Y_2O_3) eutectic at similar temperatures (Fig. 44).

Figure 68 shows a polished section through a sample only partially fractured at 1630°C. The fracture path is discontinuous and is associated primarily with growth faults in the lamellar structure. Examples can also be seen, as indicated by the arrows, where cracks which were opened in the calcium zirconate matrix have been stopped by the ZrO_2 lamellae. Fracture in this material is not dictated by the weakness at grain boundaries or by the rapid propagation of fracture through a brittle crystal. Instead the material behaves in the classic composite manner wherein a relatively strong minor phase (ZrO_2) reinforces a weaker ductile matrix phase.

MgO-CaO System

The MgO-CaO system was chosen for study primarily as a model of an oxide eutectic containing two very ductile phases. The melting point of the eutectic is 2300°C and both phases are cubic (NaCl structure). Because of the tendency of the CaO phase to hydrate this eutectic cannot generally be considered as a practical engineering material.

In this eutectic system, there is fortunately a considerable background of information about the mechanical properties of the constituent phases. In both phases, the primary slip system is {110} <1$\bar{1}$0> with slip also possible on the secondary {001} <1$\bar{1}$0> slip system. MgO single crystals compressed along the [001] deform by the primary slip system and are capable of about five percent plastic strain at temperatures down to the boiling point of liquid nitrogen. CaO yields at lower stresses and is more ductile than MgO. One of the authors has measured the stresses necessary to cause plastic yielding on the two types of slip systems in both kinds of single crystals and these data are shown in Figs. 69 and 70 (Refs. 60,61).

For purposes of comparison, a normal stress applied along a [001] direction results in a resolved shear stress on the {110} <1$\bar{1}$0> system which is one-half of the normal stress. A normal stress applied along a [111] direction results in a resolved shear stress on the [001] <1$\bar{1}$0> slip system which is 0.472 times the normal stress. In order to satisfy the requirements for true polycrystalline ductility, dislocation motion must occur at similar stress levels on both the primary and secondary slip systems. This requirement is satisfied for CaO above about 1000°C while for MgO temperatures of the order of 2000°C are needed.

In the MgO-CaO eutectic system, CaO is the matrix phase and the MgO solidifies either as rods or as plates. Figure 71 shows a transverse micro-structure with both modes of solidification. X-ray examination revealed that both phases solidify with a [111] direction parallel to the direction of solidification. Unfortunately, this is the one unique direction along which application of a normal stress does not result in a resolved shear stress on any of the six possibilities in the {110} <1$\bar{1}$0> primary slip system. Thus, plastic flow in this eutectic due to stresses applied in the direction of maximum strength, which is parallel to the direction of solidification, will only occur by motion of dislocations on the secondary {001} <1$\bar{1}$0> slip system. As can be seen from Figs. 69 and 70, these stresses are high. For example, at room temperature stress levels of ~120,000 and ~600,000 psi would be required for plastic flow in the CaO and MgO phases, respectively, even in a very coarse microstructure.

Because of the volatility of both phases, especially the CaO, at temperatures above 2300°C it was difficult to maintain the eutectic composition. In order to minimize this problem, excess CaO was added and attempts were made to process each sample through exactly the same sequence of melting steps. All runs were made at 20 cm/hr. Despite these efforts, the microstructures obtained were relatively poor. Figure 72 shows the microstructure present in a typical bend sample, in which colonies and dendrites can be seen. Figure 73 shows bend strengths at various temperatures. The strength levels are not exceptional and this is probably due at least in part to the poor quality of the microstructures.

The controlled solidification of good structure in 3/8 in. diameter ingots suitable for the preparation of work-to-fracture specimens was more difficult. The microstructures were especially poor near the centers of the ingots. Figure 74 shows a transverse microstructure and the presence of dendrites and voids. Despite the quality of the microstructure, high values for the energy to propagate a crack through this material were observed, particularly at temperatures above 1000°C. This data is shown in Fig. 75 with comparison data for polycrystalline alumina. The value given at 1550°C should be much higher than is shown because there was a considerable amount of reaction and melting at the center sapphire loading pin. Thin platinum foil spacers were used to prevent reactions at the end supports which rested on polycrystalline alumina.

An explanation for the increase in work-to-fracture energies at the higher temperatures can be deduced by examination of the fracture surfaces and from the known critical stresses for yielding in the single crystals shown in Figs. 69 and 70. Below 1000°C, little or no interaction of the fracture path with the microstructure was observed. Figure 76 shows an example of a fracture surface at 1000°C where no interaction is seen for a crack moving perpendicular to the plane of the lamellae. From the strength data shown in Fig. 73 and the critical normal stress for yielding in the [111] shown in Fig. 69, yielding in the softer CaO phase would not be expected below about 600°C even without the presence of the MgO reinforcement.

Examination of fracture surfaces produced at 1250°C indicate that the CaO matrix phase is yielding plastically and that the MgO phase is not as would be expected. Figures 77 and 78 show examples of lamellar and rod-like fracture surfaces produced at 1250°C. In Fig. 78 the round MgO whiskers have been pulled from the matrix and broken without apparent necking. The arrow in Fig. 78 indicates a brittle fracture in the MgO where both parts of the crystal still remain.

Figures 79 and 80 show fracture surface detail for both rod and lamellar microstructures at 1550°C. The pullout of the whiskers is more extensive and for the lamellar case the completely ductile CaO phase can be pulled down to a knife edge after the MgO lamellae break. The arrows in Fig. 80 indicate sharp wedges of CaO between the lamellae. In other areas the CaO wedges have apparently been broken away.

SUMMARY AND CONCLUSIONS

In a review of research directed toward the development of ceramics with optimum mechanical properties, it is pointed out that little effort has been directed toward melt formed ceramic microstructures and that the highest potential probably rests with directionally solidified eutectic composites. The most important special mechanisms and qualities which should lead to improved properties in eutectics include: (1) the elimination of dissolved gases and pores, (2) the presence of a fine uniform microstructure which can limit the size of critical flaws, (3) the effect of the structure in blocking the motion of dislocations, (4) the possibility of prestressing the matrix in compression, (5) the presence of a dispersed phase which may possess the strength properties characteristic of whiskers, and (6) the ability in certain systems to delaminate as a means for retarding crack propagation and/or initiation.

Because casting from the melt and, in particular, controlled directional solidification are unusual methods of forming ceramic materials, a considerable investigation was made in search of the optimum experimental technique. In order to prepare ingots with constant liquid-solid thermal gradients independent of ingot length, a modified Bridgman-Starkbarger technique was developed which involved water quenching one end of a refractory oxide containment tube inside a furnace. Problems with ingot porosity were overcome by creation of a vacuum over the melt prior to solidification or by insertion of an inert high frequency probe into the melt. It was difficult to form perfect microstructures and to avoid the presence of colonies using this approach apparently because of a slight impurity pick-up from the containers and too low a liquid-solid thermal gradient.

Demonstration experiments in which melts were held in platinum crucibles and cooled from the bottom illustrated that the poor thermal conductivity of the solidified ingot quickly lowered the liquid-solid thermal gradients to unacceptable values. After one inch of solidification the gradient in the $BaWO_4-WO_3$ eutectic system was only 17°C/cm.

It was concluded that the floating molten zone technique was the best solidification approach because high liquid-solid thermal gradients are created which are constant independent of ingot length. For melting temperatures up to 1700°C the best zone heating arrangement consisted of precious metal strip heaters or immersion wire heaters in direct contact with the melt. At higher temperature the best zone heating technique evolved consisted of an insulated carbon ring susceptor in an R.F. field in an atmosphere of argon.

Two modifications of the floating molten zone technique are described which allowed preparation of ingots with diameters of at least one inch. Another successfully demonstrated variation permitted the directional solidification of plate shapes.

The Al_2O_3-ZrO_2 (Y_2O_3) eutectic forms with the C-axis of the Al_2O_3 matrix and the $[1\bar{1}0]$ axis of the stabilized ZrO_2 whiskers parallel to the direction of solidification. Colony microstructures were formed at all solidification speeds greater than ~0.8 cm/hr. The flexural strength for this eutectic solidified at 20 cm/hr with an after heater ranged from 100,000 psi at room temperature to 74,000 psi at 1575°C. Work-to-fracture energies varied from 0.93×10^5 ergs/cm² at room temperature to 1×10^5 ergs/cm at 1500°C. During fracture at 1500°C, the ZrO_2 whiskers apparently continue to connect between the fracture faces after the Al_2O_3 matrix fails. Subsequently, the deformed whiskers break at one of the faces and the stub spheroidizes into a faceted ball.

The microstructure of the ZrO_2-Y_2O_3 eutectic is lamellar and occurs at 10.2 w/o ZrO_2. Room temperature bend strengths were independent of solidification speed at rates from 1.5 to 40 cm/hr (interlamellar spacings from 8.5 to 2.4μ). This independence may reflect the presence of critical flaws resulting from poor eutectic microstructures and/or stresses created during ingot fabrication or sample preparation. The critical flaw size was estimated to be the order of the smallest spacing produced. The bend strength was approximately 38,000 psi and essentially independent of temperature up to 1500°C. Fracture surfaces, particularly those created at room temperatures, contained extensive areas of uniform steps indicating that the propagation of cracks was affected by the presence of the eutectic microstructure.

The fracture behavior of the $CaO \cdot ZrO_2$-ZrO_2 eutectic (m.p. 2300°C) directionally solidified at 10 cm/hr was studied using the work-of-fracture technique and detailed examinations of the fracture surfaces. Below 1000°C, the lamellar structure appeared to have only a minor effect on the path of fracture when the direction of crack propagation was exactly perpendicular to the lamellae. There were usually appreciable effects for all other orientations. Above 1000°C, the eutectic behaved in the classic composite manner wherein a relatively strong minor phase (ZrO_2) reinforces a weaker ductile matrix phase. The energy required to propagate a slow moving crack through this microstructure increased by a factor of 28 from room temperature to 1500°C (0.44 to 11.4 $\times 10^5$ ergs/cm²). The flexural strength of this eutectic was approximately 48,000 psi independent of temperature up to 1600°C and independent of solidification speed over the range from 3 to 40 cm/hr.

The CaO-MgO eutectic can solidify with either a rod-like or lamellar microstructure. Both phases form with their [111] direction parallel to the direction of solidification. The microstructures of ingots prepared in this program were relatively poor, primarily because of the high volatility of both of the constituent phases. The flexural strengths varied from 25,000 psi at room temperatures to 35,000 psi at 1500°C. The work-to-fracture energies varied from 0.8×10^5 erg/cm^2 at room temperatures to 11.0×10^5 ergs/cm^2 at 1500°C. The dramatic increase in work-to-fracture energies at elevated temperatures reflects a property of this type of microstructure in which a ductile matrix phase (CaO) is reinforced by a strong whisker phase (MgO).

Considering all of the strength data, it is clear that the preparation of oxide materials as directionally solidified eutectics can result in new materials with exceptional mechanical properties.

ACKNOWLEDGEMENTS

REFERENCES

1. C. Hulse and J. Batt, "The Effect of Eutectic Microstructures on the Properties of Ceramic Oxides", Tech. Rept. J910803-3, United Aircraft Corp., Feb. 1970.

2. C. Hulse and J. Batt, "Effect of Eutectic Microstructures on the Properties of Ceramic Oxides", Tech. Rept. K910803-5, United Aircraft Corp., May 1971.

3. C. Hulse and J. Batt, "The Effect of Eutectic Microstructures on the Mechanical Properties of Ceramic Oxides", Tech. Rept. L910803-7, United Aircraft Corp., June 1972.

4. C. Hulse and J. Batt, "Preparation of Ceramic Eutectics by the Floating Molten Zone Technique", Symposium Advanced Materials: Composites and Carbon, Pub. Amerc. Ceram. Soc., pp 133-141 (1972).

5. C. Hulse and J. Batt, "Preparation and Properties of Directionally Solidified $ZrO_2-Y_2O_3$ Eutectic", Proceedings of the Conference on In Situ Composites, Sept. 5-8, 1972, Lakeville, Con·., NMAB 308I, Jan. 1973, pp 129-140.

6. C. Hulse and J. Batt, "Fracture of Directionally Solidified $CaO \cdot ZrO_2-ZrO_2$ Eutectic", Fracture Mechanics of Ceramics, Vol. 2, edited by R. C. Bradt, D. P. H. Hasselman, and F. F. Lange, Plenum Pub. Corp., pp 483-494.

7. R. Rice, "Transparent Crystalline Ceramics", presented at Annual Meeting Am. Ceram. Soc., April 1972, Washington, D.C.

8. J. Stravrolakis and F. Norton, "Measurement of the Torsion Properties of Alumina and Zirconia at Elevated Temperatures", J. Am. Ceram. Soc., 33, pp 263-68 (1950).

9. A. Paladino and R. Coble, "Effect of Grain Boundaries on Diffusion Controlled Processes in Aluminum Oxide", J. Am. Ceram. Soc., 46, pp 133-136 (1963).

10. F. VerSnyder and M. Shank, "Development of Columnar Grain and Single Crystal High Temperature Materials through Directional Solidification", Mater. Sci. Eng., 6, pp 213-247 (1970).

11. F. Lemkey and M. Salkind, "The Growth and Properties of Carbide Whisker-Reinforced Refractory Metals from the Melt", Crystal Growth, Pergamon Press, Oxford, p 171 (1967).

12. E. Thompson and F. George, "Eutectic Superalloys", SEE Paper No. 690689 (1969).

13. R. Hertzberg, F. Lemkey, and J. Ford, "Mechanical Behavior of Lamellar ($Al-CuAl_2$) and Whisker Type ($Al-Al_3Ni$) Unidirectionally Solidified Eutectic Alloys", Trans. AIME, Vol. 233, pp 342-54 (1965).

14. F. Lange, "Effect of Microstructure on Strength of Si_3N_4-SiC Composite System", J. Am. Ceram. Soc., 56, pp 445-450 (1973).

15. Y. Nivas and R. Fulrath, "Limitation of Griffith Flaws in Glass-Matrix Composites", J. Am. Ceram. Soc., 53, pp 188-191 (1970).

16. C. Hulse and B. Jacob, "Fiber Prestressed and Reinforced Ceramics", Tech. Rept. F110326-1, United Aircraft Corp., (1967).

17. E. Thompson, E. Kraft, and F. George, "Investigation to Develop a High Strength Eutectic for Aircraft Engine Use", Tech. Rept. J910803-4, United Aircraft Corp., July 1970.

18. B. Bayles, J. Ford and M. Salkind, "The Effect of Elevated Temperature Exposure on the Microstructure and Tensile Strength of Al_3Ni Whisker Reinforced Aluminum", Trans. AIME, Vol. 239, p 844 (1967).

19. F. Galasso, W. Darby and F. Douglas, "Unidirectional Solidification of the $BaFe_{12}O_{19}$-$BaFe_2O_4$ Eutectic", J. Am. Ceram. Soc., 50, pp 333-334 (1967).

20. D. Harrison, "Lamellar Glass-Crystal Structures in the System $ZnO-B_2O_3$", J. Crystal Growth, 4, pp 674-678 (1968).

21. D. Rowcliffe, W. Warren, W. Elliot and W. Rothwell, "The Growth of Oriented Ceramic Eutectics", J. Mat. Sci., 4, pp 902-907 (1969).

22. D. Viechnicki and F. Schmid, "Eutectic Solidification in the System Al_2O_3-$Y_3Al_5O_{12}$", J. Mat. Sci., 4, pp 84-88 (1969).

23. F. Schmid and D. Viechnicki, "Oriented Eutectic Microstructures in the System Al_2O_3-ZrO_2", J. Mat. Sci., 5, pp 470-473 (1970).

24. F. Schmid and D. Viechnicki, "Ceramic Eutectics", Tech. Rept. AMMRC TR 72-8, Army Materials and Mechanics Research Center (1972).

25. F. Schmid and D. Viechnicki, "Mechanical Properties of Eutectics in the $Al_2O_3-ZrO_2-Y_2O_3$ System", presented at the Annual Meeting of the American Ceramic Society, Washington, D.C., Apr 1 1972.

26. F. Schmid and D. Viechnicki, "Seeding and Growth of Large Eutectic Ingots", Proceedings of the Conf. on In Situ Composites, Lakeville, Conn., Sept. 1972, National Academy of Sciences Printing Office, Washington, D.C.

27. F. Kennard, R. Bradt and V. Stubican, "Eutectic Solidification of MgO-$MgAl_2O_4$", J. Am. Ceram. Soc., 56, pp 566-569 (1973).

28. F. Kennard, "Directional Solidification of High Temperature Eutectics", Ph.D. Thesis, Pennsylvania State University, Dec. 1973.

29. F. Kennard, R. Bradt and V. Stubican, "Directional Solidification of ZrO_2-MgO Eutectic", Submitted to J. Am. Ceram. Soc. (1974).

30. J. Spiers, "Eutectic Solidification in Some Oxide Systems", B.S. Thesis, Pennsylvania State University, June 1973.

31. P. Nelson and J. Rasmussen, "Composite Solidification in Systems Cr_2O_3-Mo, Cr_2O_3-Re, Cr_2O_3-W, and MgO-W", J. Am. Ceram. Soc., 53, p 527 (1970).

32. A. Chapman, G. Clark and D. Hendrix, "UO_2-W Cermets Produced by Unidirectional Solidification", J. Am. Ceram. Soc., 53, p 60 (1970).

33. P. Hart, "New Class of Ceramic Composites", Ceramic Age, p 29 (1972).

34. T. Johnson and J. Benzel, "Unidirectional Solidification of Stabilized HfO_2-W", J. Am. Ceram. Soc., 56, p 234 (1973).

35. N. Claussen, "Hot-Pressed Eutectics of Oxides and Metal Fibers", J. Am. Ceram. Soc., 56, p 442 (1973).

36. Contract N00019-74-C-0271, Naval Air Systems Command to United Aircraft Research Laboratories, Feb. 1974.

37. M. Watson, T. Johnson, J. Benzel and A. Chapman, "Unidirectional Solidification of Tungsten in Stabilized Zirconia and Hafnia," Proceedings of the Conference on In Situ Composites, Lakeville, Conn., Sept. 1972, National Academy of Sciences Printing Office, Washington, D.C.

38. P. Hart, "Observations on Oxide-Metal Eutectic Systems", Proceedings of the Conference on In Situ Composites, Lakeville, Conn., Sept. 1972.

39. M. Bright and M. Lewis, "Controlled Solidification of the Eutectic LiF-MgF$_2$", J. Mat. Sci., 6, pp 1012-1020 (1971).

40. J. Batt, F. Douglas and F. Galasso, "Optical Properties of Unidirectionally Solidified NaF-NaCl Eutectic", Ceram. Bull., 48, pp 622-626 (1969).

41. F. Galasso, F. Douglas and J. Batt, "Recent Studies of Eutectics for Nonstructural Applications", J. of Metals, pp 3-7 (1970).

42. J. Moore and L. Van Vlack, "Some Properties of Eutectic Crystals of MnO-MnS", Anisotropy in Single-Crystal Refractory Compounds, Vol. I, pp 299-315, Plenum Press (1968).

43. F. Carpay and W. Cense, "In Situ Growth of Aligned Composites from the Vitreous State. The Li$_2$O-B$_2$O$_3$ System", Scripta Metallurgica, 8, pp 11-14 (1974).

44. G. Chadwick, J. Inst. Metals, 91, p 169 (1963).

45. B. Chalmers, Principles of Solidification, J. Wiley & Sons, 1964.

46. W. Tiller and J. Rutter, Can. J. Phys., 34, p 96 (1956).

47. J. Hunt and K. Jackson, Trans. Met. Soc. AIME, 236, p 843 (1966).

48. U. S. Patent 3,471,266, Oct. 1969.

49. L. Simpson, J. Am. Ceram. Soc., 56, p 7 (1973).

50. J. Coppola and R. Bradt, J. Am. Ceram. Soc., 55, p 455 (1972).

51. J. Lynch, C. Ruderer, and W. Duckworth, "Engineering Properties of Selected Ceramic Materials", Pub. Am. Ceram. Soc. (1966).

52. Technical Literature, Norton Co. (1972).

53. "High Temperature High Strength Nickel Base Alloys", The International Nickel Co., Inc., New York, N. Y. (1964).

54. E. Levin, C. Robbins and H. McMurdie, Phase Diagrams for Ceramists, Pub. Am. Ceram. Soc. (1964).

55. P. Duwez, F. Brown and F. Odell, "The Zirconia-Yttria System", <u>J. Electro. Chem. Soc.</u>, 98, p 356 (1951).

56. R. Davidge and G. Tappin, "The Effects of Temperature and Environment on the Strength of Two Polycrystalline Aluminas", <u>Proc. Brit. Ceram. Soc.</u>, 15, p 47 (1970).

57. W. Brown and J. Srawley, "Plain Strain Crack Toughness Testing of High Strength Metallic Materials", ASTM Spec. Tech. Publ. No. 410 (1967).

58. J. Tinklepaugh, Twelfth Sagamore Army Mat. Res. Conf. (1965).

59. J. Funk, Graduate Thesis, Alfred Univ. (1964).

60. C. Hulse, "Mechanical Properties of CaO Single Crystals", Accepted for pub. J. Am. Ceram. Soc.

61. C. Hulse, "Plastic Anisotropy of MgO and Other NaCl Type Crystals", <u>Anisotropy in Single Crystal Refractory Compounds</u>, pp 307-319, Vol. II, Plenum Press (1968).

FIG. 1

TENSILE STRENGTH OF Ni₃Al–Ni₃Cb EUTECTIC AS A FUNCTION OF TEMPERATURE AND (INTERLAMELLAR SPACING)^{-½}

INTERLAMELLAR SPACING, λ – MICRONS

$\lambda^{-½}$ – MICRONS $^{-½}$

5-2
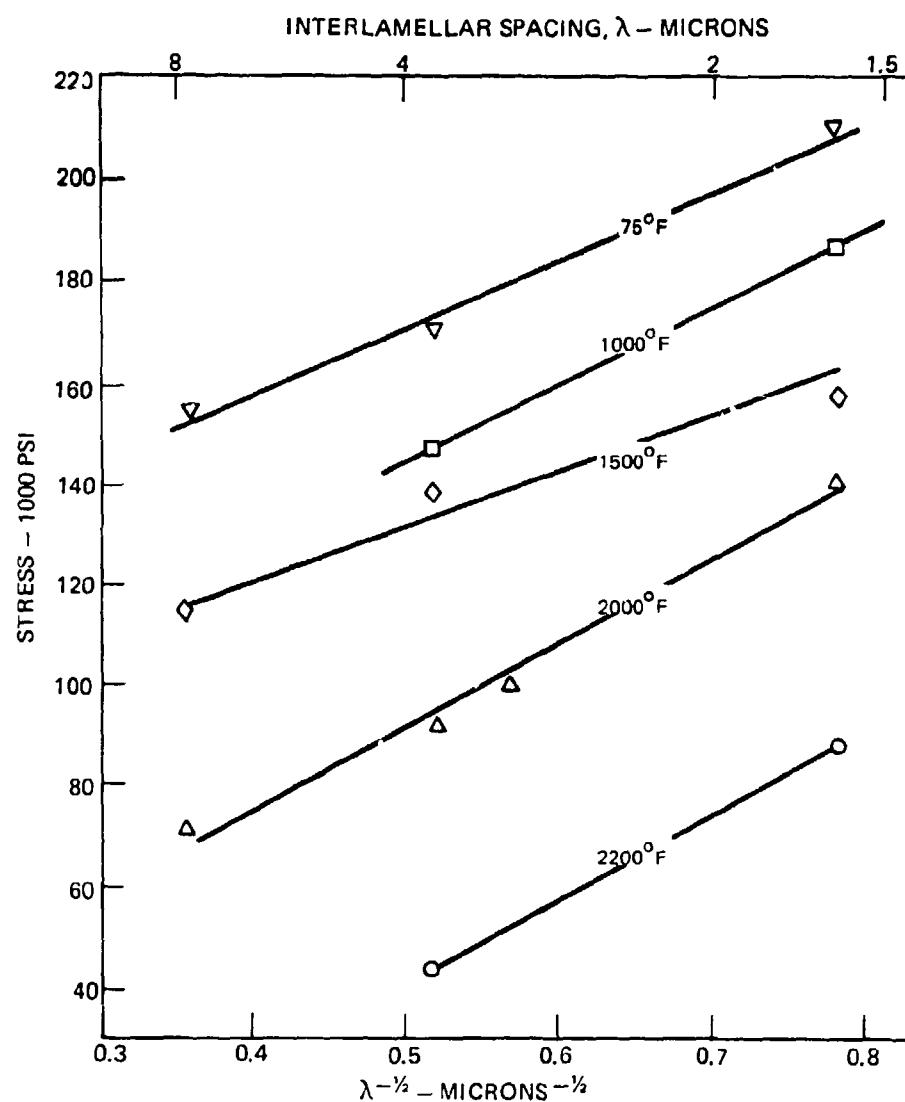
FIG. 2

NON-PROPAGATING CRACKS GENERATED IN FATIGUE SPECIMEN OF $Ni_3Al - Ni_3Cb$ TESTED AT $\pm$ 135 KSI

20_μ

FIG. 3
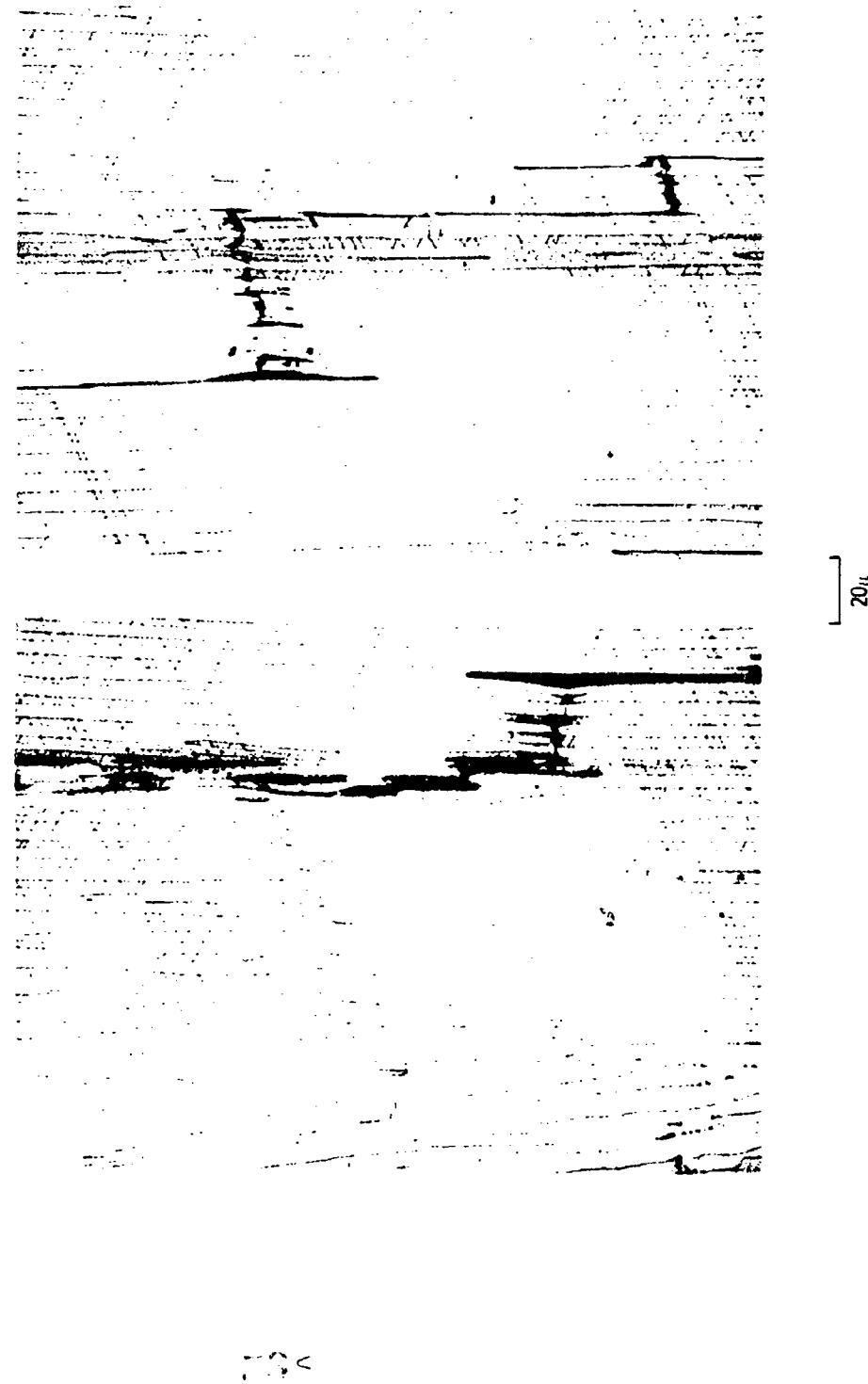
MODIFIED BRIDGMAN-STARKBARGER FURNACE FOR UNIDIRECTIONAL SOLIDIFICATION OF EUTECTICS

(VERTICAL SECTION VIEW)

Al_2O_3 TUBE

CONTROL THERMOCOUPLE

KANTHAL A-1 WIRE FURNACE

LIQUID-SOLID INTERFACE IN INGOT

COPPER WASHER

POROUS OXIDE BAFFLE RING

H_2O

Pt-Rd WIRE FURNACE

H_2O

H_2O

CIRCULAR WATER TANK

SUPPORT BRACKET FROM TRANSVERSE MECHANISM

FIG. 4
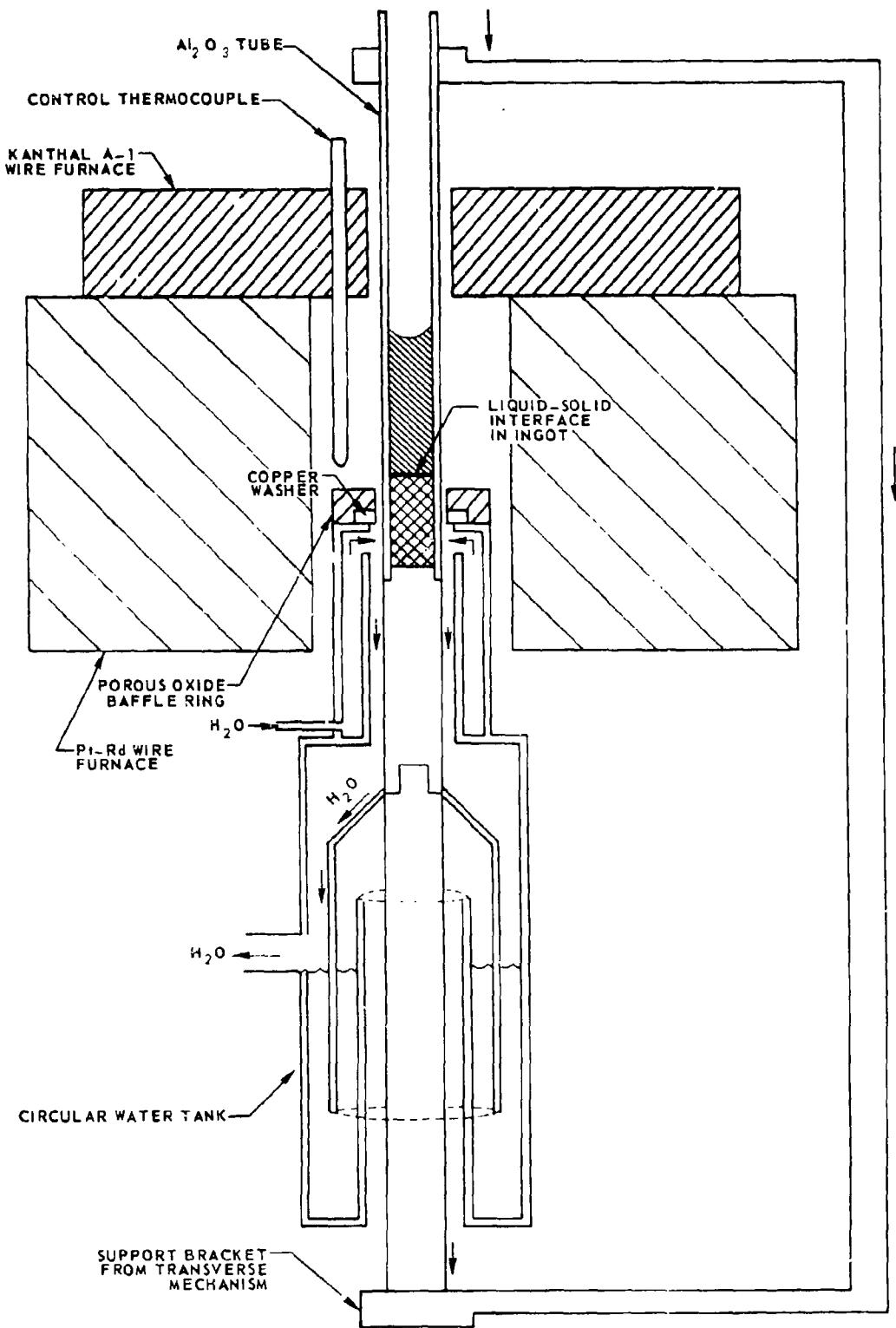
ALUMINA TUBE ASSEMBLY AND VIBRATING PROBE

VIBRATOR

WINDOW OR PROBE ENTRY

GAS OR VACUUM INLETS

ALUMINA PROBE

SEALED COPPER PLUG

FIG. 5
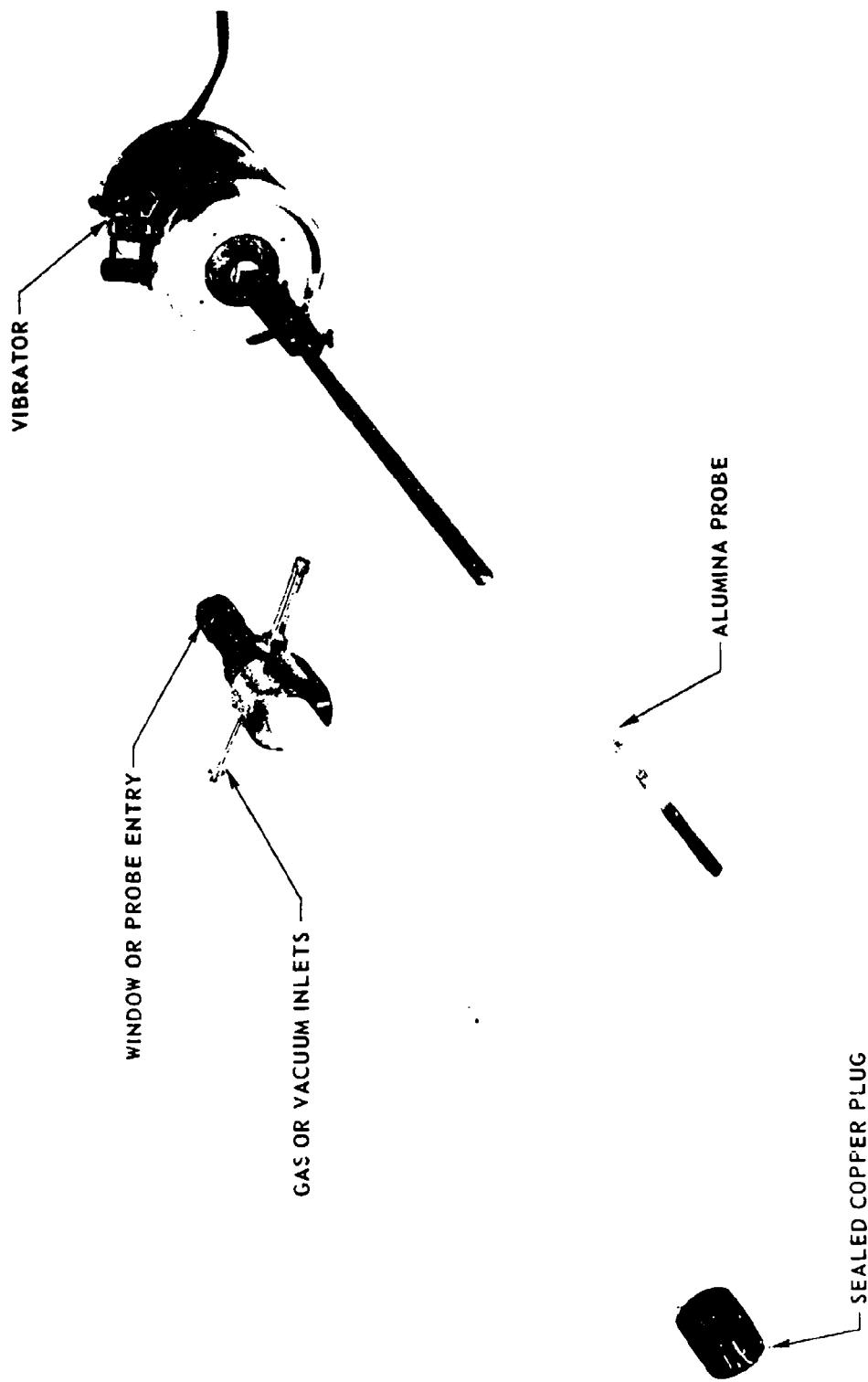
EUTECTIC INGOTS OF $Bi_2O_3 - Bi_2O_3 \cdot Fe_2O_3$ SOLIDIFIED UNDER VARIOUS CONDITIONS

A—AIR

B—EVACUATED, BACK FILLED WITH OXYGEN

C—VIBRATING PROBE, AIR

D—WITH LAYER OF PT FOIL BETWEEN MELT AND ALUMINA, EVACUATED, BACK FILLED WITH OXYGEN

RL-70-26-B
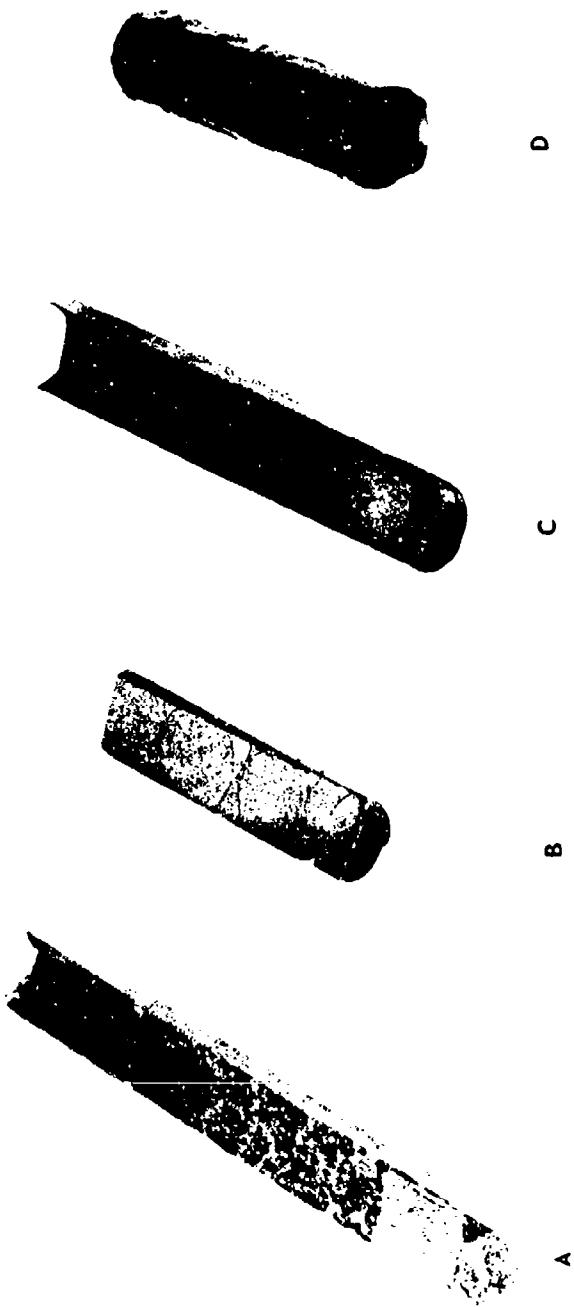
INITIAL FURNACE UNIDIRECTIONAL SOLIDIFICATION OF DISCS OF OXIDE EUTECTICS
(VERTICAL SECTION VIEW)

FIXED WIRE SUPPORT

REFRACTORY PLUG

SIC RESISTANCE TUBE HEATER

FURNACE
INSULATION

MELT

Al_2O_3 INSULATION PLATE

WATER COOLED POST
CONNECTED TO CONTROLLED
TRANSVERSE MECHANISM

H_2O

H_2O

57<

N05–221–1

FIG. 7
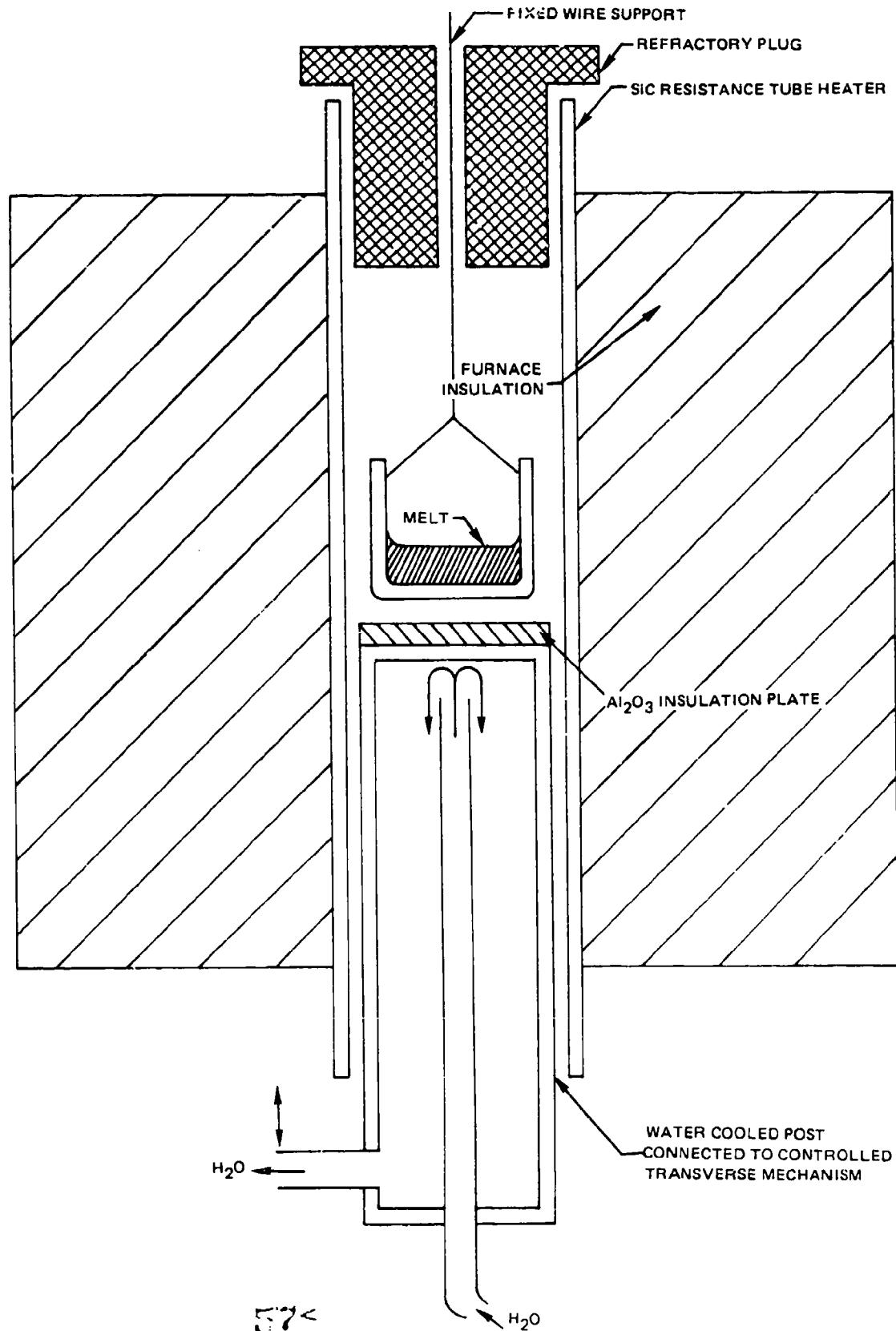
GLOBAR HEATED FURNACE FOR UNIDIRECTIONAL SOLIDIFICATION OF OXIDE EUTECTICS

(VERTICAL SECTION VIEW)

WINDOW OR THEROMOCOUPLE PROBE ENTRANCE

VACUUM OR CONTROLLED ATMOSPHERE PORT

Al_2O_3 TUBE

INSULATION

GLOBAR HEATER

FURNACE INSULATION

CRUCIBLE WITH MELT

CONTROL THERMOCOUPLE

CERAMIC PEDASTAL

CROSSHEAD SUPPORTED WITH MOVEABLE SCISSOR JACK (NOT SHOWN)

HEIGHT OF COOLING PROBE, ADJUSTABLE THROUGH VACUUM FITTING

H_2O

H_2O

BALL BUSHING (BOTH SIDES)
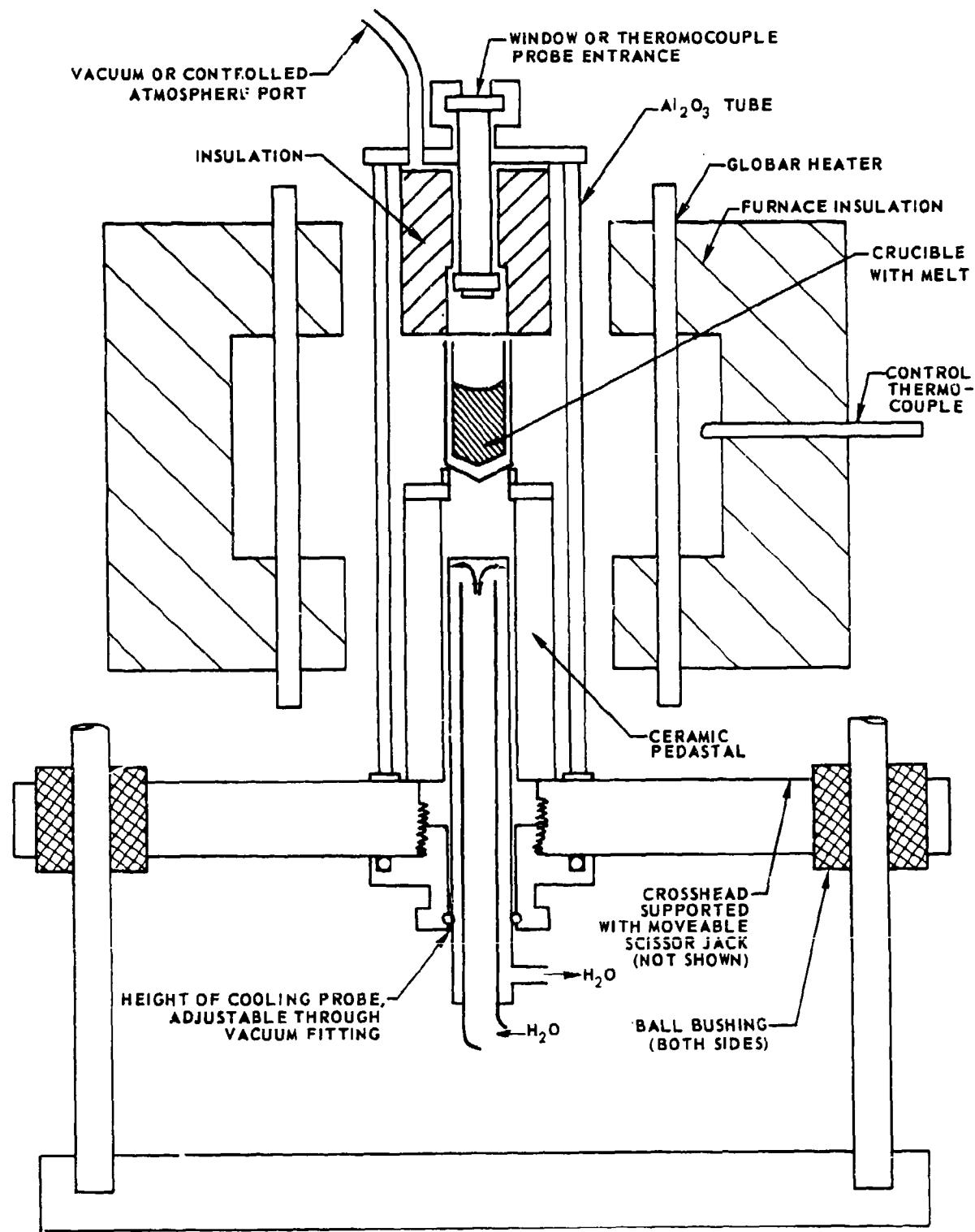
PICTURES OF INGOTS SOLIDIFIED IN COMPOSITE MULLITE-PLATINUM CRUCIBLE
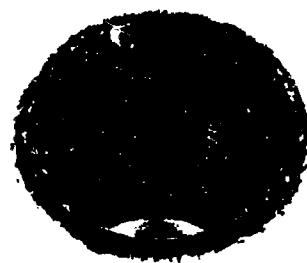
CRUCIBLE

TiO_2 WHISKERS IN
$SiO_2-B_2O_3-Na_2O$ GLASS

$Bi_2O_3 - Fe_2O_3$ EUTECTIC

FIG. 9

LIQUID–SOLID THERMAL GRADIENTS IN BaWO$_4$–WO$_3$ EUTECTIC WITH BOTTOM COOLING
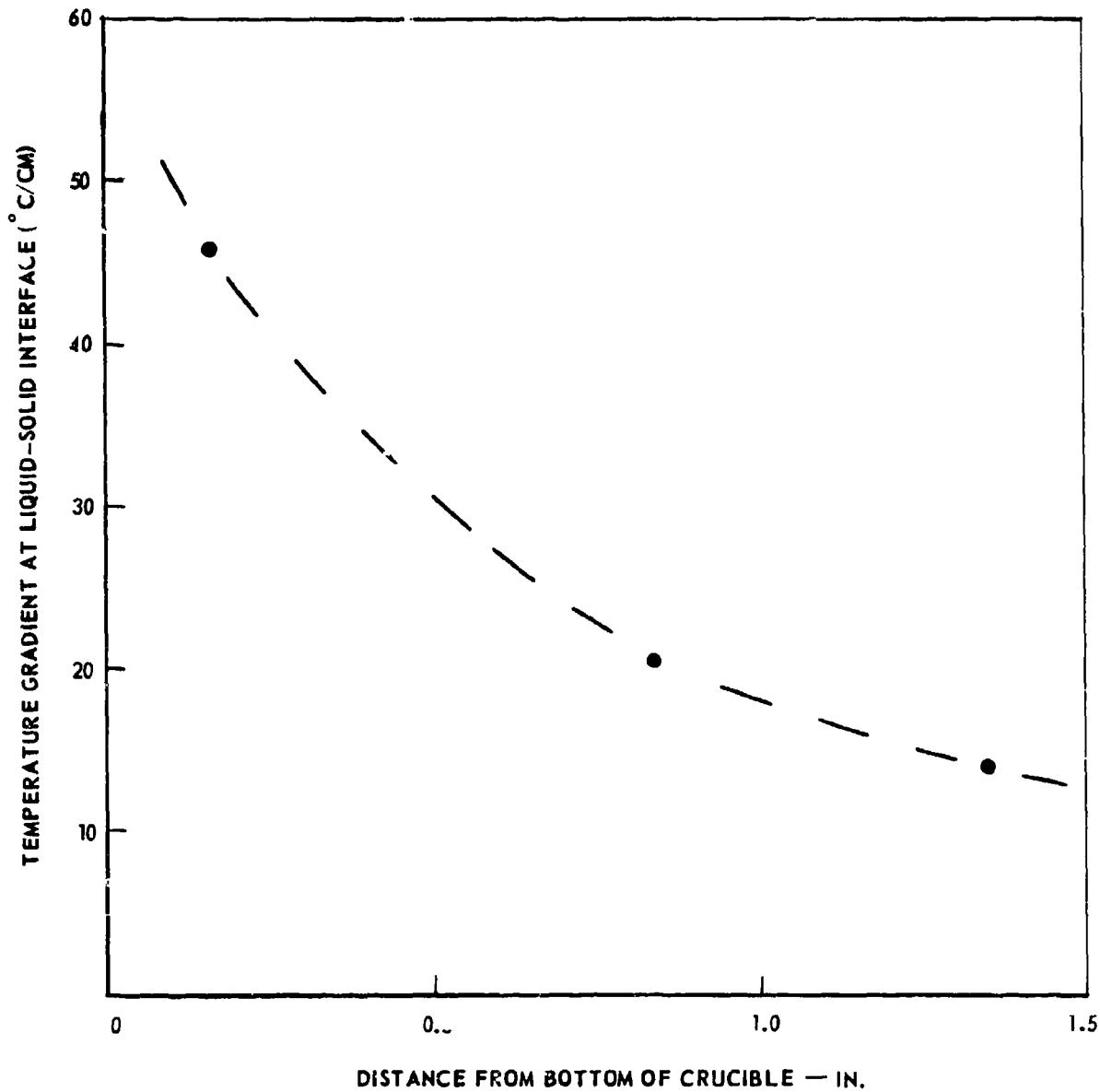
FIG. 10

FLOATING—ZONE TEMPERATURE PROFILE
$PbO-3PbO \cdot Nb_2O_5$ EUTECTIC

S.S. SHIELDED CHROMEL—ALUMEL THERMOCOUPLE (0.040 IN. DIA.)

CENTERED IN 0.25 IN. DIA. ROD, 10 CM/HR

61<

FIG. 11
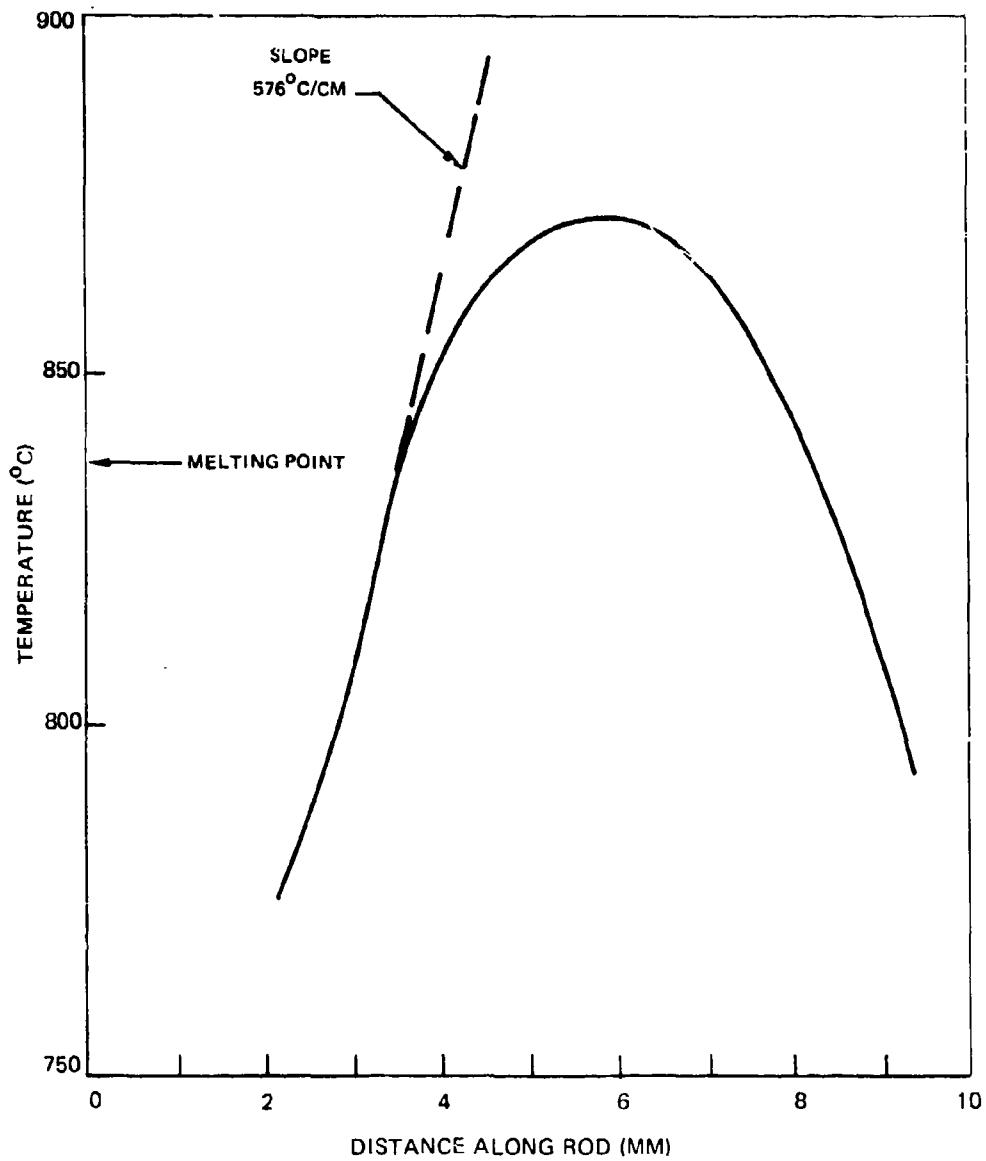
PLATINUM OR IRIDIUM STRIP HEATER FOR FLOAT ZONE EUTECTICS

Pt TABS

A

A

SOLID EUTECTIC

SIDE VIEW

MELT

2 MIL STRIP HEATER

TACK WELDS

TOP VIEW THROUGH MELT
(SECTION A–A)

FIG. 12
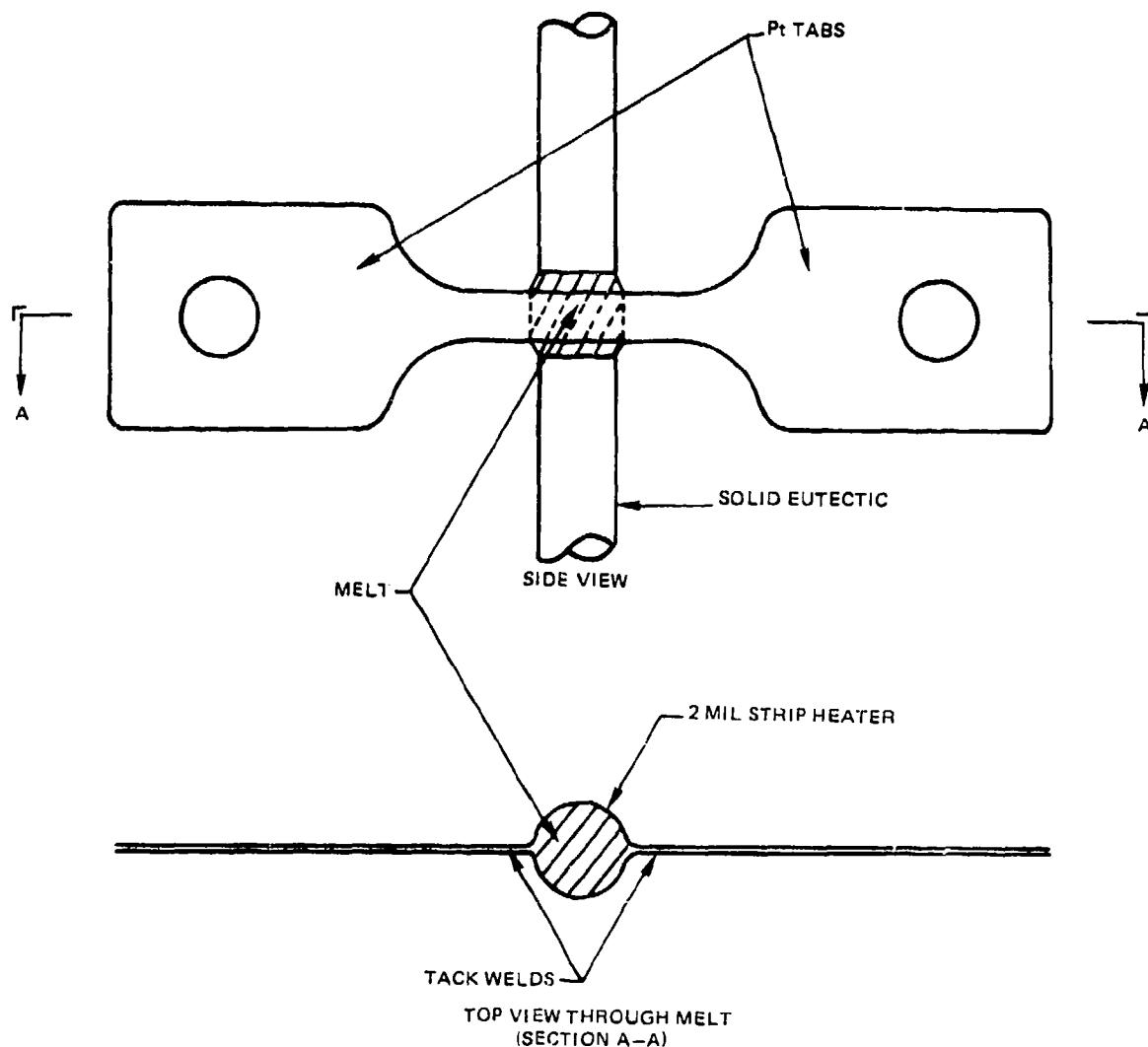
WIRE IMMERSION HEATER FOR FLOAT ZONE EUTECTICS

Pt TABS

MELT

SIDE VIEW

SOLID EUTECTIC

Pt OR Ir WIRE HEATER

TOP VIEW THROUGH MELT (SECTION A–A)

FIG. 13
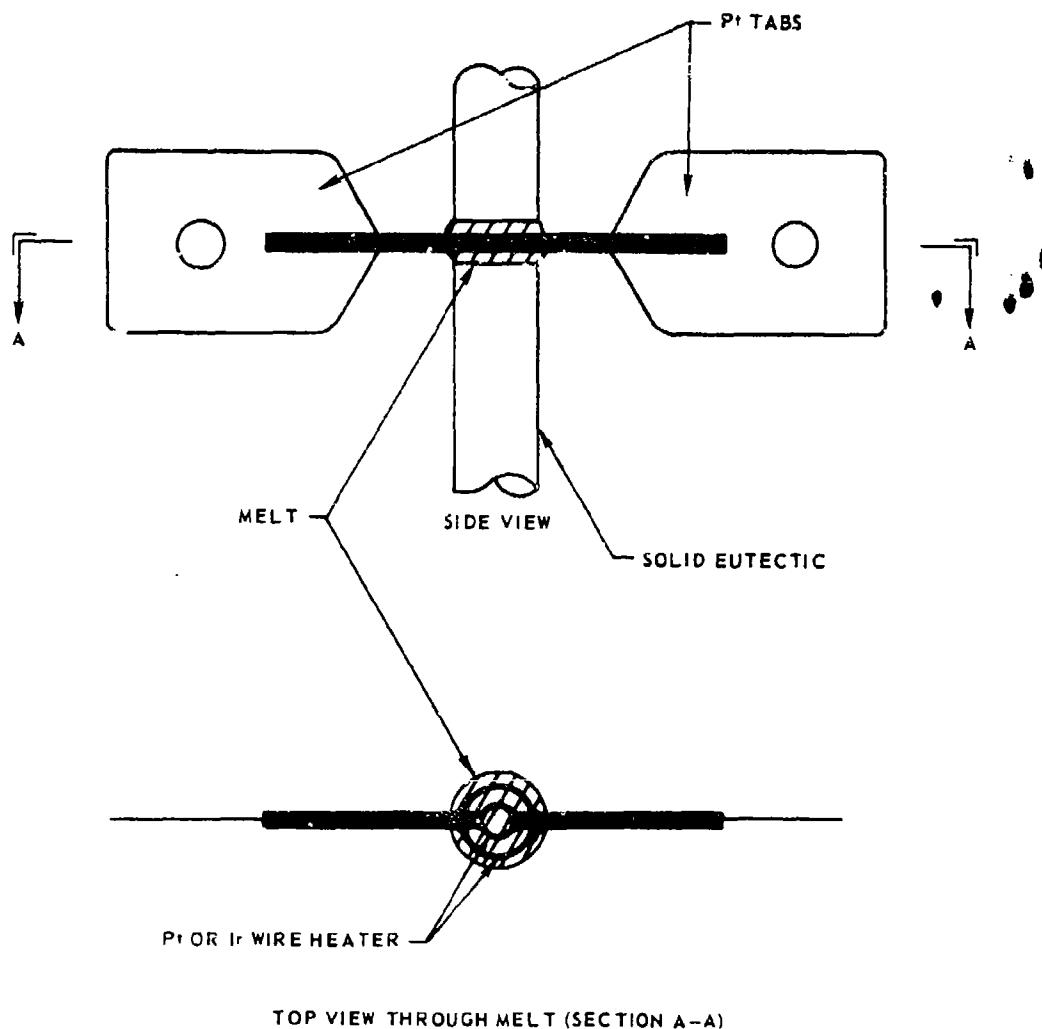
TUNGSTEN HEATER FOR ZONE MELTING OF EUTECTIC RODS

SIDE VIEW, VERTICAL CENTER SECTION

FIG. 14
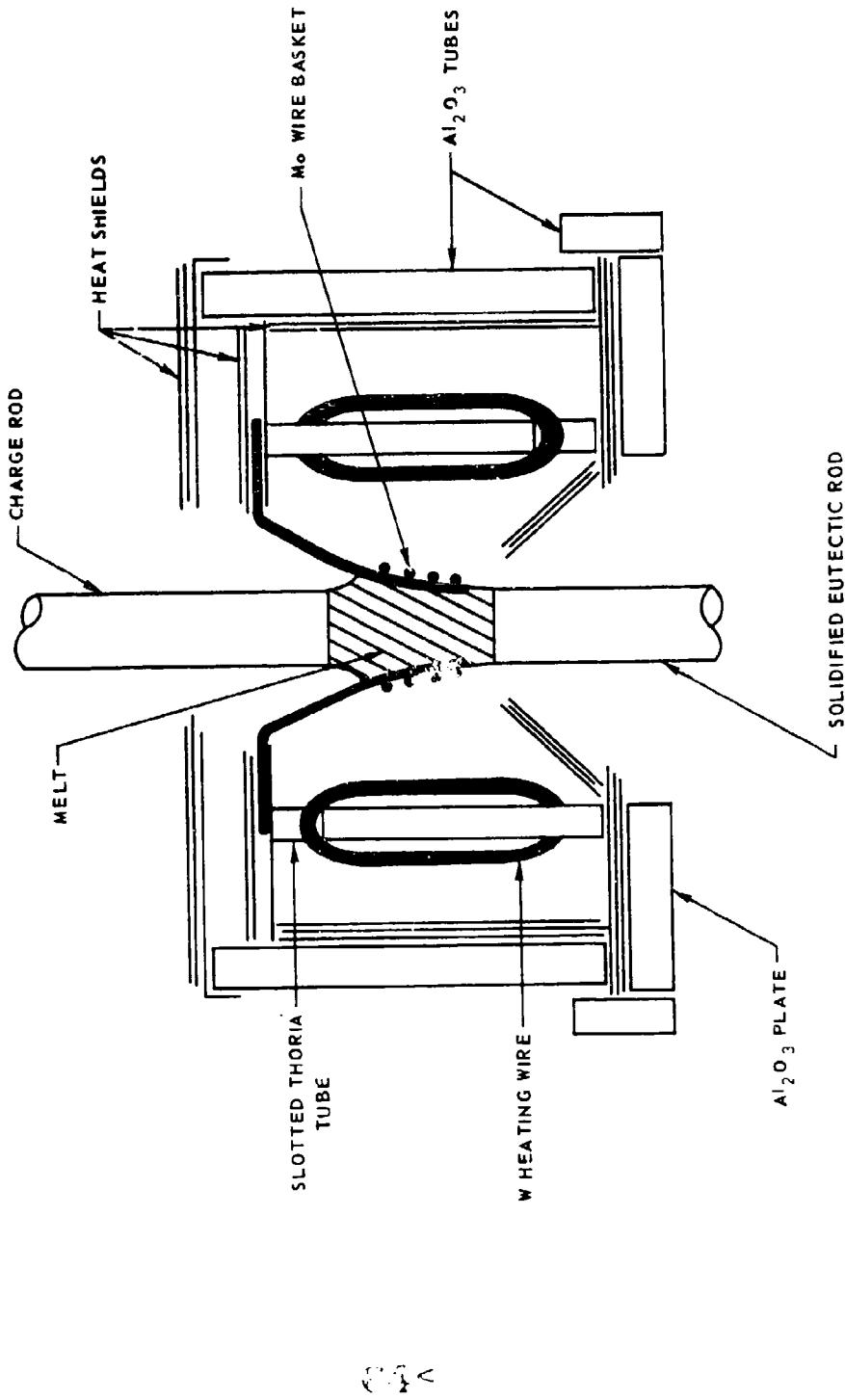
SCHEMATIC OF DIRECTIONAL SOLIDIFICATION EQUIPMENT FOR CERAMIC OXIDE EUTECTICS

VERTICAL SECTION VIEW THROUGH CENTER OF CYLINDRICAL FURNACE

65<
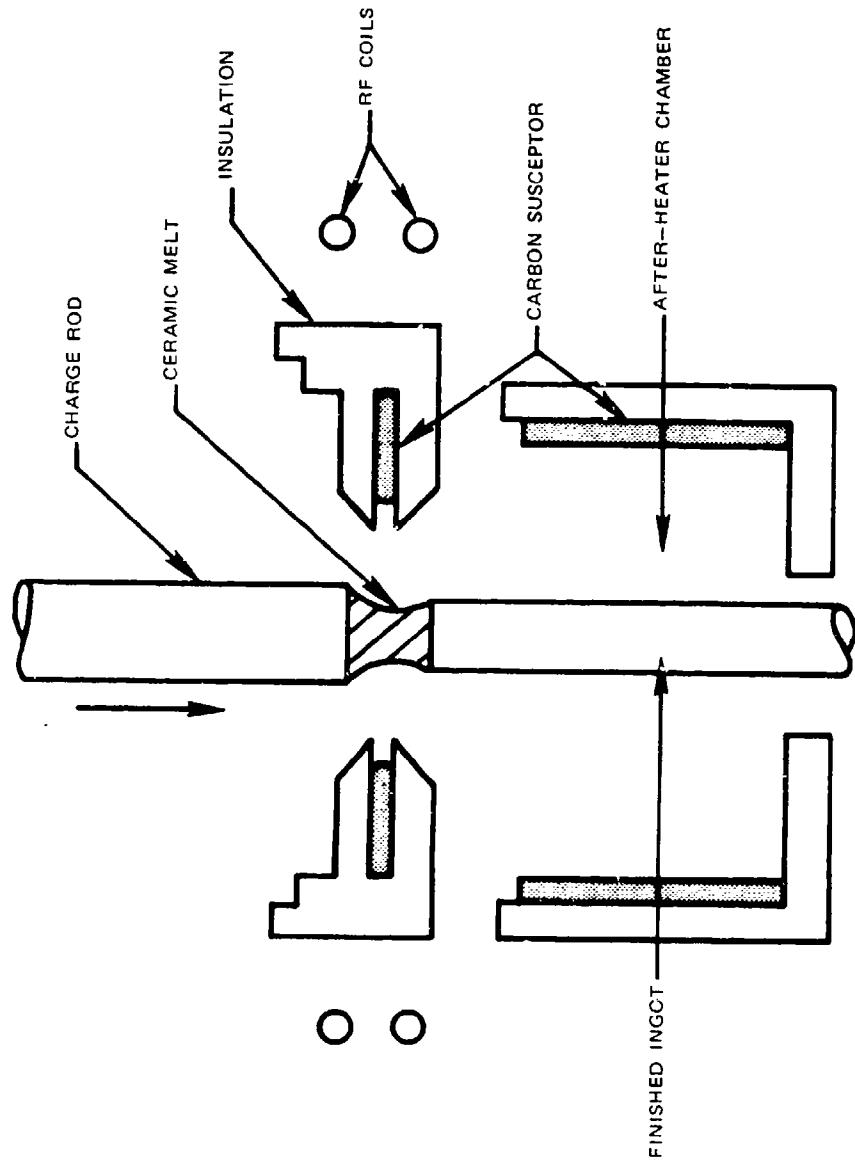
SCHEMATIC OF DIRECTIONAL SOLIDIFICATION EQUIPMENT FOR MAKING LARGER SIZED INGOTS

CHARGE ROD

MOLYBDENUM
CRUCIBLE

CERAMIC MELT

R.F. COILS

CARBON
SUSCEPTOR

D.S. INGOT
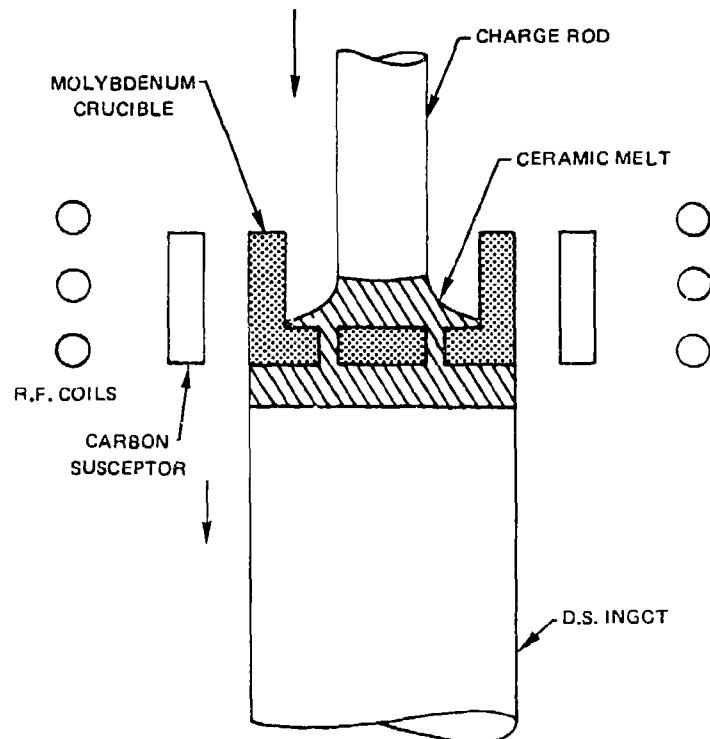
VERTICAL SECTION THROUGH CENTER OF CYLINDRICAL FURNACE

>86<

MOLYBDENUM SURFACE DEVICE FOR MAKING
LARGER SIZE INGOTS

FIG. 17

SCHEMATIC OF FLOATING MOLTEN ZONE FOR MAKING LARGER SIZED INGOTS
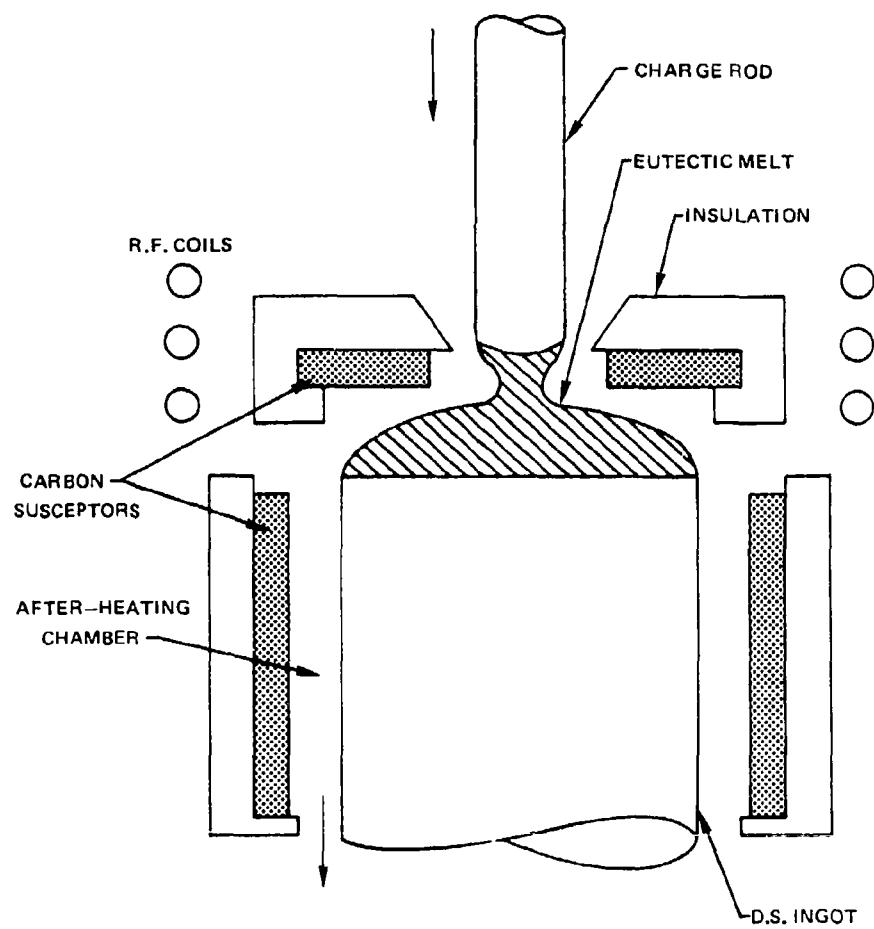
VERTICAL SECTION VIEW THROUGH CENTER OF CYLINDRICAL FURNACE

FIG. 18

LARGE DIAMETER INGOT OF $Al_2O_3-ZrO_2$ (Y_2O_3)
FABRICATED WITHOUT USE OF CONTAINER
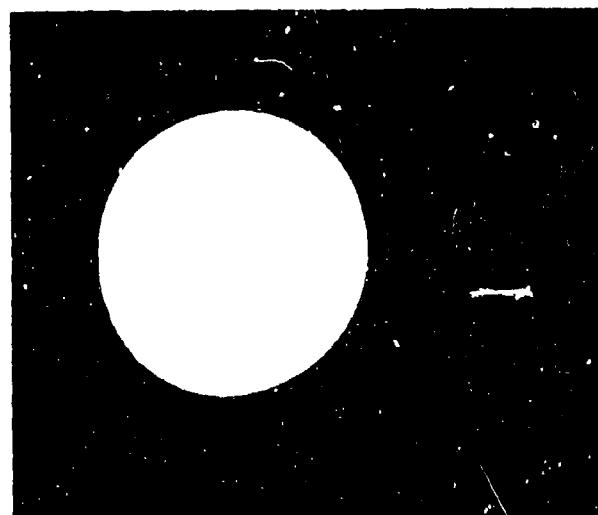
TOP VIEW

SIDE VIEW

SCHEMATIC OF FLOATING MOLTEN ZONE VARIATION FOR MAKING D.S. PLATES

TOP VIEW SECTION A–A

R.F. COIL

INSULATION

EUTECTIC MELT

B

B

SUSCEPTORS

EUTECTIC MELT

INSULATION

A

A

R.F. COILS

D.S. PLATE

LOWER SUPPORT ROD

SIDE VIEW SECTION B–B

FIG. 20
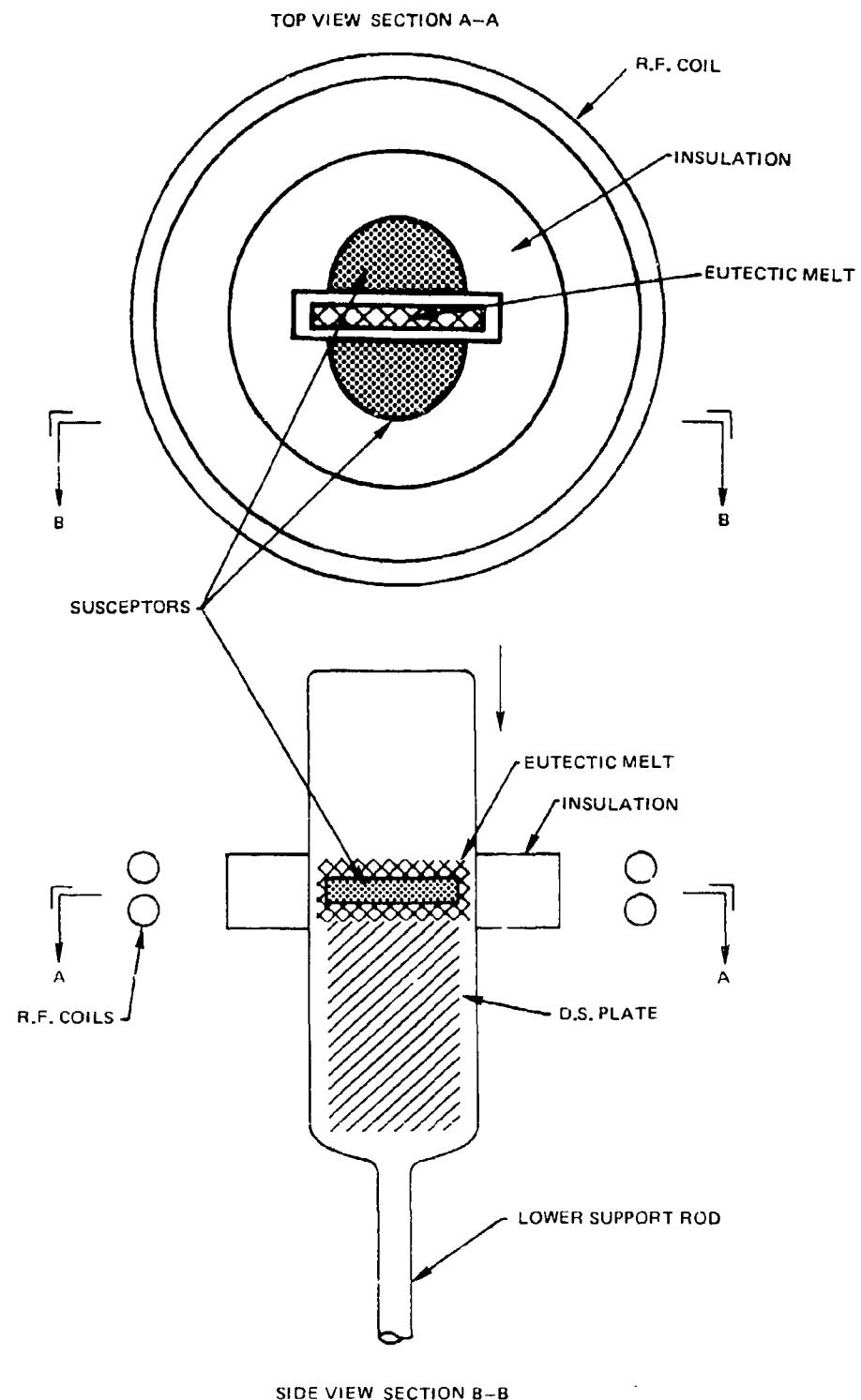
PLATE OF $Al_2O_3-ZrO_2$ (Y_2O_3) EUTECTIC PREPARED BY MODIFICATION TO FLOATING MOLTEN ZONE TECHNIQUES

EDGE VIEW   SIDE VIEW

FIG. 21
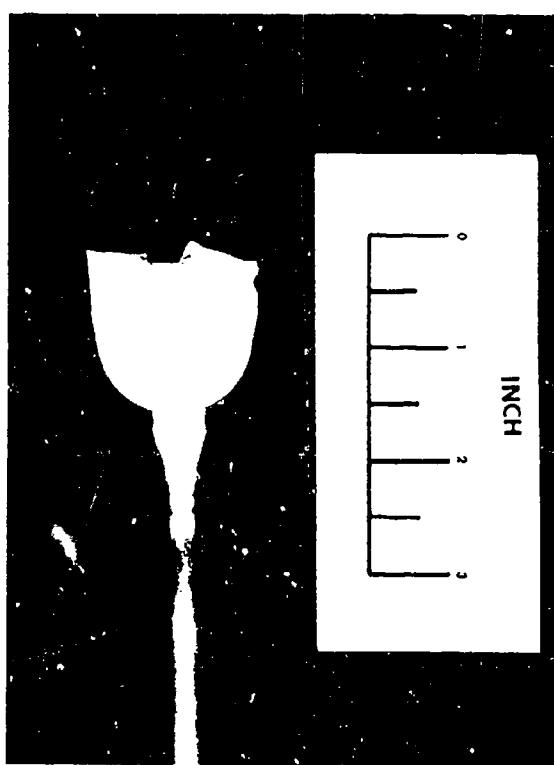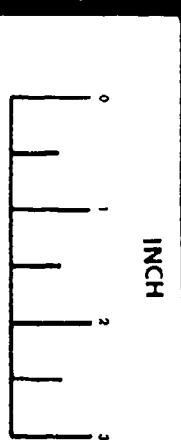
TECHNIQUE FOR CASTING EUTECTIC CHARGE RODS

PT. CRUCIBLE

CAST ROD

QUARTZ TUBE

COPPER HEAT SINK
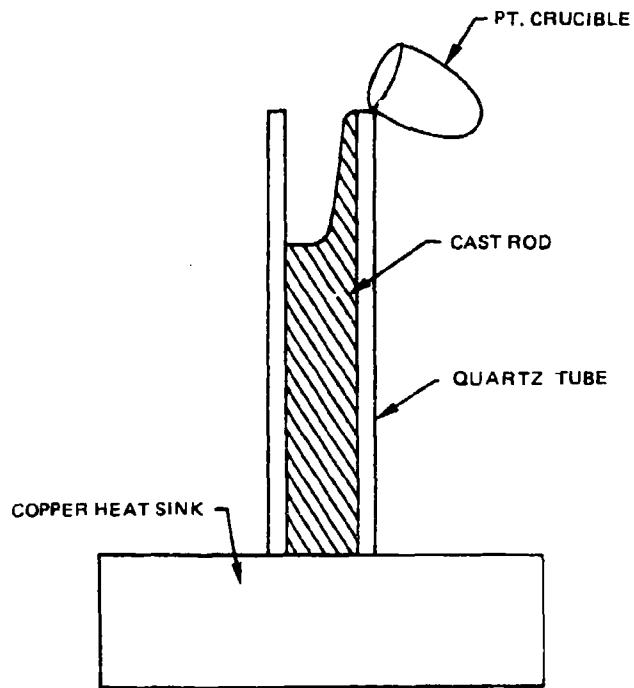
FIG 22

TINIUS OLSEN TESTING MACHINE USED FOR FLEXURAL TESTING OF OXIDE EUTECTICS

FIG 23
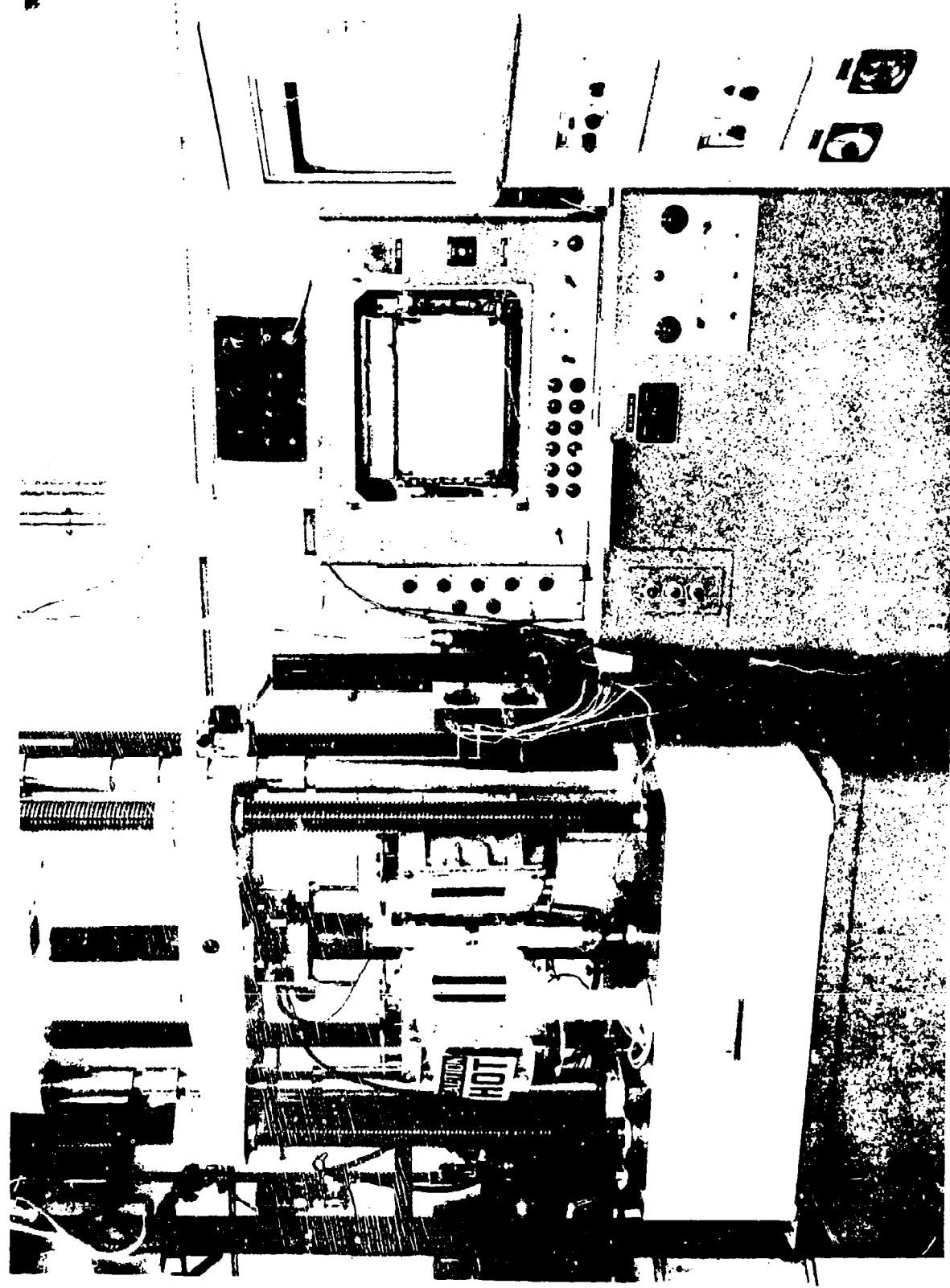
CAST MICROSTRUCTURE OF $SrO \cdot WO_3 - WO_3$ EUTECTIC

20 µ
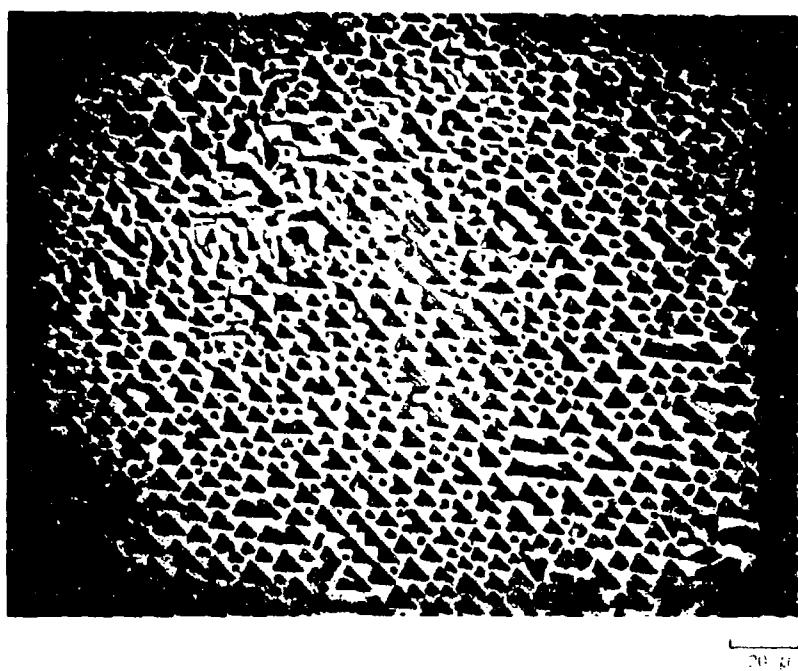
FIG. 24

UNDIRECTIONALLY SOLIDIFIED PbO-3PbO·Nb$_2$O$_5$ EUTECTIC

TRANSVERSE, 200X   (67-653-3)
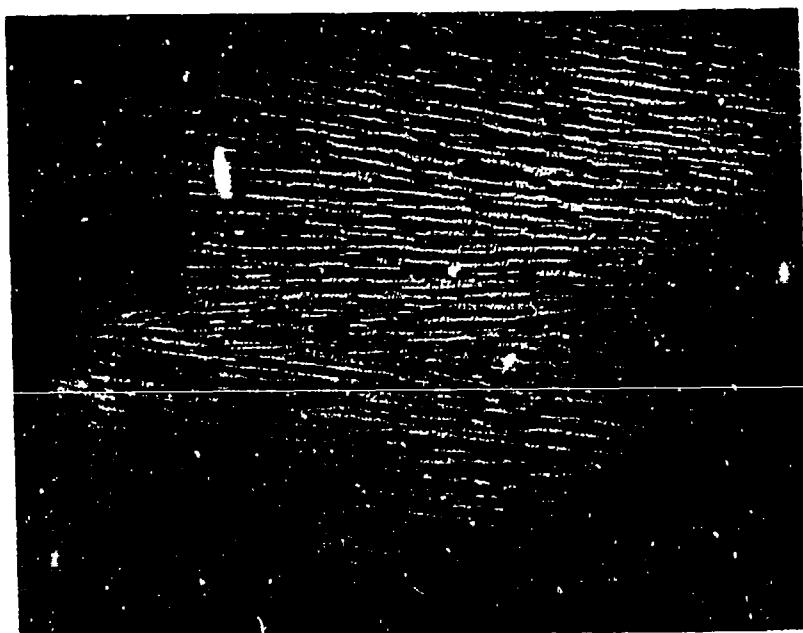
LONGITUDINAL, 500X (69-653-3)

UNIDIRECTIONALLY SOLIDIFIED PbO-2PbO·Fe$_2$O$_3$ EUTECTIC
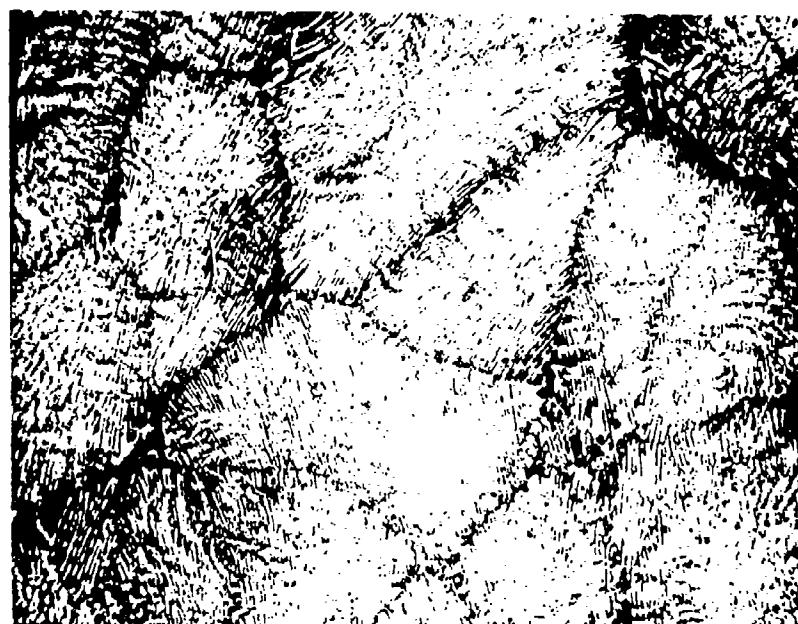
TRANSVERSE, 200X (69-150-1
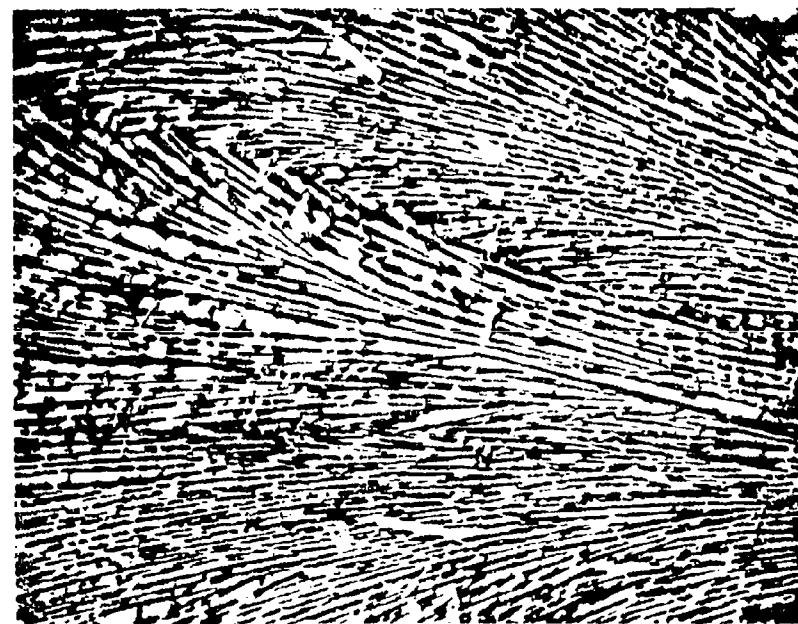
LONGITUDINAL, 500X (69-150-6)

UNIDIRECTIONALLY SOLIDIFIED Bi$_2$O$_3$-Bi$_2$O$_3$·Fe$_2$O$_3$ EUTECTIC

TRANSVERSE, 700X (69−055−9)
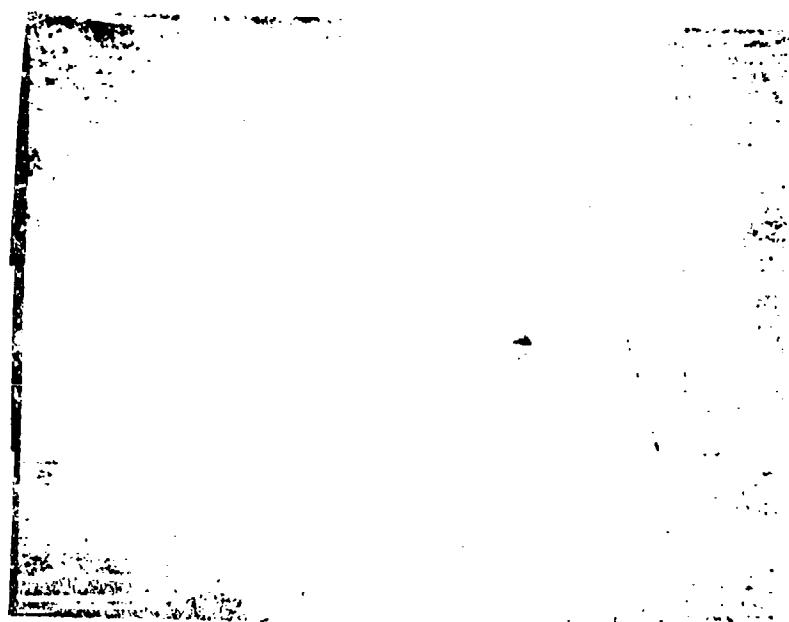
LONGITUDINAL, 500X (69−055−9)

FIG. 27

UNIDIRECTIONALLY SOLIDIFIED $Bi_2O_3 - Bi_2O_3 \cdot Fe_2O_3$ EUTECTIC SHOWING
BREAKDOWN OF ALIGNED STRUCTURE NEAR CENTER OF CELLS
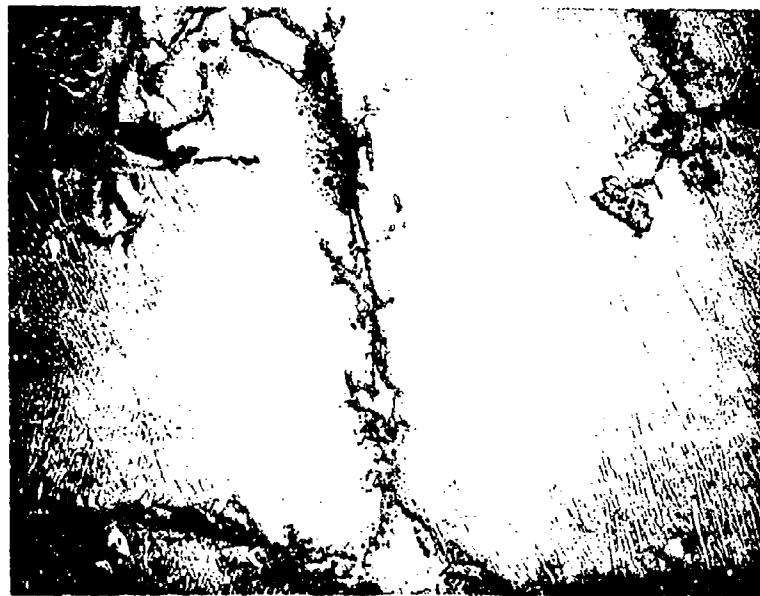
TRANSVERSE, 200X (A69 055 10)

TRANSVERSE, 200X (A69 ...)

FIG. 28
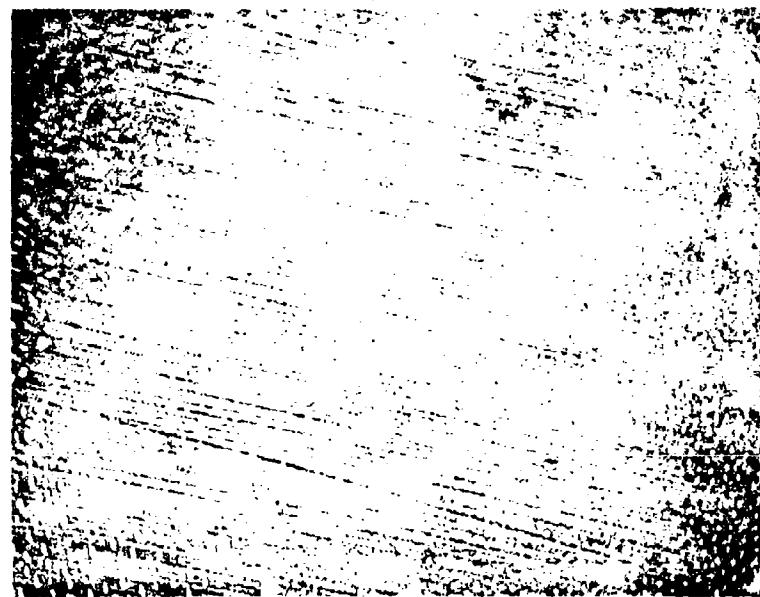
UNIDIRECTIONAL SOLIDIFIED $Bi_2O_3 - 15 Bi_2O_3 \cdot 2ZnO$ EUTECTIC
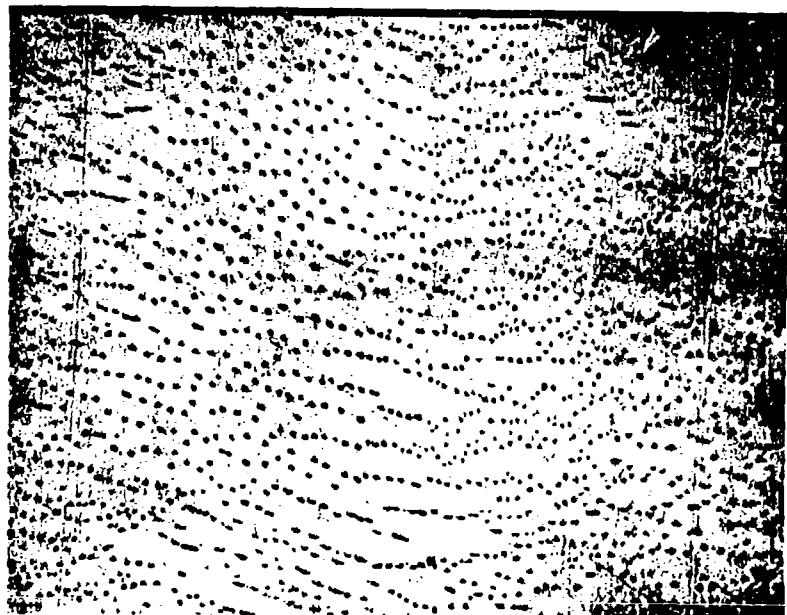
TRANSVERSE, 1000X (70-025-1)

FIG. 29

TRANSMITTED LIGHT VIEWS OF Fe_2O_3 – $LaFe_{12}O_{19}$ EUTECTIC
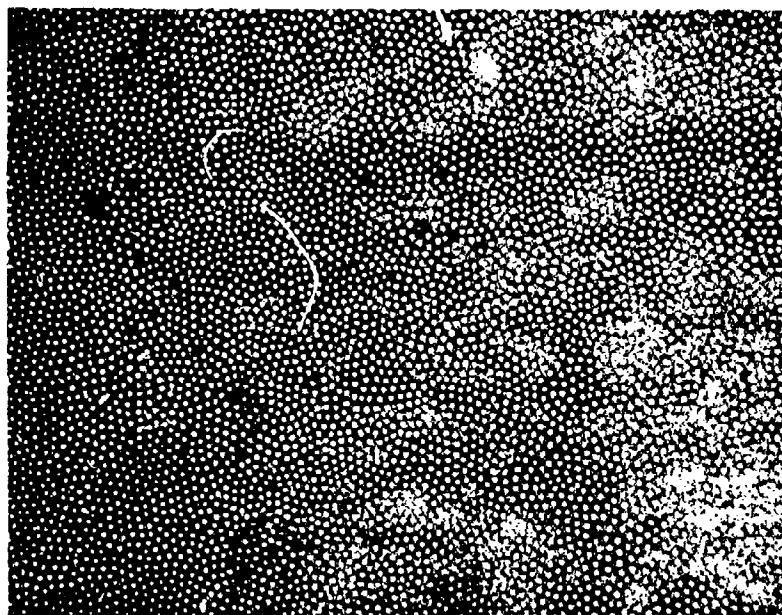
TRANSVERSE, WHITE LIGHT, 500X (70-C23-1)
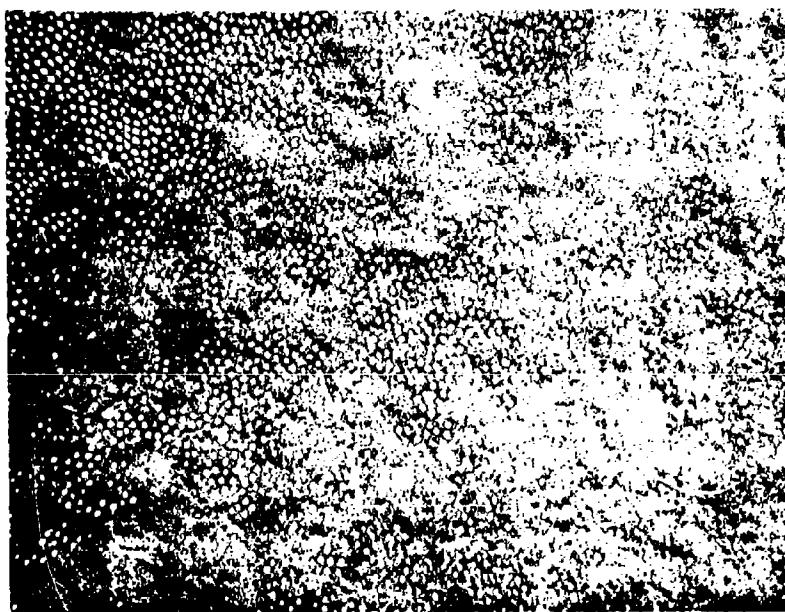
POLARIZED LIGHT, ANALYZER ROTATED TO RETARD TRANSMISSION
THROUGH SOME OF WHISKERS, (A70-C23-1)

FIG. 30

MICROSTRUCTURE OF DIRECTIONALLY SOLIDIFIED $BaWO_4$–WO_3 EUTECTIC

TRANSVERSE SECTION
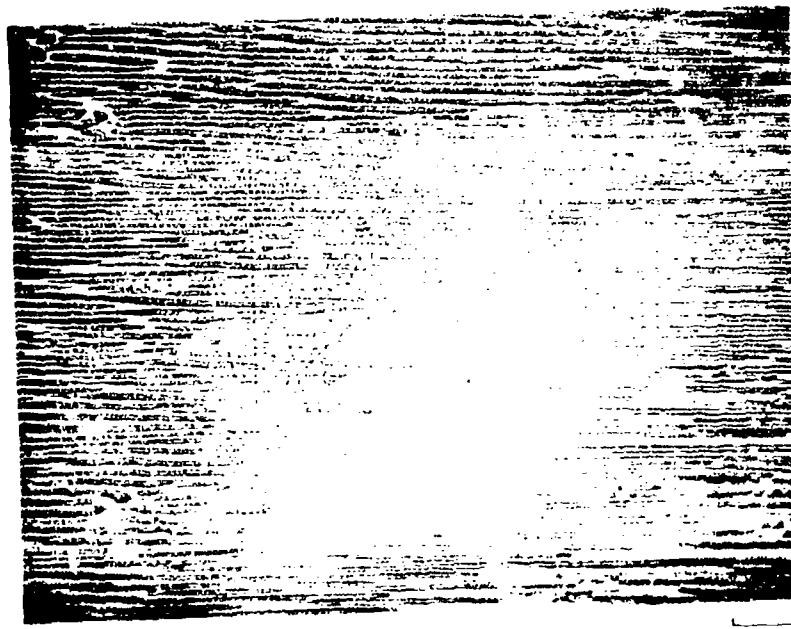
LONGITUDINAL SECTION

EFFECT OF SOLIDIFICATION SPEED ON INTERLAMELLAR SPACING
PbO–3PbO·Nb$_2$O$_5$ EUTECTIC
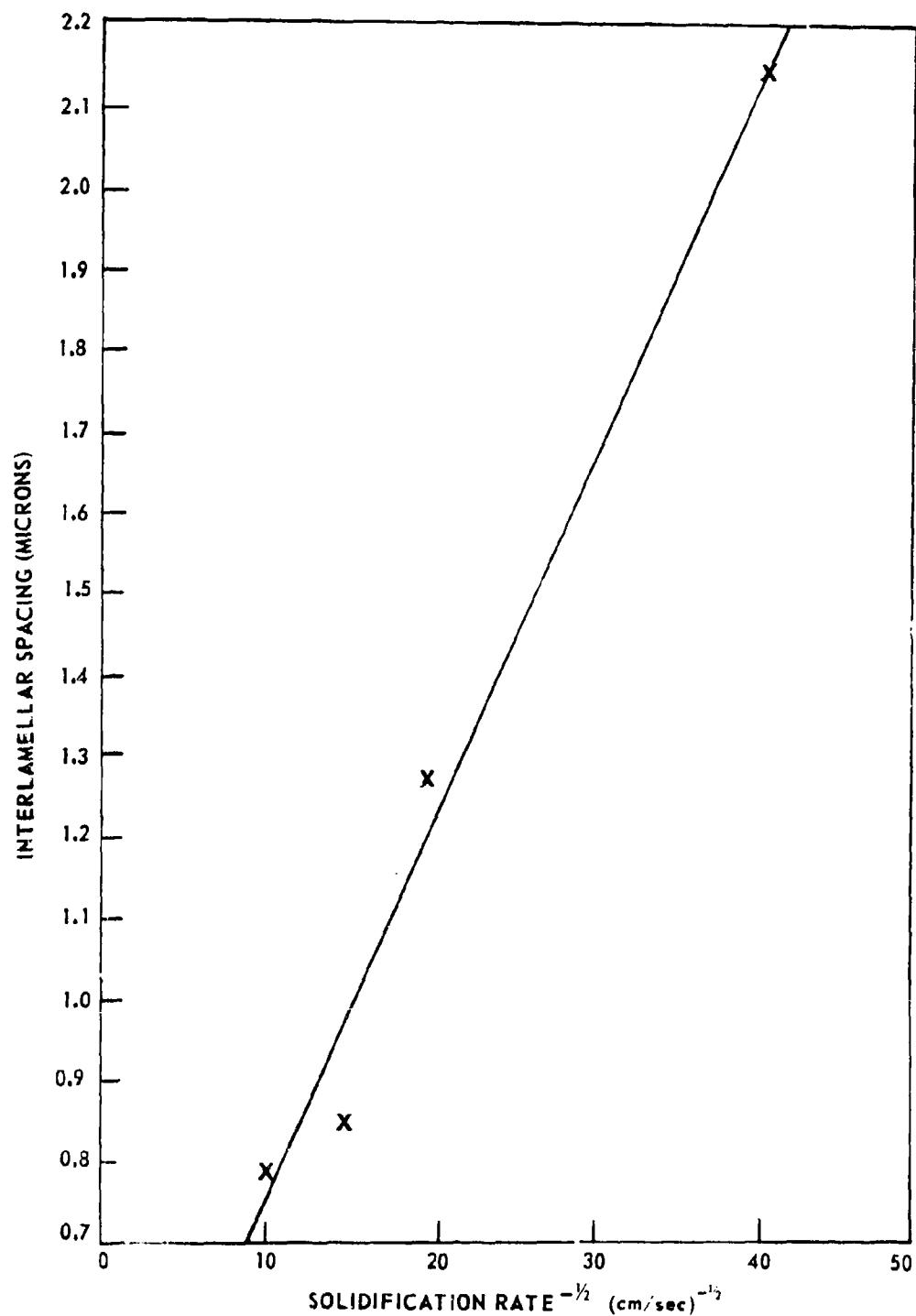
CRACK DEVIATION BY LAMELLAR MICROSTRUCTURE OF PbO–3PbO · Nb_2O_5
EUTECTIC SOLIDIFIED AT 2.2 cm/hr, ETCHED

$\overline{10\mu}$

FIG. 33

LONGITUDINAL SECTION $BaTiO_3$–Ba_2TiO_4 EUTECTIC 2 cm/hr, AS POLISHED

100μ

FIG. 34
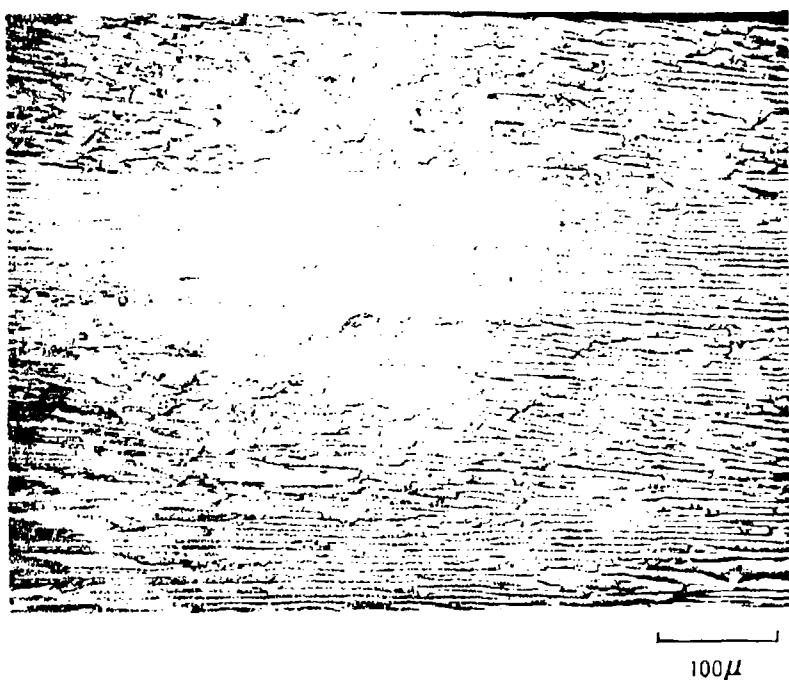
LONGITUDINAL SECTION OF $Al_2O_3-ZrO_2$ (Y_2O_3) EUTECTIC
DIRECTIONALLY SOLIDIFIED AT 0.8 CM/HR
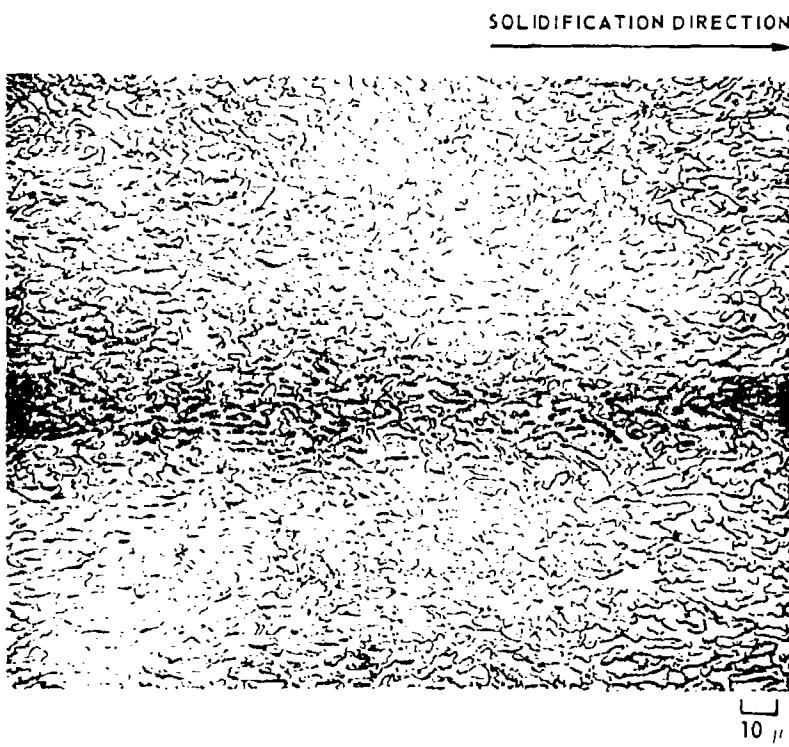
SOLIDIFICATION DIRECTION

10 μ

TRANSVERSE SECTION OF CELLULAR MICROSTRUCTURE IN $Al_2O_3-ZrO_2$ (Y_2O_3)
EUTECTIC SOLIDIFIED AT 20 CM/HR

10 μ

FIG. 36
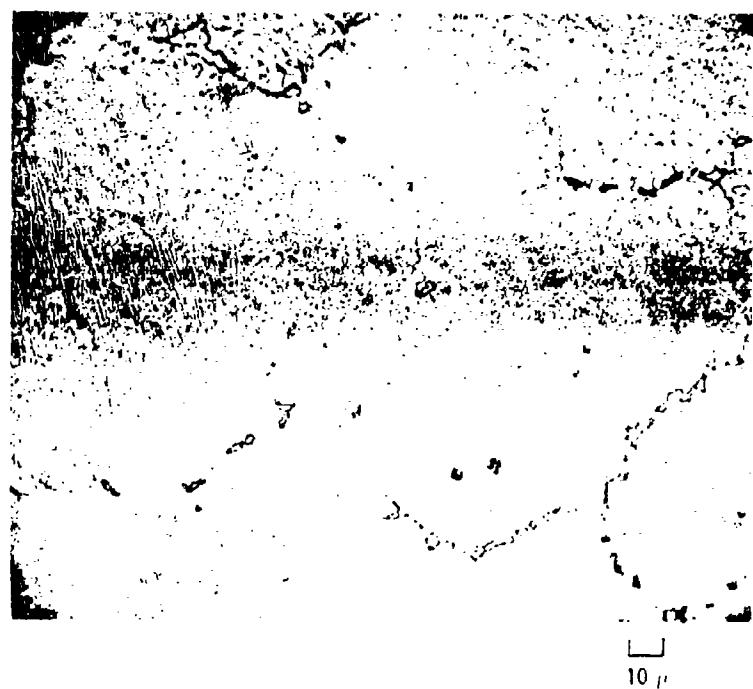
THREE-POINT BEND STRENGTH $Al_2O_3-ZrO_2$ (Y_2O_3)
EUTECTIC AND POLYCRYST, Al_2O_3

1575°C

$Al_2O_3-ZrO_2$ (Y_2O_3)
EUTECTIC

POLYCRYST, Al_2O_3
WESGO 995

FLEXURAL STRESS $-LB/IN.^2$ ×1000

ESTIMATED DEFORMATION , e $-IN./IN.$
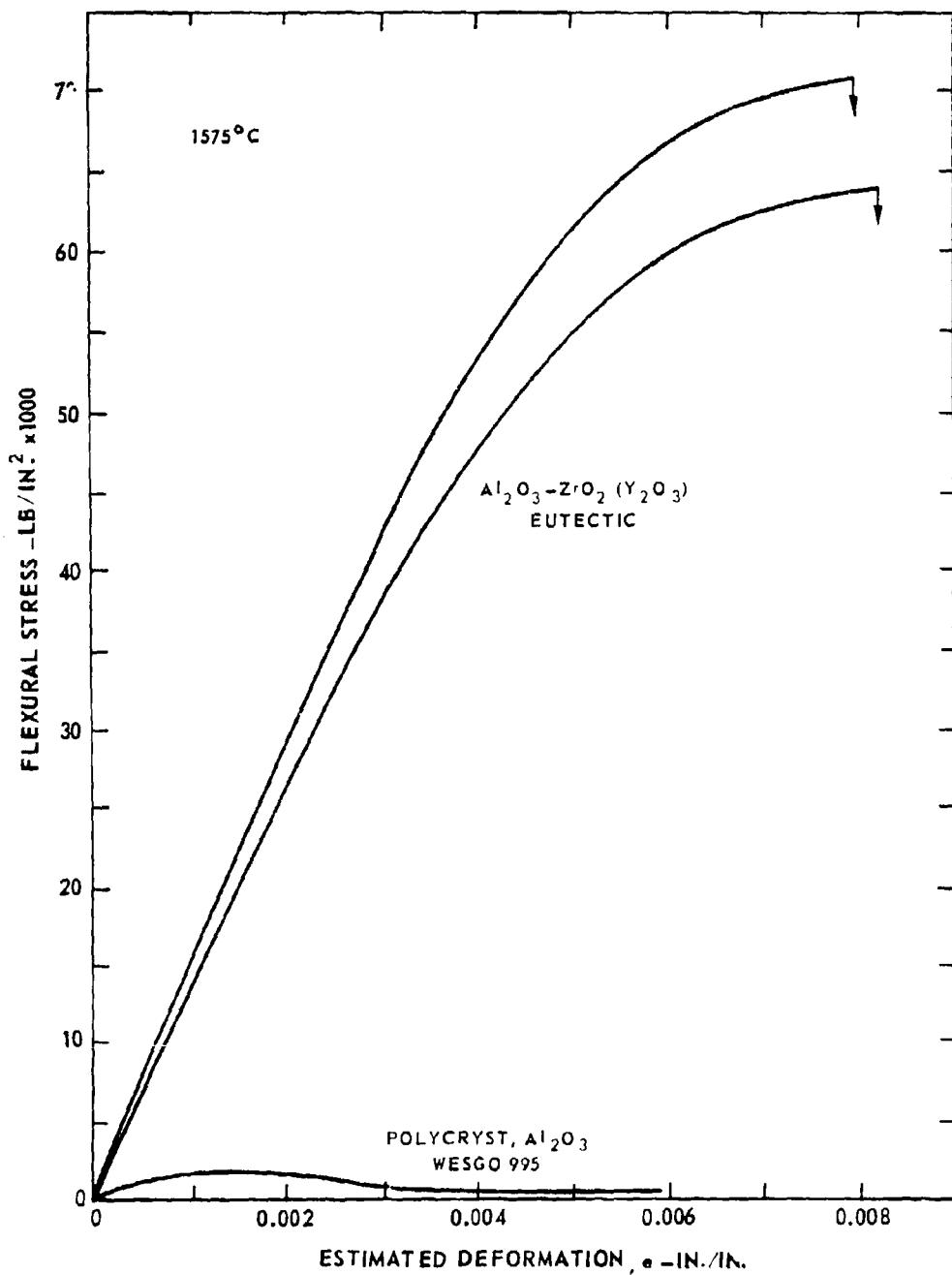
STRENGTH OF Al_2O_3–ZrO_2 (Y_2O_3) EUTECTIC AT 1575°C ($\sim$2900° F)
COMPARED WITH POLYCRYST Al_2O_3
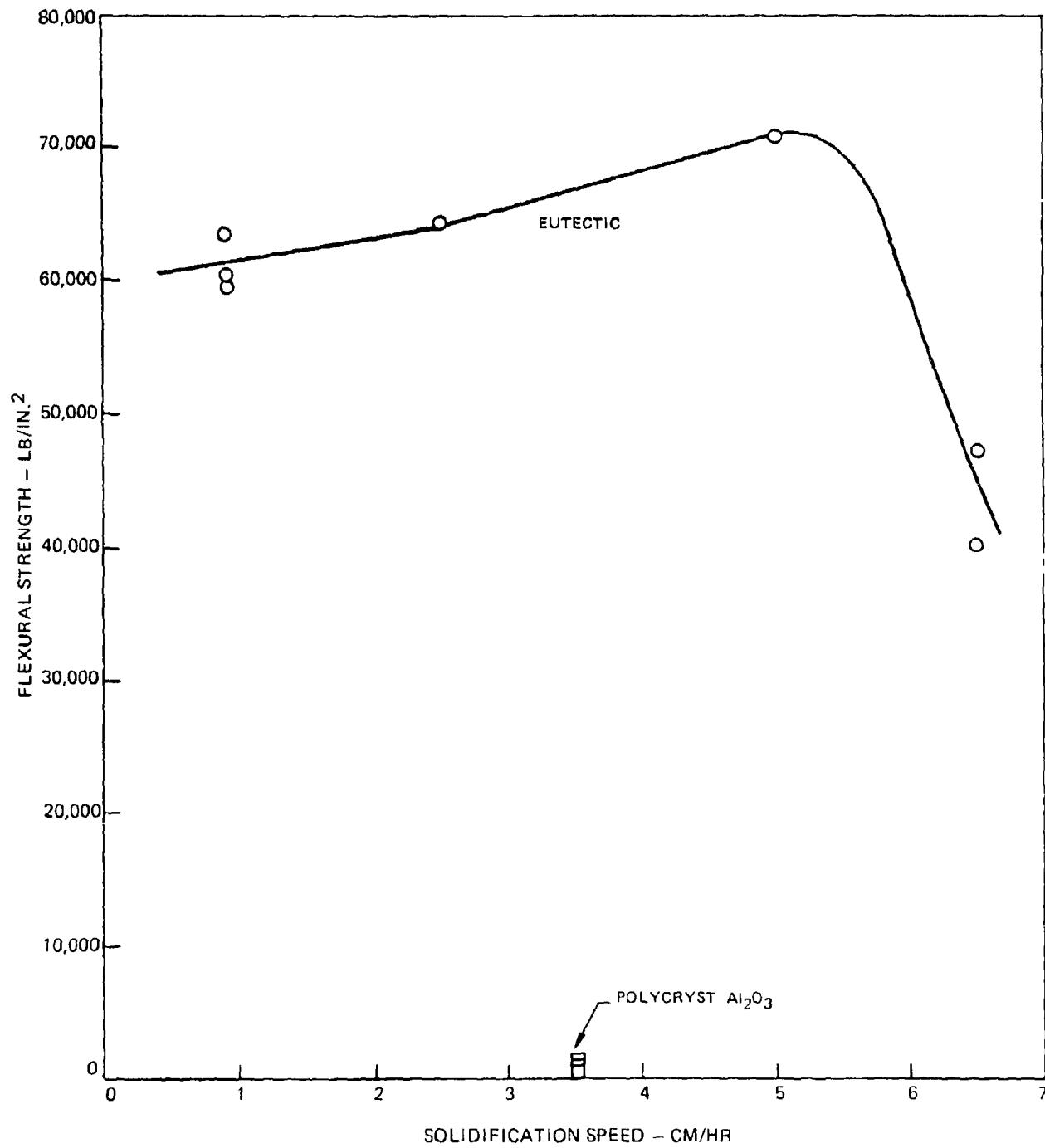
STRENGTH OF UNIDIRECTIONALLY SOLIDIFIED $Al_2O_3-ZrO_2$ (Y_2O_3) EUTECTIC COMPARED WITH HOT—PRESSED ALUMINA, SILICON NITRIDE AND B—1900
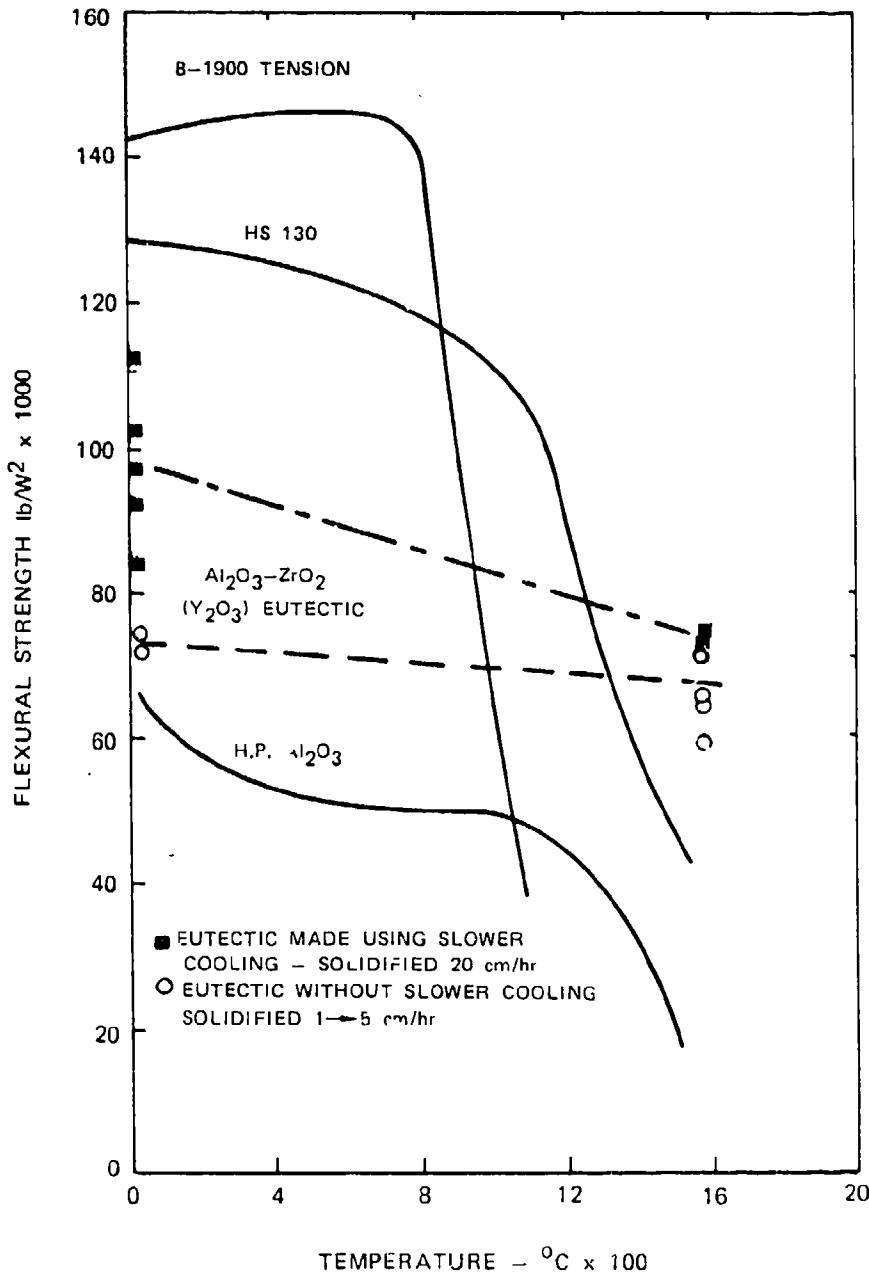
B-1900 TENSION

HS 130

$Al_2O_3-ZrO_2$
(Y_2O_3) EUTECTIC

H.P. Al_2O_3

■ EUTECTIC MADE USING SLOWER
  COOLING — SOLIDIFIED 20 cm/hr
○ EUTECTIC WITHOUT SLOWER COOLING
  SOLIDIFIED 1—5 cm/hr

FLEXURAL STRENGTH lb/w^2 x 1000

TEMPERATURE — ^{0}C x 100

FIG. 39

TRANSVERSE SECTION OF CELLULAR MICROSTRUCTURE IN $Al_2O_3-ZrO_2$ (Y_2O_3)
EUTECTIC SOLIDIFIED AT 20 CM HR

100 μ
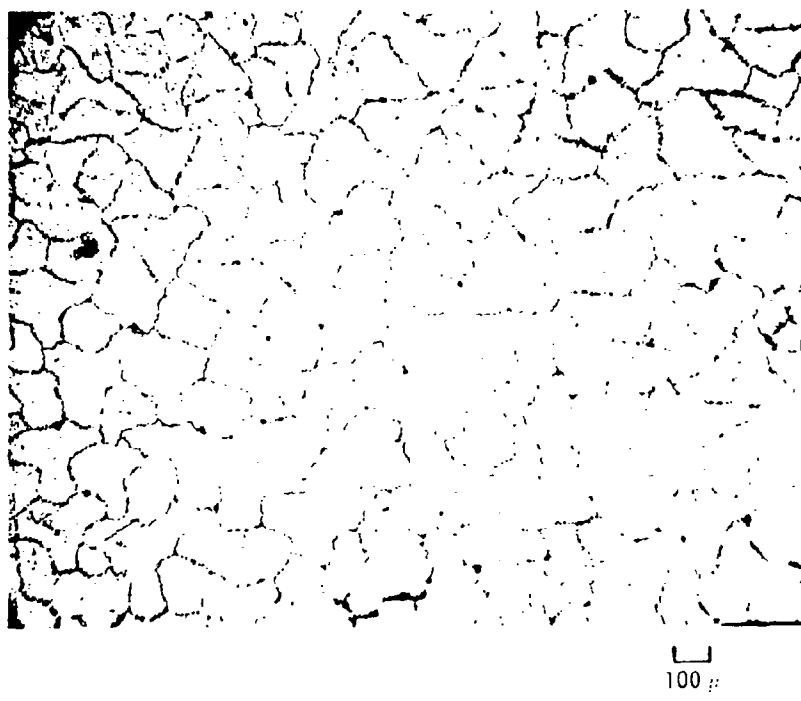
FIG. 40

TRANSVERSE SECTION OF CELLULAR MICROSTRUCTURE IN $Al_2O_3-ZrO_2$ (Y_2O_3)
EUTECTIC SOLIDIFIED AT 2.5 CM/HR

$\vdash\!\!-\!\!\dashv$
$10\,\mu$
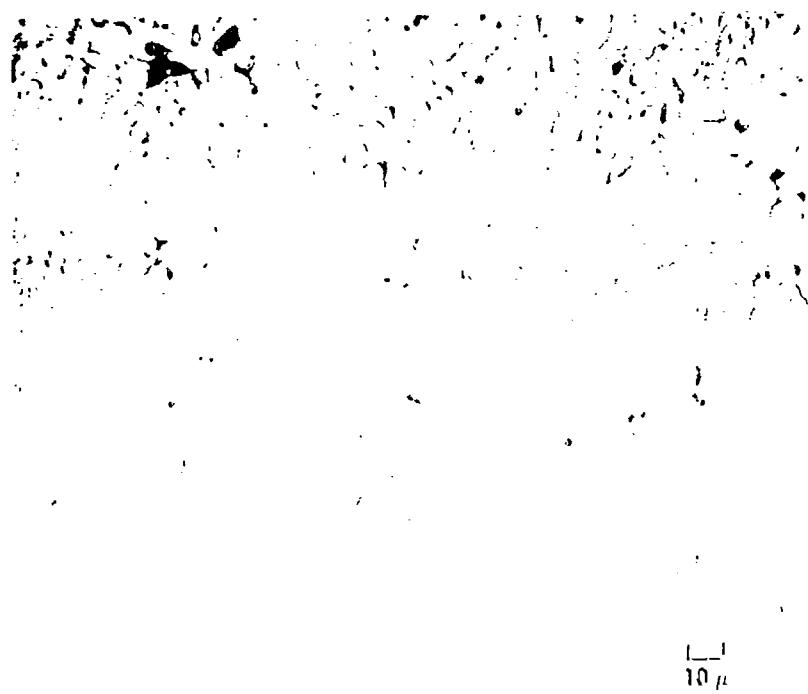
WORK–TO–FRACTURE OF Al_2O_3–ZrO_2 (O_3) EUTECTIC,
POLYCRYSTALLINE AND SINGLE CRYSTAL Al_2O_3 VS TEMPERATURE
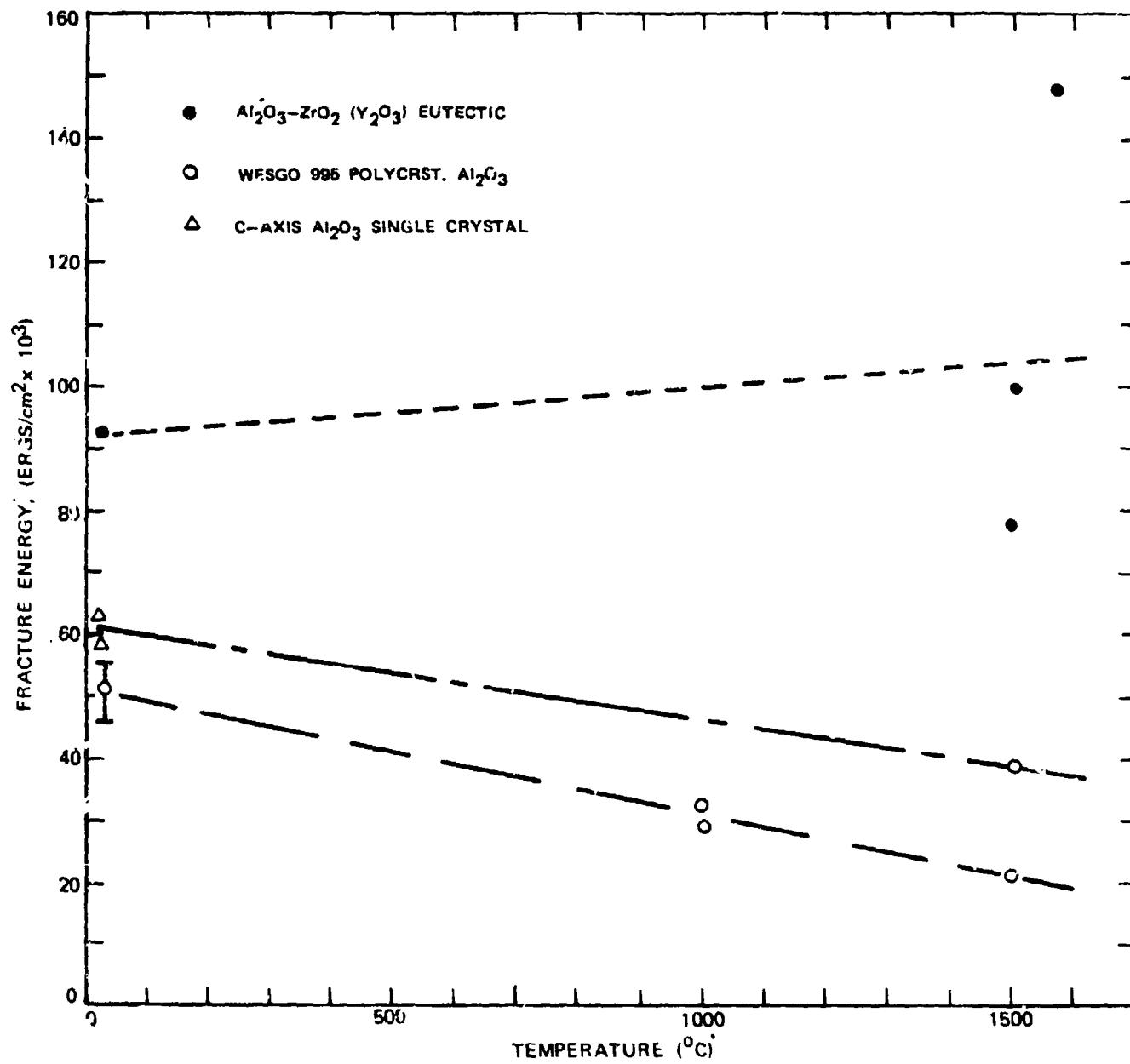
FRACTURE SURFACE OF $Al_2O_3-ZrO_2$ (Y_2O_3)
EUTECTIC AT R.T. SHOWING ONE CELL.
(SOLIDIFIED AT 20 cm/hr).
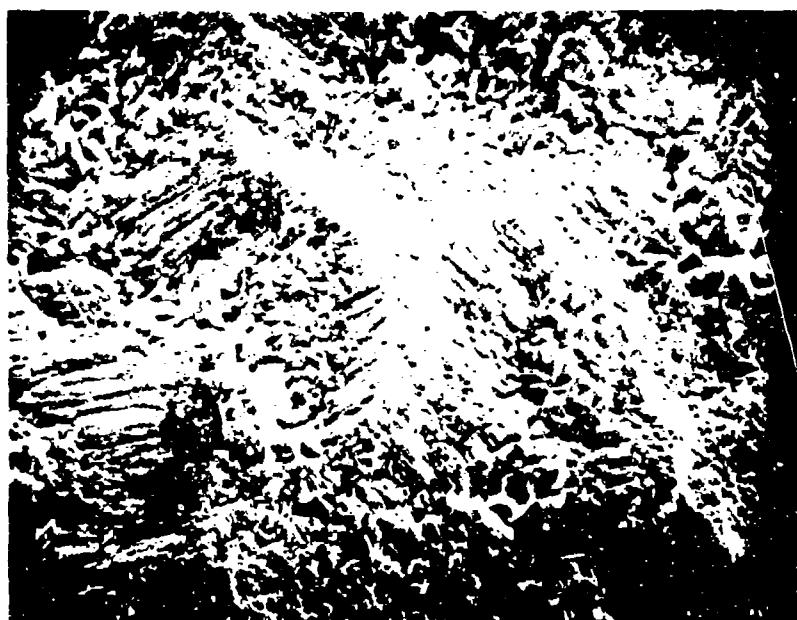
FRACTURE SURFACE NEAR CENTER OF CELL

IN $Al_2O_3-ZrO_2$ (Y_2O_3) EUTECTIC AT 1500 C

(SOLIDIFIED AT 20 cm/hr).

FIG 44

VIEW PARALLEL TO FRACTURE SURFACE OF
$Al_2O_3-ZrO_2$ (Y_2O_3) EUTECTIC AT 1500 °C
(SOLIDIFIED AT 20 cm/hr).

FIG. 45

SUGGESTED FRACTURE MODE FOR $Al_2O_3-ZrO_2(Y_2O_3)$ EUTECTIC AT 1500°C

Al_2O_3 MATRIX

$ZrO_2 (Y_2O_3)$ WHISKERS

CRACK PROPAGATION DIRECTION

FIG. 46
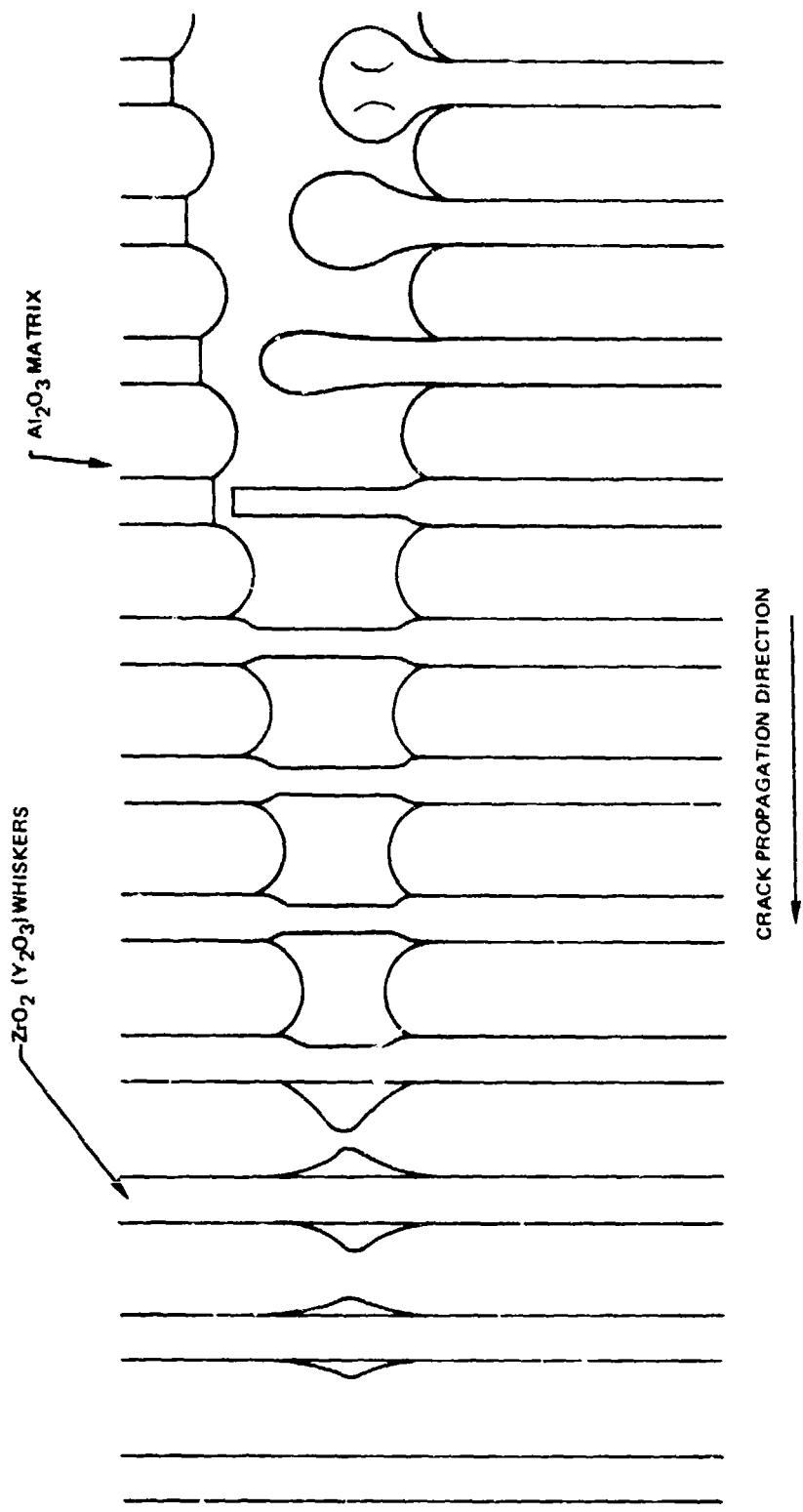
MICROSTRUCTURE OF $Al_2O_3-ZrO_2$ (Y_2O_3) EUTECTIC SEEDED WITH SAPPHIRE
SINGLE CRYSTAL TO GROW AT 2 cm/hr PARALLEL TO $[02\bar{2}4]$.

TRANSVERSE
SECTION

└──┘

10 μ

LONGITUDINAL
SECTION

└──┘

5 μ

FIG. 47

UNIDIRECTIONALLY SOLIDIFIED Al_2O_3-ZrO_2 (CaO) MELT

SOLIDIFICATION DIRECTION

50 µ
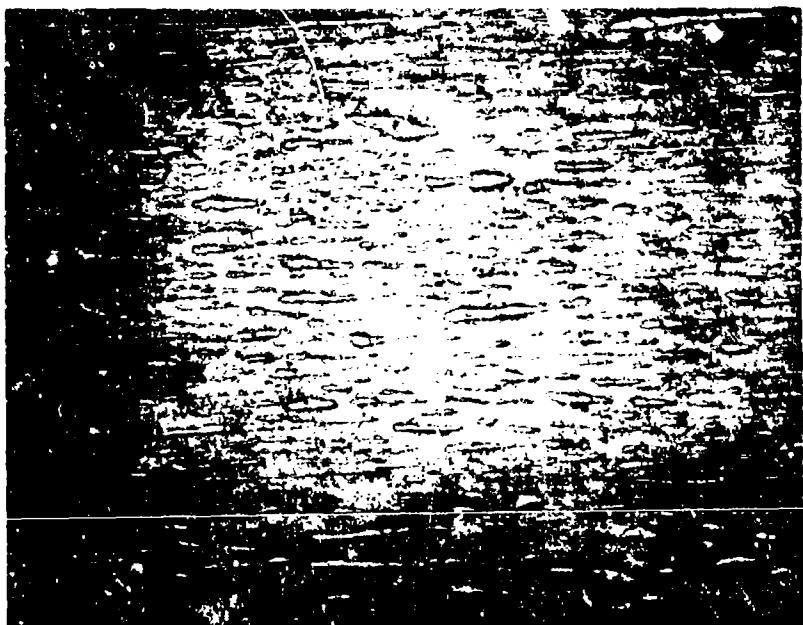
FIG. 48

CONTINUOUS MATRIX EUTECTIC IN UNIDIRECTIONALLY SOLIDIFIED
$Al_2O_3 - ZrO_2$ (Ca O) MELT

$\llcorner \quad \lrcorner$
$10 \; \mu$

FIG. 49
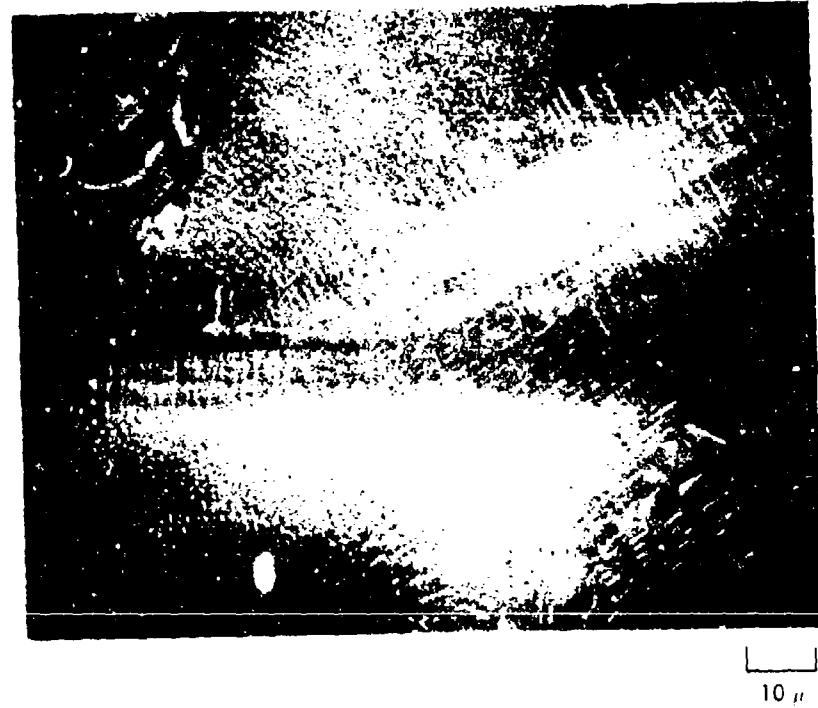
PHASE DIAGRAM FOR ZrO_2-Y_2O_3 SYSTEM
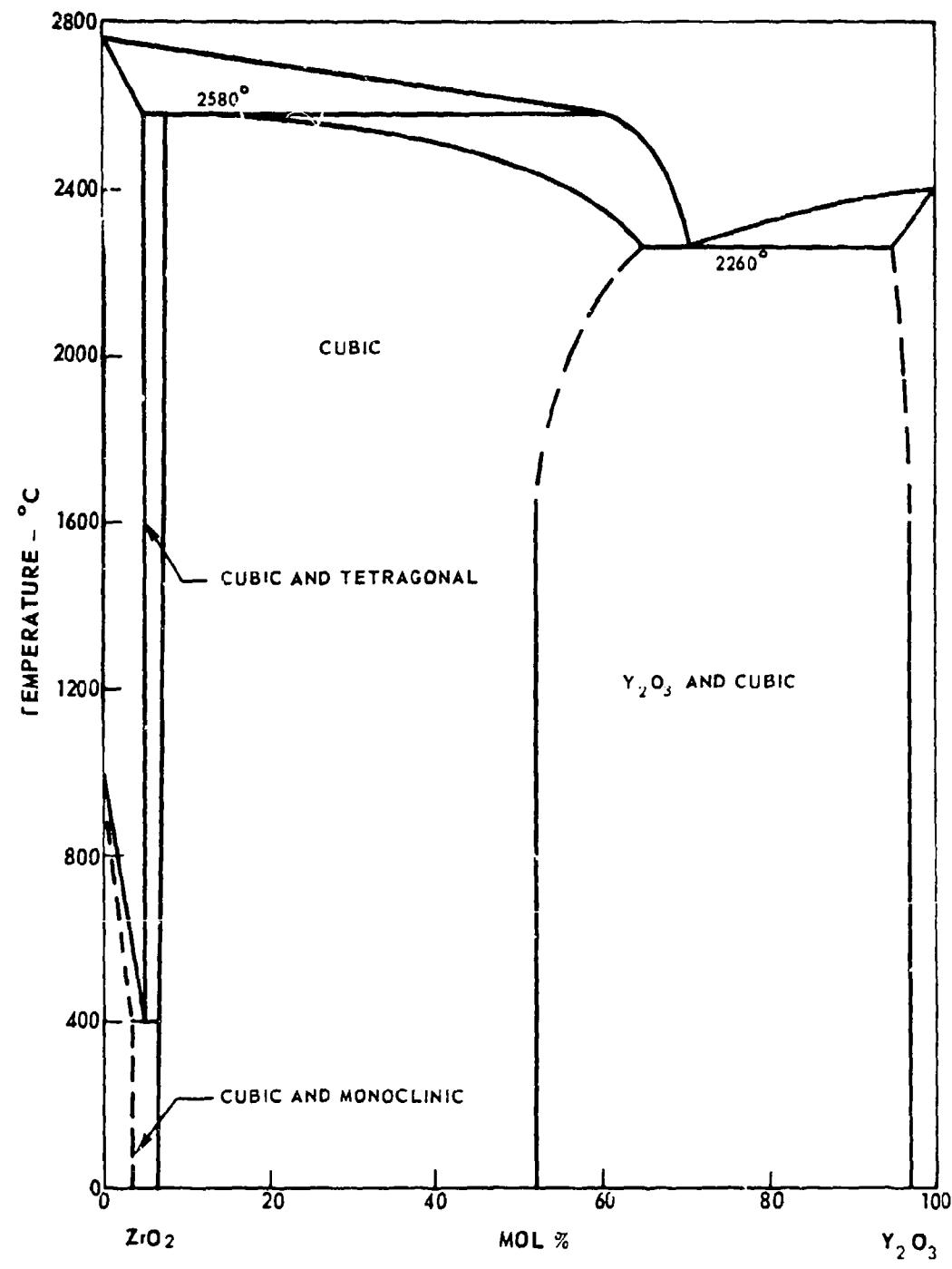
FIG. 50

TRANSVERSE MICROSTRUCTURE OF ZrO$_2$–Y$_2$O$_3$ EUTECTIC SOLIDIFIED AT 5.7 CM/HR

200 μ

LONGITUDINAL MICROSTRUCTURE OF $ZrO_2-Y_2O_3$ EUTECTIC SOLIDIFIED AT 40 CM/HR

SOLIDIFICATION DIRECTION

50 μ
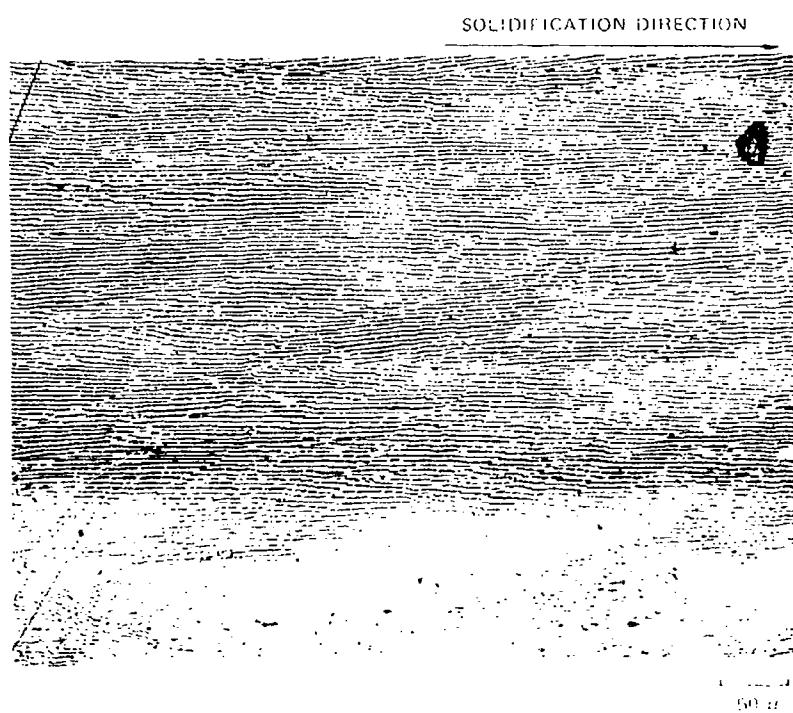
LAMELLAR SPACING VERSUS SOLIDIFICATION SPEED OF DIRECTIONALLY SOLIDIFIED $ZrO_2-Y_2O_3$ EUTECTIC
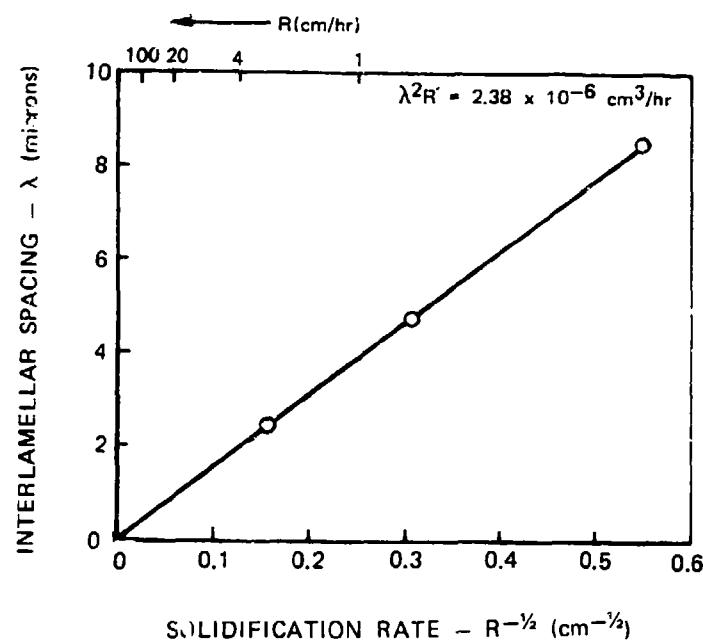
BEND STRENGTH VERSUS SOLIDIFICATION SPEED OF DIRECTIONALLY SOLIDIFIED $ZrO_2-Y_2O_3$

FIG. 54
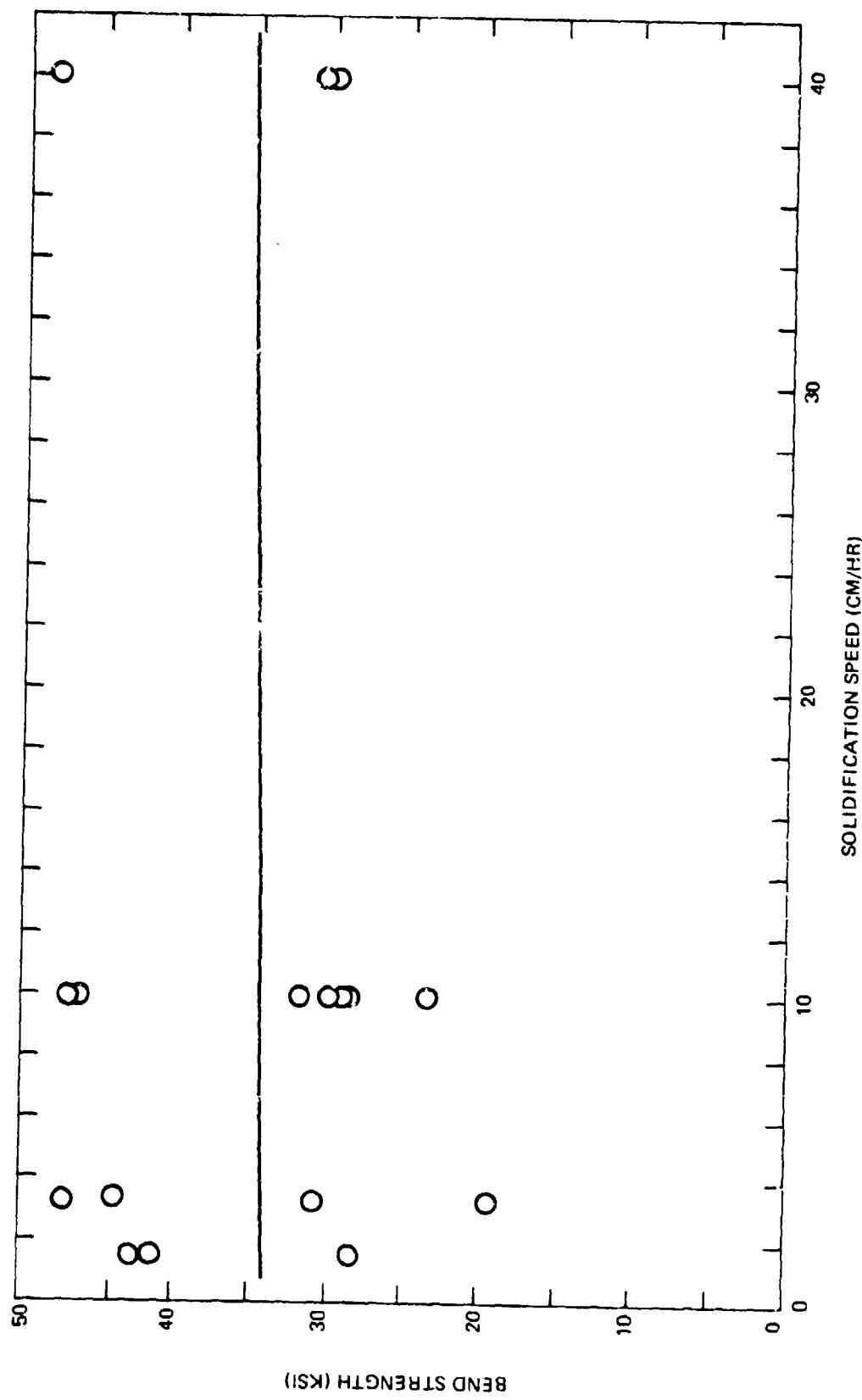
BEND STRENGTH VERSUS TEMPERATURE OF $ZrO_2-Y_2O_3$ EUTECTIC
DIRECTIONALLY SOLIDIFIED AT 40 CM/HR
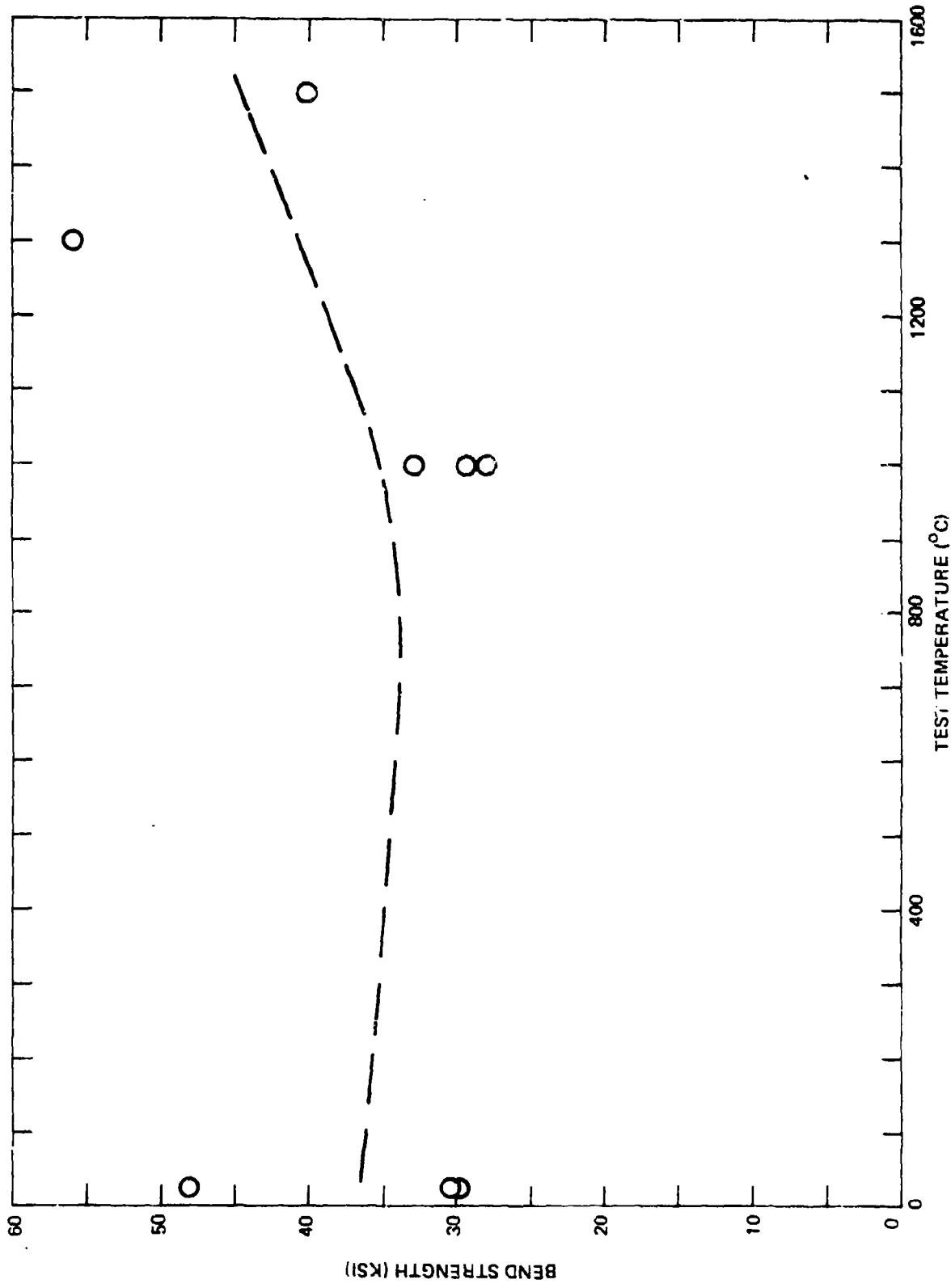
ROOM TEMPERATURE FRACTURE SURFACE OF
$ZrO_2-Y_2O_3$ EUTECTIC DIRECTIONALLY SOLIDIFIED AT 1.8 cm/hr

FIG 56
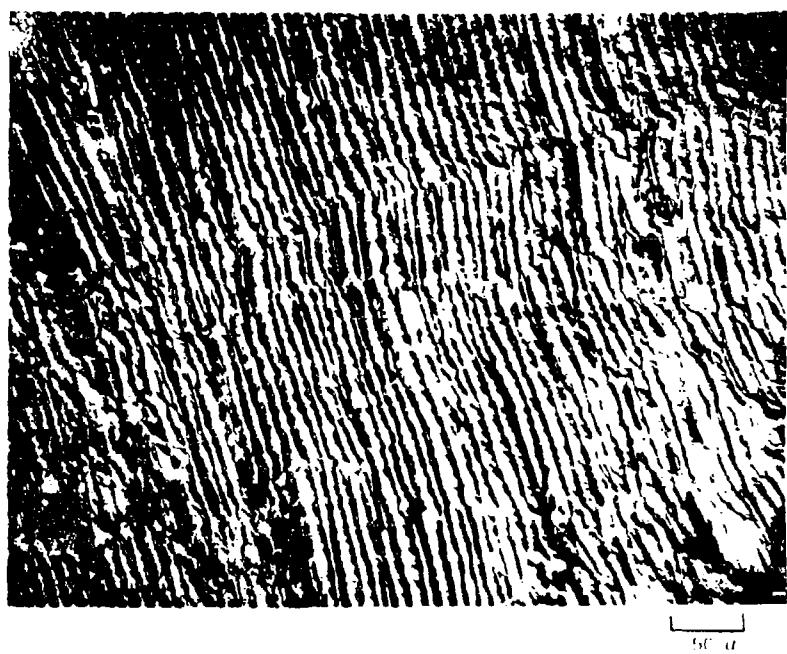
FRACTURE SURFACE WITH CRACK DIRECTION NORMAL TO LAMELLAE OF
$ZrO_2-Y_2O_3$ EUTECTIC (10 CM/HR)

20 μ
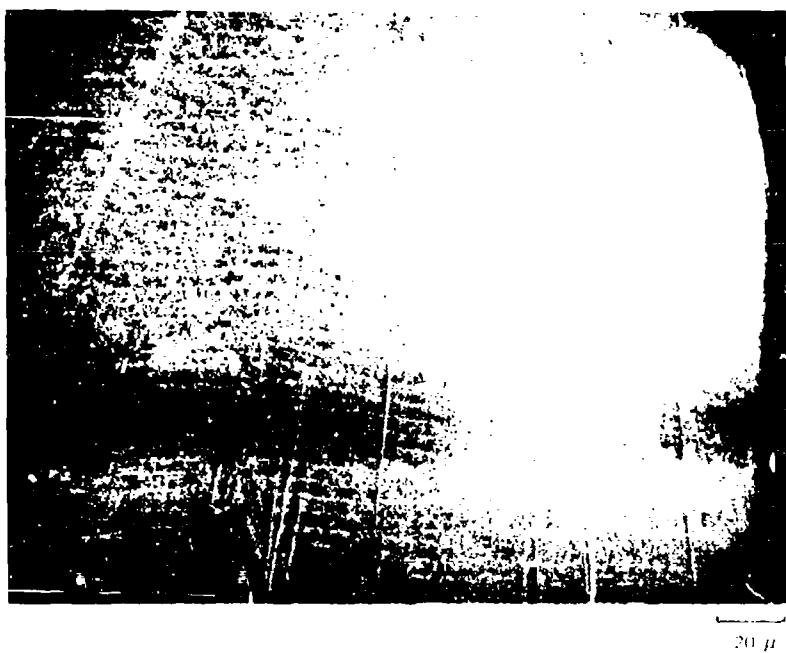
FRACTURE SURFACE OF ZrO_2 Y_2O_3 EUTECTIC DIRECTIONALLY SOLIDIFIED AT 40 CM HR AND BROKEN AT 1500° C

LONGITUDINAL SECTION OF CaO·ZrO$_2$-ZrO$_2$ EUTECTIC (SOLIDIFIED 10 CM/HR)
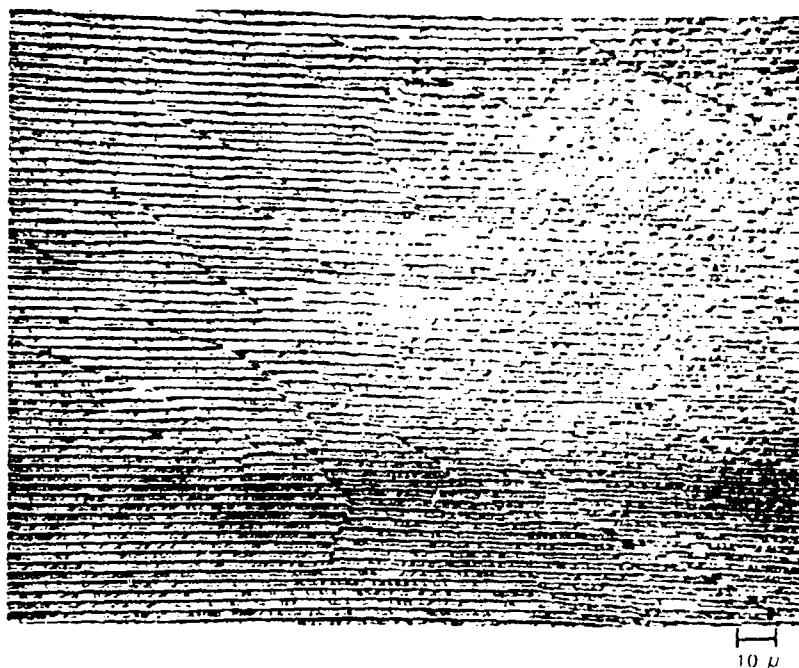
10 μ

EFFECT OF SOLIDIFICATION SPEED ON FLEXURAL STRENGTH (3-POINT) OF
UNIDIRECTIONALLY SOLIDIFIED $ZrO_2-CaO \cdot ZrO_2$ EUTECTIC

FIG. 60
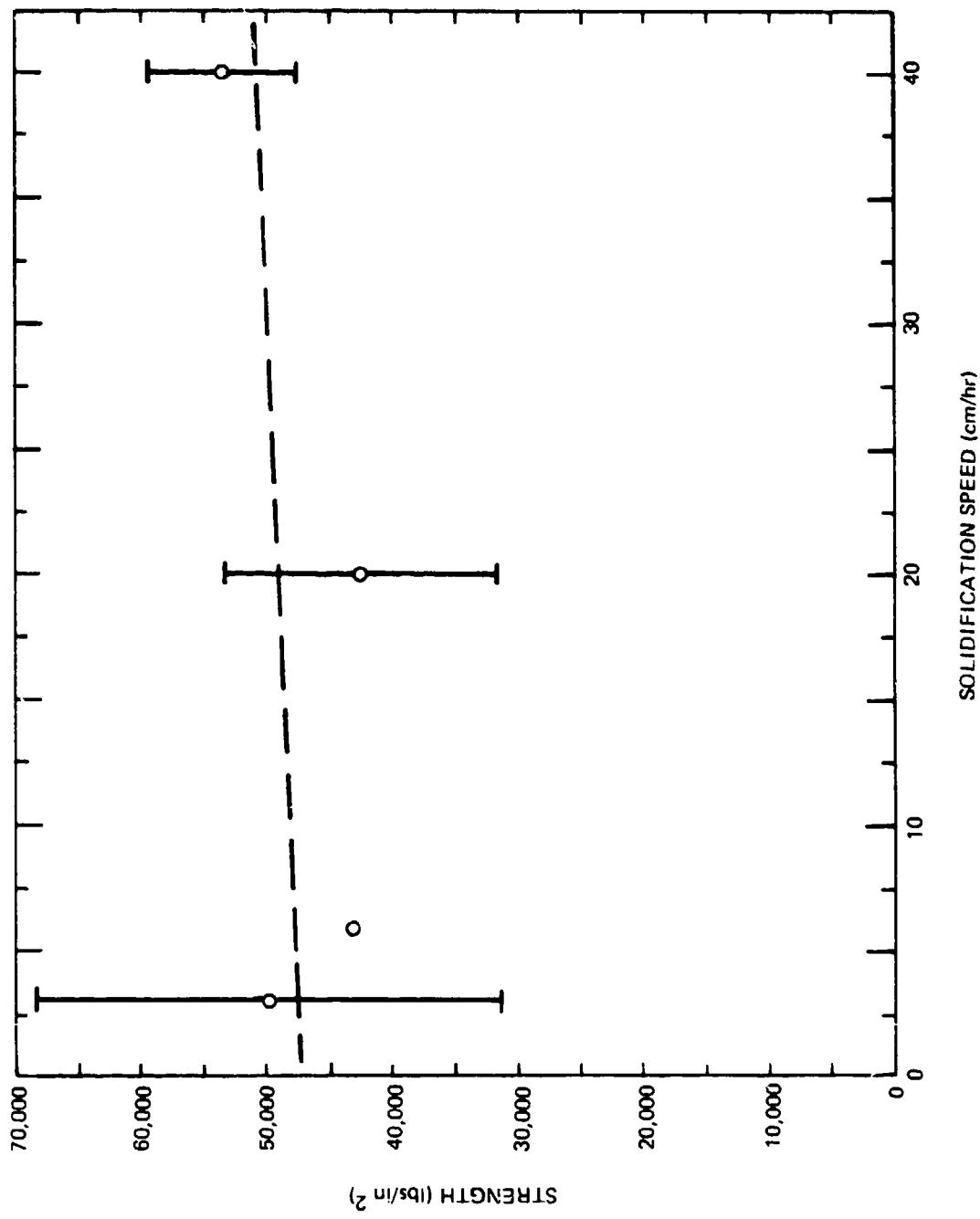
EFFECT OF TEMPERATURE ON FLEXURAL STRENGTH (3–POINT) OF
UNIDIRECTIONALLY SOLIDIFIED ZrO_2– $CaO \cdot ZrO_2$ EUTECTIC
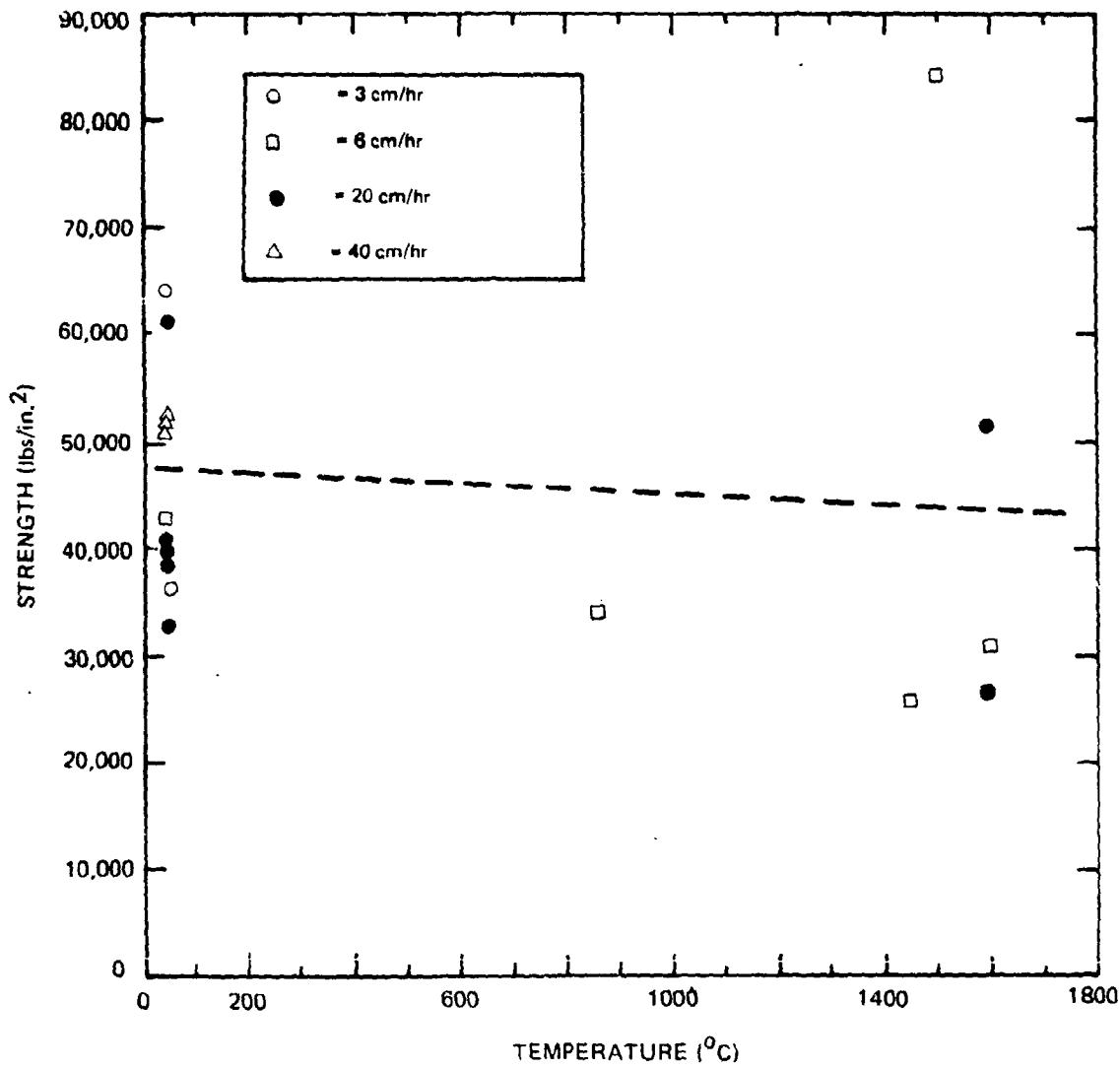
TRANSVERSE VIEW OF CaO·ZrO_2–ZrO_2 EUTECTIC MICROSTRUCTURE NEAR CENTER OF INGOT

25 μ

FIG. 62

FRACTURE SURFACE OF CaO · ZrO_2–ZrO_2 EUTECTIC AT ROOM TEMPERATURE

FIG. 63

WORK–TC–FRACTURE FORCE/DEFLECTION CURVES FOR CaO · ZrO_2–ZrO_2
EUTECTIC AT SEVERAL TEMPERATURES

FIG. 64
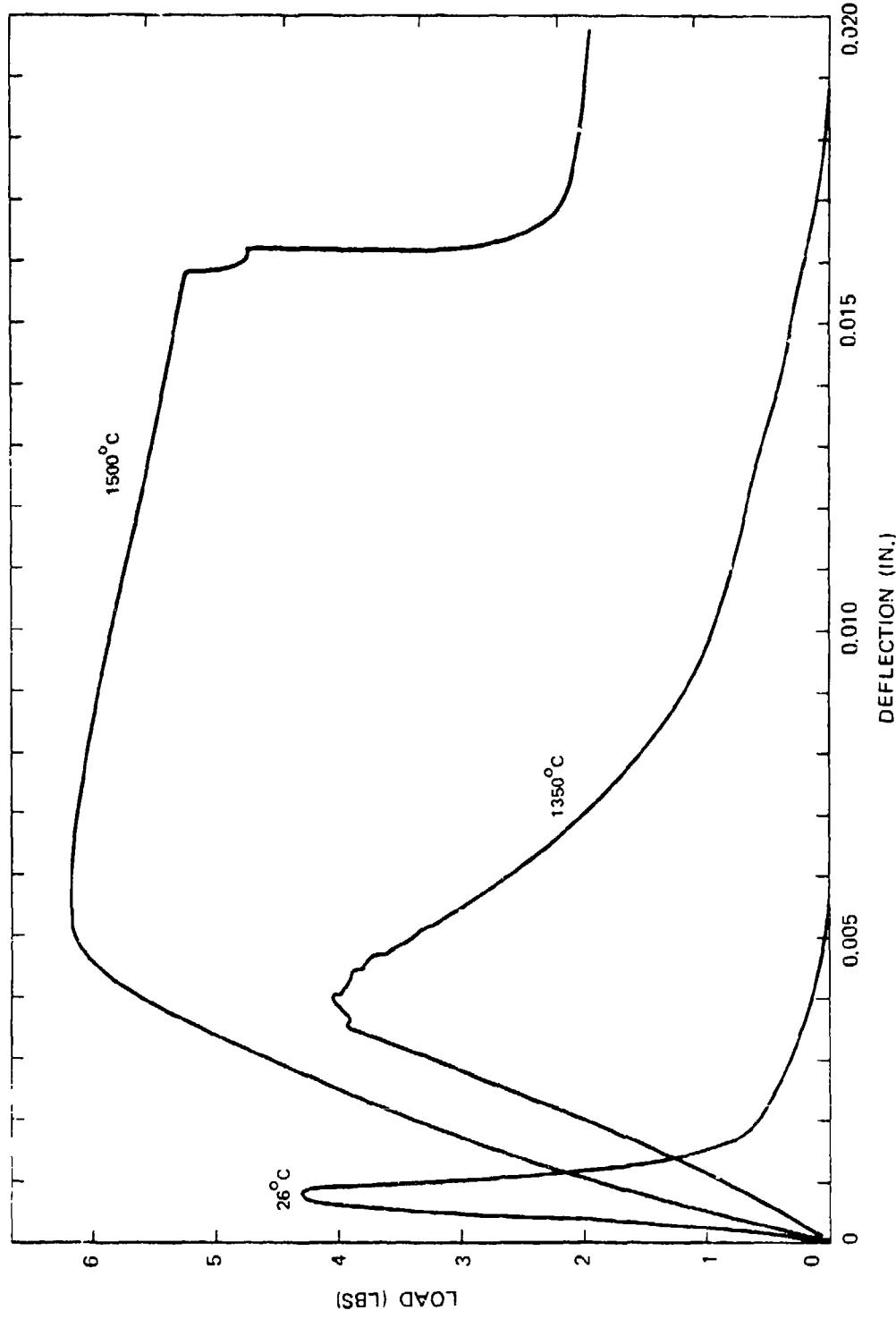
WORK-TO-FRACTURE OF CaO·ZrO₂-ZrO₂ EUTECTIC DIRECTIONALLY SOLIDIFIED AT 10 CM/HR AND POLYCRYST Al₂O₃ VERSUS TEMPERATURE

Legend:
- O DIRECTIONALLY SOLIDIFIED CaO·ZrO₂-ZrO₂ EUTECTIC
- △ POLYCRYST Al₂O₃ - VESGO 995 (R.T. DATA NOT SHOWN)

Curve labels: Al₂O₃, CaO·ZrO₂-ZrO₂

X-axis: TEMPERATURE (°C)
Y-axis: WORK-TO-FRACTURE (ERG/CM² x 10⁴)

FIG. 65
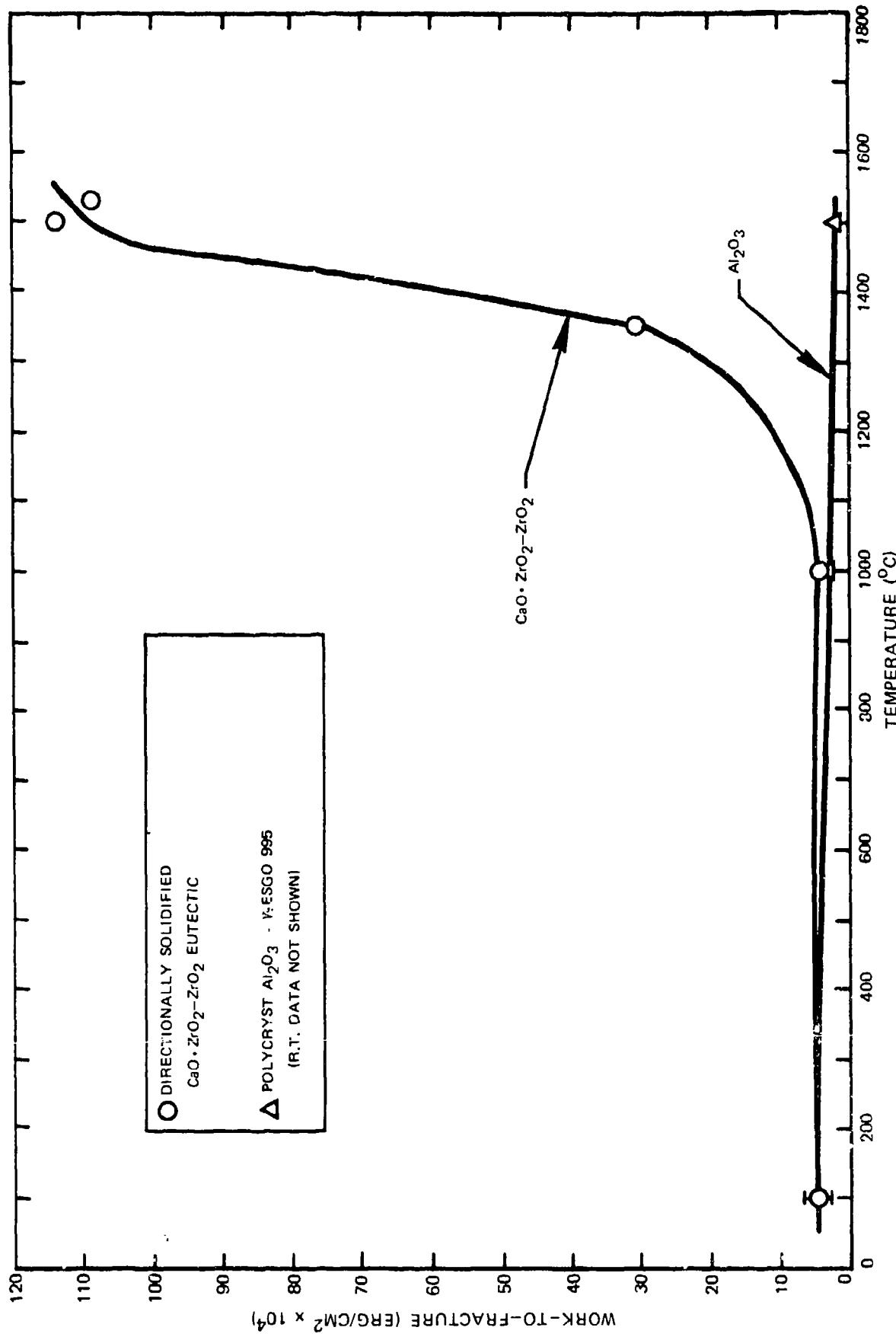
FRACTURE SURFACE OF $CaO_2 \cdot ZrO_2 - ZrO_2$ EUTECTIC AT $1000^\circ C$

FRACTURE SURFACE OF CaO·ZrO_2–ZrO_2 EUTECTIC AT 1500°C

FIG. 67

FRACTURE SURFACE OF CaO · ZrO$_2$–ZrO$_2$ EUTECTIC AT 1500°C (30" TILT)

EDGE VIEW OF FRACTURE IN CaO·ZrO_2–ZrO_2 EUTECTIC AT 1630°C

5 μ
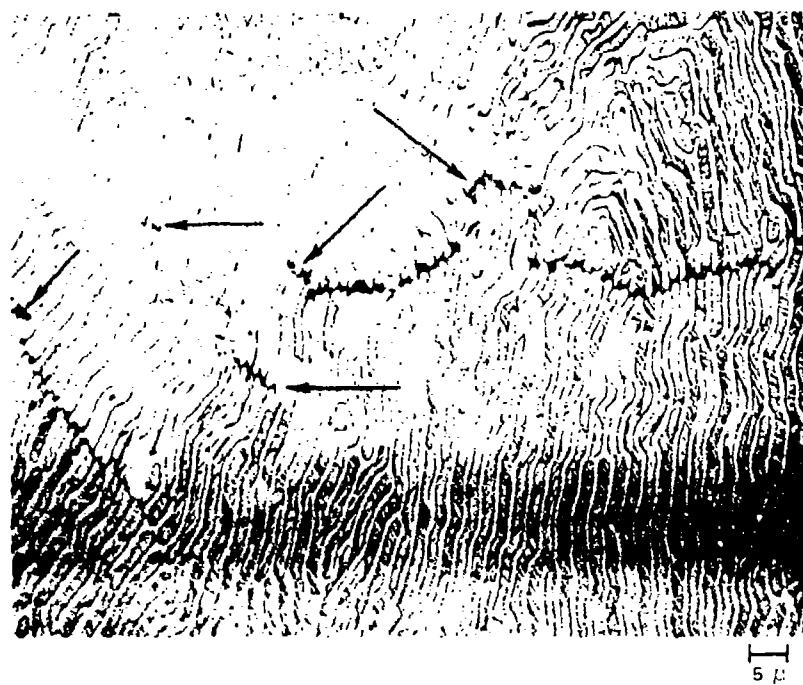
NORMAL STRESSES REQUIRED FOR PLASTIC YIELDING ON {001} <$1\bar{1}0$> AND {110} <$1\bar{1}0$> SLIP SYSTEMS IN CaO SINGLE CRYSTALS

FIG. 70
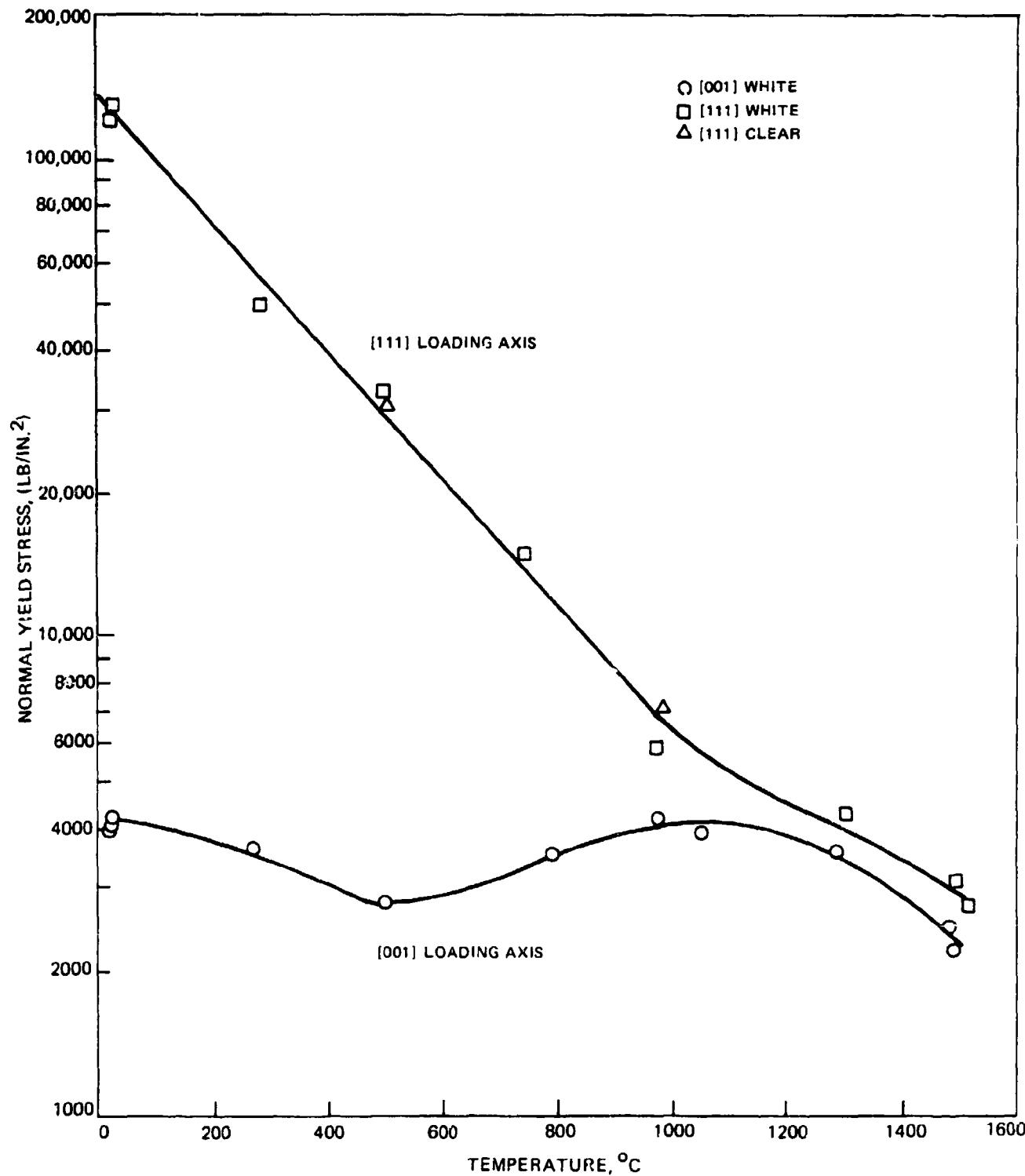
SHEAR STRESSES REQUIRED FOR PLASTIC YIELDING ON {001}
<1$\bar{1}$0> AND {110} <1$\bar{1}$0> SLIP SYSTEMS IN MgO
SINGLE CRYSTALS
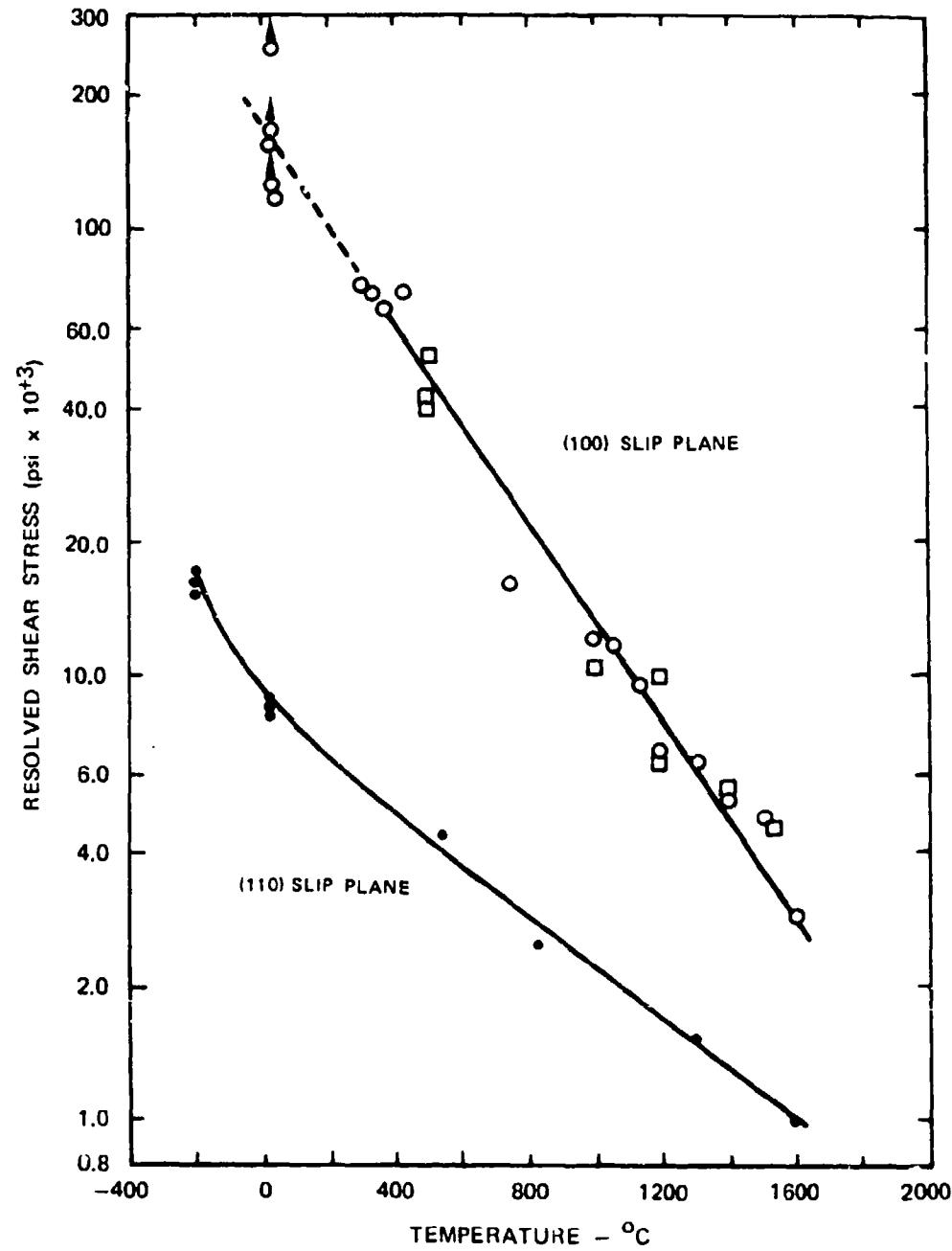
TRANSVERSE MICROSTRUCTURE OF MgO–CaO EUTECTIC SOLIDIFIED AT 20 CM/HR

10 μ

FIG. 72

TYPICAL LONGITUDINAL MICROSTRUCTURE OF MgO—CaO
EUTECTIC SOLIDIFIED AT 20 CM/HR.
(BEND SAMPLES)

100 μ
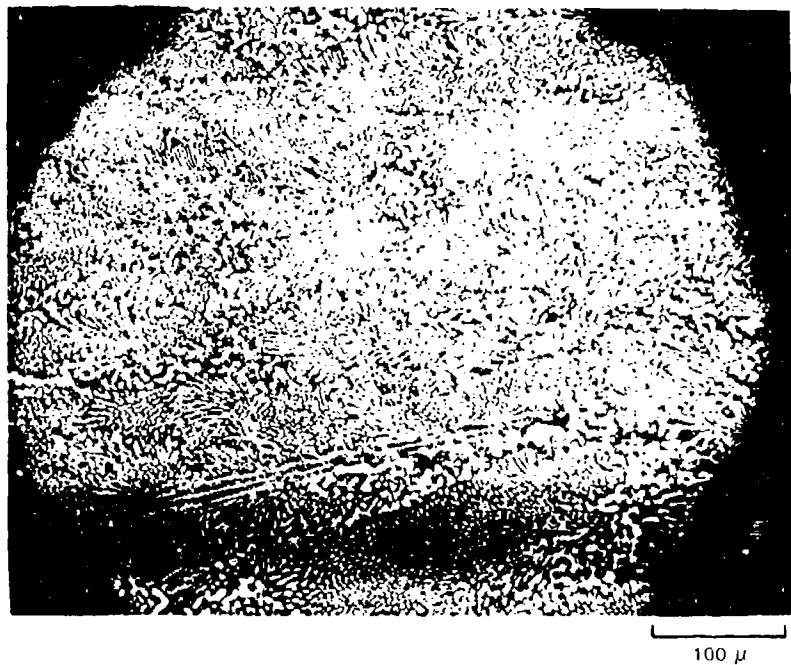
FIG. 73

STRENGTH IN 3–POINT –BENDING CaO–MgO EUTECTIC UNIDIRECTIONALLY SOLIDIFIED AT 20 CM/HR

ARGON ATMOSPHERE

TEMPERATURE (^{o}C)

FLEXURAL STRENGTH (LBS/IN.^{2})
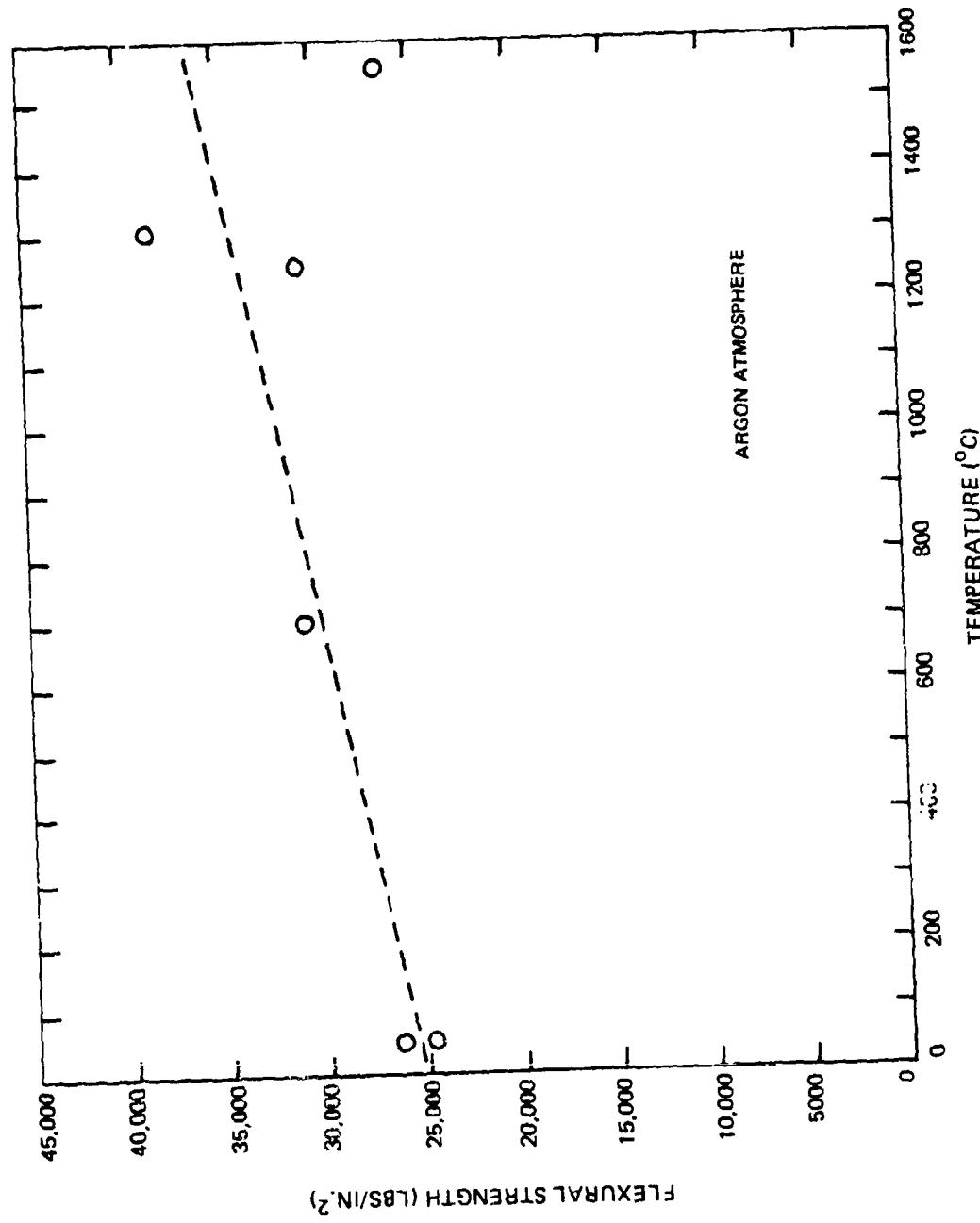
FIG. 74

TYPICAL TRANSVERSE MICROSTRUCTURE FOR POOR WORK—OF—FRACTURE SAMPLES
OF MgO—CaO EUTECTIC SOLIDIFIED AT 20 CM/HR.

100 μ

FIG. 75
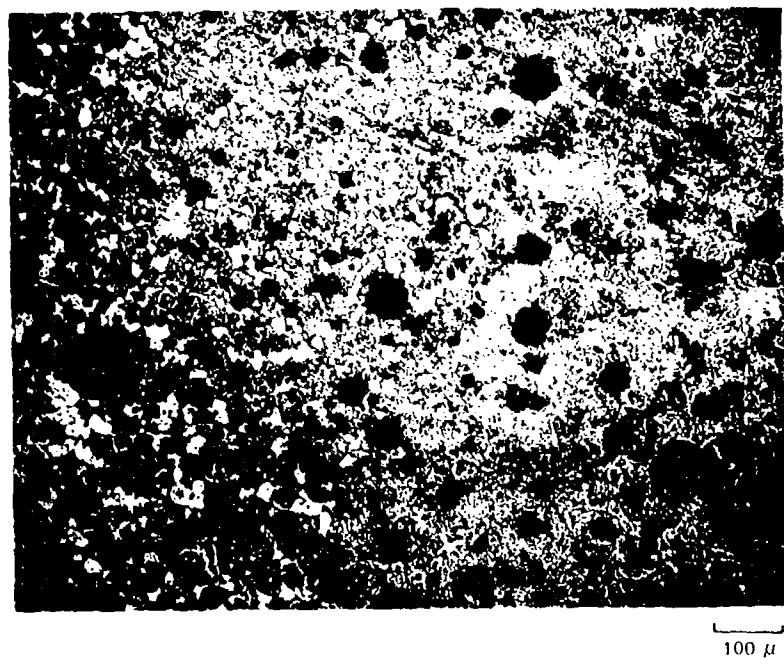
WORK–TO–FRACTURE OF CaO–MgO EUTECTIC UNIDIRECTIONALLY SOLIDIFIED AT 20 CM/HR AND POLYCRYSTALLINE Al$_2$O$_3$ VERSUS TEMPERATURE


125<
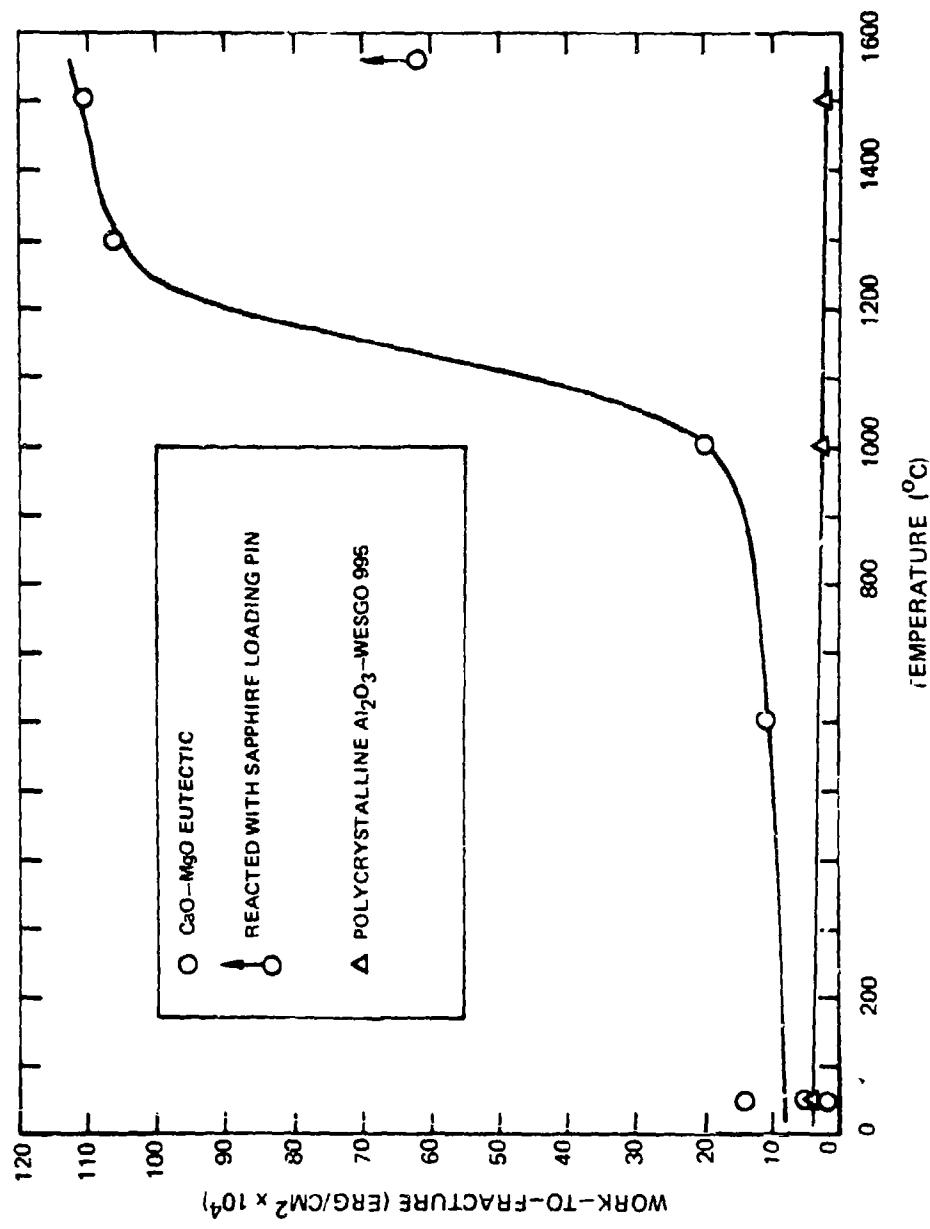
FRACTURE SURFACE AT 1000°C OF CaO–MgO EUTECTIC SOLIDIFIED AT 20 CM/HR.

5 μ

FIG. 77

FRACTURE SURFACE AT 1250°C OF CaO–MgO EUTECTIC SOLIDIFIED AT 20 CM/HR.

5 μ

FIG. 78

FRACTURE SURFACE AT 1250°C OF CaO—MgO EUTECTIC SOLIDIFIED AT 20 CM/HR.

3 μ

FIG. 79

FRACTURE SURFACE AT 1550°C OF CaO–MgO EUTECTIC SOLIDIFIED AT 20 CM/HR

$2\,\mu$

FRACTURE SURFACE AT 1550°C OF CaO–MgO EUTECTIC SOLIDIFIED AT 20 CM/HR.